British Geological Survey
NATURAL ENVIRONMENT RESEARCH COUNCIL

ENVIRONMENT AGENCY

United Utilities

Investigation into the physical and chemical characteristics of the Abbey Arms Wood observation borehole, Delamere, Cheshire

Groundwater Systems and Water Quality Programme

Commissioned Report CR/02/317

BRITISH GEOLOGICAL SURVEY

COMMISSIONED REPORT CR/02/317

Investigation into the physical and chemical characteristics of the Abbey Arms Wood observation borehole, Delamere, Cheshire

Kinniburgh, D G, Bloomfield, J P, Davies, J, Newell, A J, Milodowski, A E, Ingram, J and Merrin, P D

Contributors

Neumann, I, Cobbing, J E, Buckley, D K, Williams, P J and Ward, R

Key words

Delamere; arsenic; water quality; borehole.

Front cover

The drilling rig in operation (John Ingram, EA)

Bibliographical reference

KINNIBURGH, D G, BLOOMFIELD, J P, DAVIES, *J ET AL.*. 2002. Investigation into the physical and chemical characteristics of the Abbey Arms Wood observation borehole, Delamere, Cheshire. *British Geological Survey Commissioned Report*, CR/02/317. 105pp.

Keyworth, Nottingham British Geological Survey 2002

BRITISH GEOLOGICAL SURVEY

The full range of Survey publications is available from the BGS Sales Desks at Nottingham and Edinburgh; see contact details below or shop online at www.thebgs.co.uk

The London Information Office maintains a reference collection of BGS publications including maps for consultation.

The Survey publishes an annual catalogue of its maps and other publications; this catalogue is available from any of the BGS Sales Desks.

The British Geological Survey carries out the geological survey of Great Britain and Northern Ireland (the latter as an agency service for the government of Northern Ireland), and of the surrounding continental shelf, as well as its basic research projects. It also undertakes programmes of British technical aid in geology in developing countries as arranged by the Department for International Development and other agencies.

The British Geological Survey is a component body of the Natural Environment Research Council.

Keyworth, Nottingham NG12 5GG

☎ 0115-936 3241 Fax 0115-936 3488
e-mail: sales@bgs.ac.uk
www.bgs.ac.uk
Shop online at: www.thebgs.co.uk

Murchison House, West Mains Road, Edinburgh EH9 3LA

☎ 0131-667 1000 Fax 0131-668 2683
e-mail: scotsales@bgs.ac.uk

London Information Office at the Natural History Museum (Earth Galleries), Exhibition Road, South Kensington, London SW7 2DE

☎ 020-7589 4090 Fax 020-7584 8270
☎ 020-7942 5344/45 email: bgslondon@bgs.ac.uk

Forde House, Park Five Business Centre, Harrier Way, Sowton, Exeter, Devon EX2 7HU

☎ 01392-445271 Fax 01392-445371

Geological Survey of Northern Ireland, 20 College Gardens, Belfast BT9 6BS

☎ 028-9066 6595 Fax 028-9066 2835

Maclean Building, Crowmarsh Gifford, Wallingford, Oxfordshire OX10 8BB

☎ 01491-838800 Fax 01491-692345

Parent Body

Natural Environment Research Council, Polaris House, North Star Avenue, Swindon, Wiltshire SN2 1EU

☎ 01793-411500 Fax 01793-411501
www.nerc.ac.uk

Foreword

This report is the published product of a joint study by the British Geological Survey (BGS), the Environment Agency (EA) and United Utilities (UU). The Environment Agency's R&D project number for this study is P2-267/U/1. Project details are given below.

Project Title: Delamere Arsenic Investigation borehole
Start date: November 2001
End date: August 2002

Agency Project Manager: John Ingram
Agency Project Executive: Rob Ward
Address: Environment Agency
National Groundwater and Contaminated Land Centre
Olton Court
10 Warwick Road
Olton
Solihull B92 7HX
Telephone: 0121 711 5841
Fax: 0121 711 5925
Email: rob.ward@environment-agency.gov.uk

BGS project manager: David Kinniburgh
British Geological Society
Maclean Building
Crowmarsh Gifford
Wallingford OX10 8BB
Telephone: 01491 692293
Fax: 01491 692345
Email: dgk@bgs.ac.uk

UU project manager: Phil Merrin
United Utilities
Thirlmere House
Lingley Mere Business Park
Great Sankey
Warrington WA5 3LP
Telephone: 01925 234000
Fax: 01925 464766
Email: phil.merrin@uuplc.co.uk

Acknowledgements

We would like to thank Laura Bellis for a copy of her M.Sc. thesis and Pauline Smedley for review and comments.

Contents

FIGURES

PLATES

TABLES

Summary

In March 2002, a 150-m borehole was drilled in Abbey Arms Wood, Delamere, Cheshire UK. It was located in an embayment of the outcrop of the Helsby Sandstone Formation (part of the Sherwood Sandstone Group) and was cored throughout its entire length. The area is known to give rise to relatively high arsenic (10–50 μg L^{-1}) groundwaters. The aims were (i) to provide a better understanding of the geology of the area in order to provide the Environment Agency and United Utilities with an improved understanding of the local hydrogeological conditions, and (ii) to determine the location and nature of possible sources of the arsenic in the local groundwater and to determine whether any engineering solutions could lead to a mitigation of the arsenic problem, e.g. by screening out high source zones.

The results indicated that a perched water table existed at 26 m bgl and the main water table was at about 40 m. The underlying Wilmslow Sandstone formation was found at 48.9 m and below. The physical properties of the cored sandstone were constant throughout its length (typical porosity of 0.19–0.21; median plug permeability of 1000 mD). Flow logging indicated a major flow horizon at 105 m while CCTV and the caliper log indicated two large cavities in a similar position in the borehole. The chemical composition of the sediments was also quite uniform although some systematic differences with depth were noted. There was a somewhat greater concentration of elements associated with clay minerals (e.g. illite) in the Wilmslow Sandstone Formation compared with the Helsby Sandstone Formation. The top 50 m of the Wilmslow Sandstone also had a low Ca content, suggesting the absence of calcite. The arsenic content of the sediments ranged from 5–15 mg kg^{-1} and averaged 8 mg kg^{-1} (n = 60) and showed no trends with depth. Porewater spun from the core showed a steadily increasing trend in As concentration with increasing depth. This ranged from 8 μg L^{-1} at 10 m (unsaturated zone) to 30 μg L^{-1} at 150 m (saturated zone). There was no convincing evidence for specific sources of As or other types of mineralization. It appears that the high-As groundwaters cannot be avoided by screening out high-As zones. Restricting intakes to the uppermost parts of the saturated zone may reduce As concentrations but will reduce yields and may risk higher nitrate concentrations.

The analyses of water samples referred to in this report were not carried out for the purposes of assessing the quality of water from each of the boreholes tested for drinking, cooking or other domestic, agricultural, or industrial purposes and do not amount to certification of potability in respect of groundwater in the region. If such information is required, specific tests should be carried out for this purpose.

1 Introduction

In 2001, as part of a programme to enhance its observation borehole network, the Environment Agency (EA), North West Region, planned to drill an observation borehole in Abbey Arms Wood, near Delamere, Cheshire. The site proposed is situated in west Cheshire and geologically is in an embayment of outcropping Helsby Sandstone Formation, part of the Sherwood Sandstone Group and is surrounded by the younger Mercia Mudstone Group. The site is situated just west of the Delamere Sand Sheet on which several groundwater-dependent meres and mosses are situated, some of which (Oakmere and Abbots Moss) are designated as Special Areas of Conservation (SAC's) under the EU Habitats Directive. It was believed that the groundwater in the Delamere Sand Sheet might be fed in part by groundwater perched above marl beds within the Helsby Sandstone Formation. One of the aims of the borehole was therefore to provide detailed information about the local geology of the area particularly with regard to the nature and distribution of marl bands and the presence of perched water tables.

Locally, groundwater is exploited for public water supply by United Utilities (UU) and through a number of private farm boreholes. Severn Trent Water also have a number of public supply sources exploiting the same sandstone aquifers at Peckforton and Tattenhall to the south of Delamere. Limited water level monitoring has shown that water levels in the sandstone aquifer in the Delamere area have been rising steadily since 1996 after a long period of decline. It is intended that the observation borehole will provide additional information on water level trends in the Delamere area.

Some of the groundwater sources in the Delamere area contain relatively high concentrations of arsenic in the raw water. This is not unique to the Delamere area. Relatively high concentrations of arsenic have also been found in other parts of the Triassic Sandstone (Edmunds et al., 1989) as well as in other UK aquifers, notably the Chalk of Lincolnshire (Smedley et al., 1995). In order to comply with the new 10 $\mu g\ L^{-1}$ drinking water standard for arsenic in the Delamere area, United Utilities has invested significantly in water treatment plants for arsenic removal. The BGS/EA 'Baseline' project is currently undertaking a more comprehensive assessment of the quality status of UK groundwaters including that of arsenic (see http://www.bgs.ac.uk/hydrogeology/baseline/home.html).

In view of the excellent opportunity for a multi-purpose groundwater investigation provided by the proposed observation borehole, the EA approached the BGS to log the borehole and to consider a proposal for a more detailed study of the source and nature of the high groundwater arsenic concentrations. A meeting between representatives of the EA (both the North West Region and the Groundwater Centre), United Utilities and the BGS was held at the Groundwater Centre on 31st August 2001 to discuss the requirements for such a project. The present project arose out of those discussions. Construction of the borehole has been funded by the EA North West Region while all other aspects of the investigation have been jointly funded by BGS, the EA Groundwater Centre and UU.

2 Aims of the project

The main aims of the project were:

(i) to provide a better understanding of the geology of the Abbey Arms wood area, Delamere, in order to provide the Environment Agency and United Utilities with an improved understanding of the local hydrogeological conditions;

(ii) to determine the location and nature of possible sources of the arsenic in the local groundwater and to determine whether any engineering solutions could lead to a mitigation of the arsenic problem, e.g. by screening out high source zones.

It was proposed that the borehole would be 150 m deep and would be cored throughout its length. It was expected that the coring would encounter a few metres of superficial sand, followed by about 70 m of Helsby Sandstone Formation with part of the Wilmslow Sandstone Formation below.

The analyses of water samples referred to in this report were not carried out for the purposes of assessing the quality of water from each of the boreholes tested for drinking, cooking or other domestic, agricultural, or industrial purposes and do not amount to certification of potability in respect of groundwater in the region. If such information is required, specific tests should be carried out for this purpose.

3 Geological and hydrogeological context

3.1 REGIONAL STRUCTURAL SETTING

The Cheshire Basin is one of the largest onshore basins in Britain (Figure 3.1). It is an important post-Variscan sedimentary basin that contains up to 4.5 km of Permian and Triassic strata (Chadwick, 1997). The Abbey Arms Wood borehole is located in the northern part of the Basin. The Cheshire Basin is a broadly asymmetrical half-graben with a slight deepening toward the Wem-Red Rock Fault system that forms its southeastern margin (Figure 3.2). The Cheshire Basin is infilled with a relatively thick Permo-Triassic sequence which has a regional dip toward the ESE and thickens gradually toward the more or less unfaulted western basin margin (Plant *et al.*, 1999).

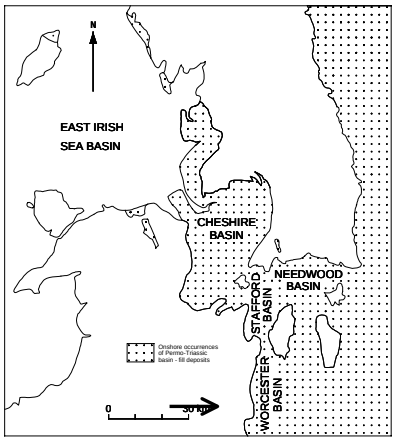

Figure 3.1 Relation between the Cheshire basin and other nearby basins (from Plant *et al.*, 1999).

The Abbey Arms Wood borehole, located in an important structural position on the 'Western Slope' of the Cheshire Basin (Figure 3.3), is less than 1 km east of the 'Overton–East Delamere Fault Zone', a major structural belt which defines the western margin of the Wem-Audlem Sub-basin (Figure 3.4) (Plant *et al.*, 1999). This fault zone is some 70 km in length and has an easterly downthrow that locally exceeds 1000 m at the top of the pre-Permian basement. The fault has an important control on the geological outcrop pattern with Sherwood Sandstone Group generally occurring to the west of the fault zone and Mercia Mudstone Group to the east (Figure 3.4).

The fault zone broadly forms the eastern margin of the 'Mid-Cheshire Ridge'. A second important feature of the fault zone is its association with base metal mineralisation. At Bickerton, 15 km south of Delamere, there is a small mineral deposit hosted in Wilmslow Sandstone with Cu, Co, As, Ni, and Fe mineralisation (Figure 3.4) (Naylor and Fallick, 1989). Sulphides are found impregnating the sandstones in a narrow zone adjacent to the fault. Mineralisation in the known sulphide ore deposits is thought to have occurred when high-density metalliferous brines from the Mercia Mudstone Group fluxed through the basin under the influence of gravity and encountered a small volume of reducing fluid in fault systems around the margins of the basin (Plant *et al.*, 1999).

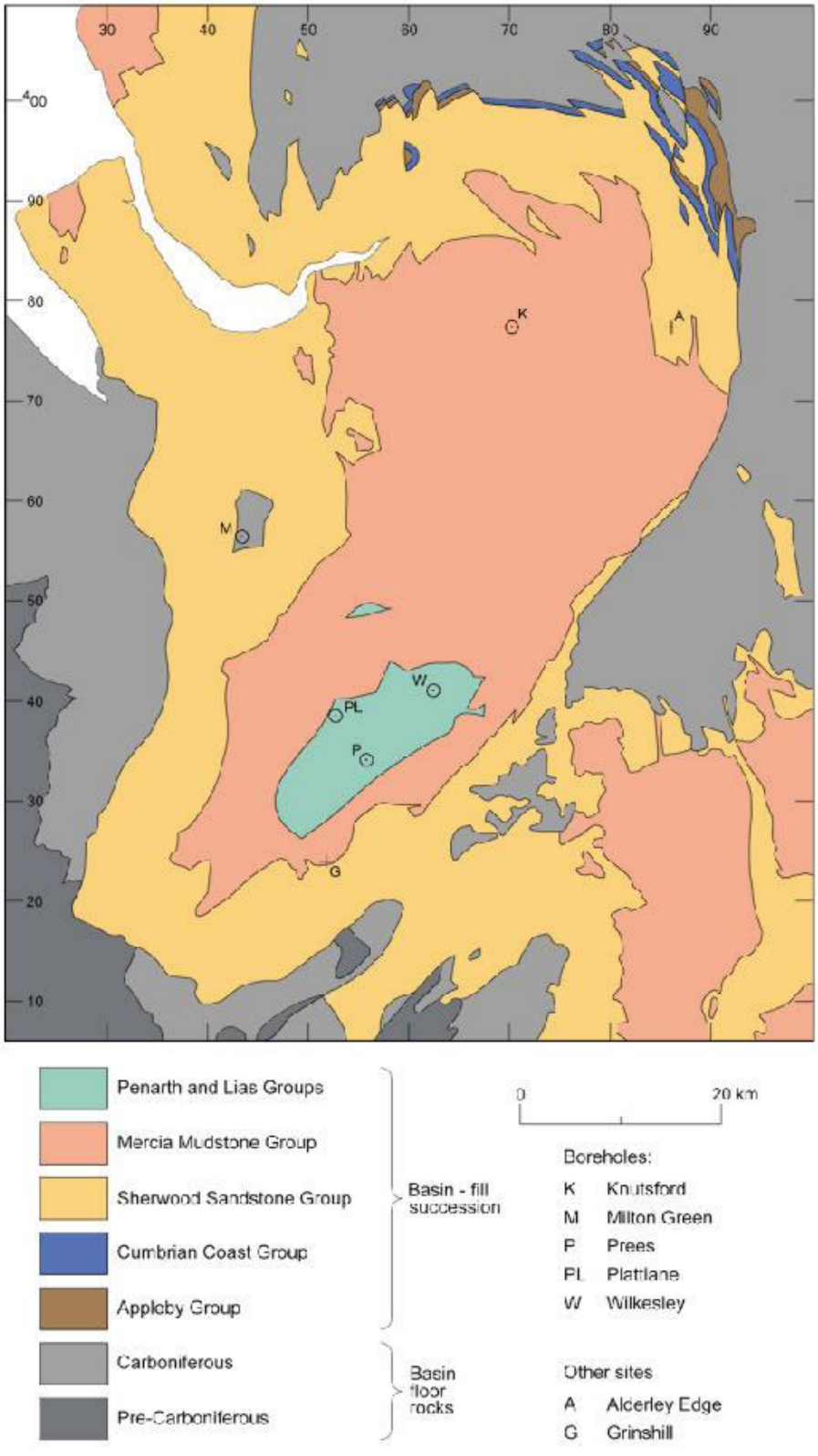

Figure 3.2 Geological map of the Cheshire Basin showing the overall geology (from Plant *et al.*, 1999).

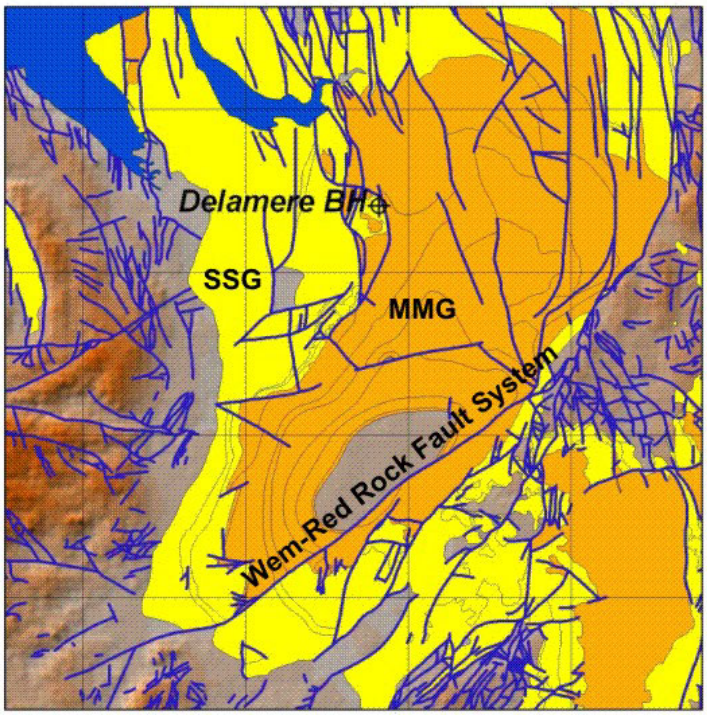

Figure 3.3 Geological map of the Cheshire Basin showing the fault system and sub-divisions of the Mercia Mudstone Group (MMG). The contours and shading relief reflect elevation. SSG=Sherwood Sandstone Group.

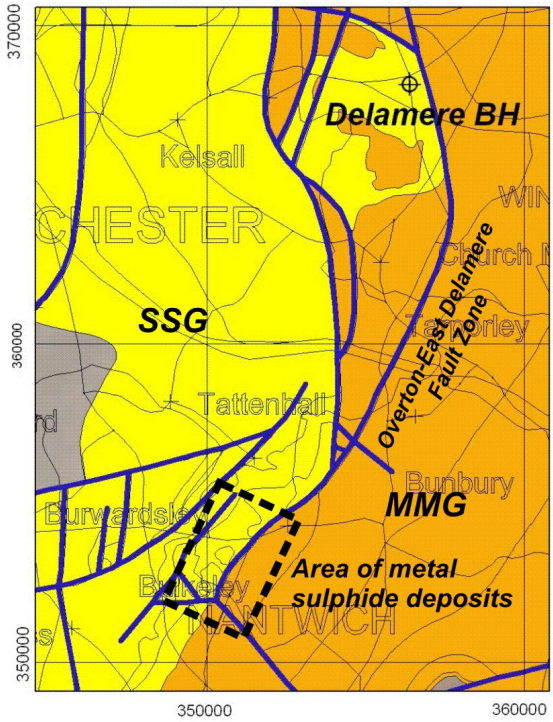

Figure 3.4 Geology of the Delamere region showing the location of the area of sulphide mineralization to the south of Delamere. SSG = Sherwood Sandstone Group; MMG = Mercia Mudstone Group. A 10 km grid is shown.

3.2 STRATIGRAPHY OF THE DELAMERE AREA

The Abbey Arms Wood borehole penetrates the Helsby Sandstone Formation and the Wilmslow Sandstone Formation. These are the two uppermost units of the Sherwood Sandstone Group, a thick succession of Triassic sandstones, mudstones and conglomerates deposited in arid continental fluvial, aeolian and lacustrine environments (Figure 3.5). In general terms, the Helsby Sandstone Formation comprises reddish brown, well-cemented, sometimes pebbly, fluvial sandstones interstratified with friable aeolian sandstones. An attempt has been made to subdivide the Helsby Sandstone into formal members (Delamere, Thuraston and Frodsham members) based on the proportion of aeolian and fluvial facies. However this scheme has generally proven difficult to apply because of complex lateral and vertical facies change (Warrington *et al.*, 1980).

The Helsby Sandstone is generally thought to rest with a sharp erosive unconformity on the underlying Wilmslow Sandstone and, in the basin centre, reaches a thickness of up to 230 m. The Wilmslow Sandstone comprises predominantly red, fine-grained, argillaceous cross-bedded sandstones with some interbedded siltstones and mudstones. The formation is 920 m thick in the Knutsford borehole in the centre of the basin. The contact between the Helsby Sandstone and Wilmslow Sandstone is relatively well-defined in the Abbey Arms Wood borehole, occurring at a depth of 48.9 m and marked by a change from relatively silty, fine-medium grained flat-bedded sandstones to clean cross-bedded sandstones and mudstones. The stratigraphic contact is well defined by the gamma-ray log (see Section 0).

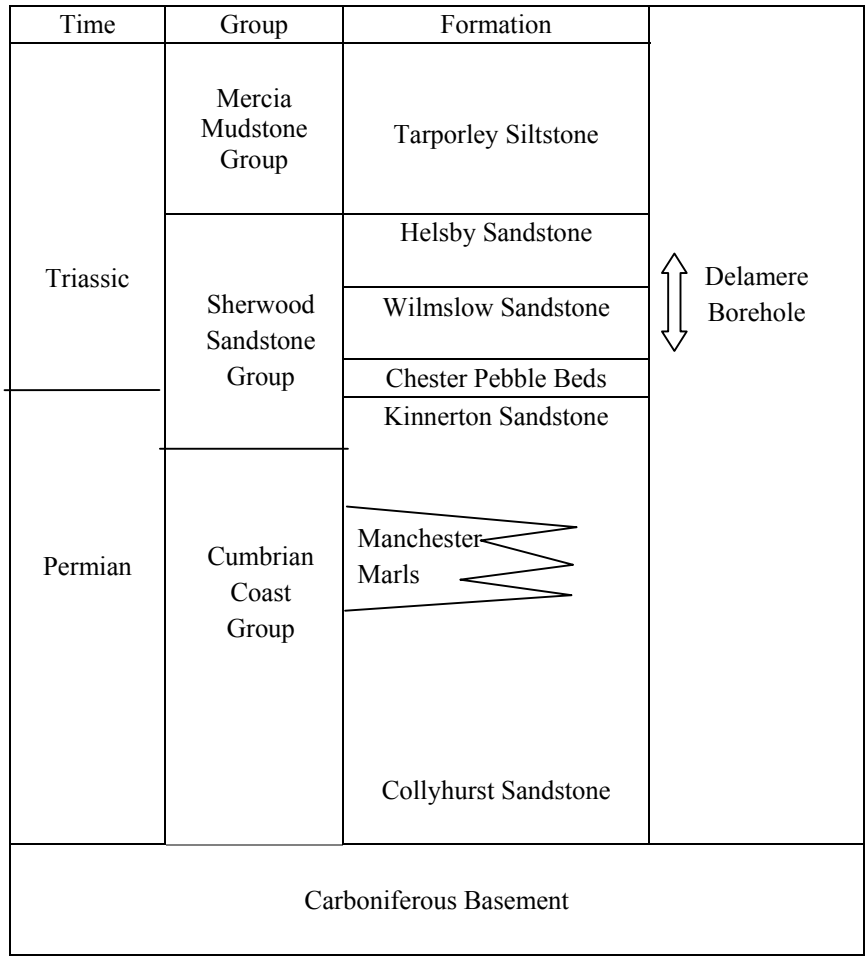

Figure 3.5 Stratigraphy of the Cheshire Basin

3.3 LITHOFACIES AND DEPOSITIONAL ENVIRONMENTS

A lithofacies is a rock unit with a distinctive set of characteristics, such as grain-size and sedimentary structure, and is generally produced by a particular process or depositional environment. Table 3.1 provides a description and interpretation of the seven main lithofacies that are encountered in the Delamere core. The Helsby and Wilmslow Sandstones are each characterised by a distinct association of lithofacies which provides the key to the identification of depositional environment.

Table 3.1 Principal lithofacies of the Helsby and Wilmslow Sandstone Formations in the Abbey Arms Wood borehole

Facies	Facies Code	Facies description	Facies interpretation
Aeolian sandy sabkha	Aw	Sandstone, generally dark reddish brown, fine-medium grained, poorly sorted, moderately cemented, distinctive wavy lamination highlighted by thin silty laminae and irregular lenses of sand	Deposition of windblown sand, silt and clay on a siliciclastic sabka by the adhesion and trapping of sediment on and under salt crusts
Aeolian sand sheet	Al	Sandstone, generally reddish brown or pale reddish brown, fine-coarse grained, moderately sorted, moderately cemented to friable, distinctive low angle/horizontal pinstripe (wind-ripple) lamination	Deposition of wind-blown sand as a low-relief sand sheet where wind-ripples form the dominant sedimentary structure and dune slip-faces are absent
Aeolian dune	Ax	Sandstone, generally reddish brown or pale reddish brown, fine-coarse grained, moderately sorted, moderately cemented to friable, high angle cross-lamination	Deposition of wind-blown sand on a slipfaced aeolian dune
Coarse-grained fluvial channel fill	Fx	Sandstone, generally reddish brown or orange brown, fine-coarse grained, moderately to well sorted, cross-bedded, contains mudclasts often lining erosion surfaces	Depostion of sand in a fluvial channel environment by the lateral and downstream migration of dunes and bars.
Fine-grained fluvial channel fill	Fl	Sandstone, generally reddish brown or orange brown, fine-grained, moderately to well sorted, laminated or ripple cross-laminated, commonly micaceous	Deposition in a fluvial channel, generally fine-grained bar-top deposits
Mudstone	M	Mudstone, dark reddish brown, generally massive	Deposition from suspension in standing water body e.g. channel plug, shallow lake
Massive sandstone	Sm	Sandstone, generally reddish brown or dark reddish brown, fine-coarse grained, moderately to well sorted, can include carbonate cemented zones generally as bedding parallel layers and nodules	Pedogenically destratified sands of fluvial or aeolian origin. Carbonates probably represent early diagenetic calcretes precipitated from Ca-rich groundwaters in the near-surface zone

3.3.1 Helsby Sandstone Formation

The Helsby Sandstone is composed predominantly of coarse-grained fluvial channel-fill sandstones interbedded with subordinate mudstones, aeolian sandstones and massive sandstones with zones of carbonate cementation. The interpretation of sandstones as fluvial is based on the presence of erosion surfaces (scoured channel bases), rounded mudclasts and the association with fine-grained micaceous sandstones and mudstone. An important feature of the fluvial sandstones is that most appear to be composed of reworked aeolian sand grains, characterised by a high degree of rounding and a frosted surface texture. The mature composition and lack of clay matrix probably accounts for the relatively low gamma-ray values of the fluvial sandstones. Overall, the association of facies is consistent with previous depositional models of the Helsby Sandstone which envisage a mixed fluvial-aeolian environment (Thompson, 1970).

3.3.2 Wilmslow Sandstone Formation

The Wilmslow Sandstone differs significantly from the Helsby Sandstone. It is primarily a monotonous succession of wavy and irregularly stratified fine to medium-grained silty sandstones (Facies Aw, aeolian sandy sabkha). These wavy bedded units are characterised by undulose, wavy crinkly and irregular stratification defined by preferentially cemented thin very fine grained and silty laminae a few mm to 1–2 cm apart. Analogous facies are developed in the Sherwood Sandstone Group in the East Irish Sea Basin where they were previously interpreted as fluvial sheetflood deposits (Meadows and Beach, 1993). However, recent work has demonstrated that these irregularly laminated silty sandstones are the product of deposition on an inland aeolian sandy sabkha, where deposition results from the trapping and adhesion of sand on and under thin surface salt crusts.

Direct evidence for evaporitic conditions is generally absent from the rock record of this environment because the salts are dissolved under conditions of sediment aggradation and rising water table. The sandy sabkha deposits are interbedded with thin units of aeolian sandsheet/dune sandstones. These sandstones are relatively ‘clean’ (free from clay and silt) compared to the sabkha deposits and have a lower gamma-ray response. They are also more poorly cemented and friable than the other lithologies and are often represented by zones of core loss. The gamma-ray curve highlights the cyclic arrangement of clean aeolian sandstones with sabkha deposits (see Section 0). These cycles may reflect periodic fluctuations in the palaeo-water table which allowed the encroachment and inundation of the sabkha by ‘dry’ aeolian deposits.

3.4 HYDROGEOLOGY OF THE DELAMERE AREA

3.4.1 Background

The sandy formations within the Sherwood Sandstone Group form the second most important aquifer in the United Kingdom after the Chalk and the most important in northern England. The porosity of the Sherwood Sandstone Group is typically 20–30%, and specific yields are relatively high at 6–14%. The high porosity and absence of sedimentary compaction are evidence that primary cementation which existed initially has now been dissolved. Annual fluctuations in water levels are therefore low, often less than 4 m in the unconfined aquifer. Porosity varies slightly between the different formations of the Sherwood Sandstone. However, no general porosity trend has been identified with depth within the top 100 m of

the aquifer. In many parts of the Cheshire Basin, groundwater levels are currently rising due to decreased groundwater abstraction rates.

Approximately 300 m to the east of the borehole site the north-south trending normal East Delamere Fault brings the Helsby Sandstone and underlying Formations into contact with the Mercia Mudstone Group, a throw of around 400 m. For several tens of kilometres to the west of the site, the Sherwood Sandstone is divided into blocks by further north-south trending faults, which brings different formations of the Sherwood Sandstone into juxtaposition at the surface. Whilst it is commonly the case that adjacent blocks of Sherwood Sandstone are in hydraulic continuity, the contact with the Mercia Mudstone is likely to constitute a hydraulic boundary with very limited groundwater flow into or out of the relatively impermeable Mercia Mudstone. However, sands and gravels overlying the Mercia Mudstone to the east of the East Delamere Fault are in hydraulic continuity with the Sherwood Sandstone to the west of the fault, and probably contribute water to the aquifer.

3.4.2 Hydrogeology of the Sherwood Sandstone Formation

Aquifer properties of the Sherwood Sandstone generally are greatly affected by the sedimentary structure and post-depositional diagenesis. For example, hydraulic conductivities may be directional, as fluvial channel deposits with higher hydraulic conductivities are found. Core studies have shown that horizontal values are generally greater than vertical ones. Argillaceous horizons, resulting from the settling of flood-overbank deposits, act as aquitards. Hydraulic stratification is greater in the Helsby Sandstone than the Wilmslow Sandstone in the vicinity of the Abbey Arms Wood borehole due to the presence of mudstone horizons. Lateral facies changes occur. Generally, intrinsic permeabilities are low, but hydraulic conductivities are greatly improved by the presence of fissures, bedding plane fractures and faults of either tectonic or diagenetic origin. These may be enhanced by additional *in situ* solution. These features provide virtually all of the permeability, and are found at depths of up to 150 m. Although faults normally increase the permeability, locally they may reduce it.

Mineralisation associated with groundwater flow along large faults may in particular reduce permeabilities in the adjacent sandstone by filling voids. Clay in-fills in fault zones may render them much less permeable than adjacent rock. These effects on permeability may be worsened by the associated compression of the adjacent rock and the presence of rock flour. Large faults may interrupt regional groundwater flows where beds of significantly different permeability are brought into contact, which is the case with the Delamere Fault which juxtaposes the Mercia Mudstone and the Sherwood Sandstone Groups.

The aquifer should therefore be considered as a dual-porosity aquifer, with water movement taking place primarily along fissures and faults, which are in turn fed by intergranular water. Transmissivities therefore vary greatly and depend on the number, size and interconnectivity of fissures that are intersected. Transmissivities have a recorded range of from 0.9 $m^2 d^{-1}$ to 4900 $m^2 d^{-1}$ in the Sherwood Sandstone of the Cheshire region as a whole (Allen *et al*.,1997) with a geometric mean of 220 $m^2 d^{-1}$ and a median of 250 $m^2 d^{-1}$. Pumping tests in the West Cheshire region, closer to the Abbey Arms Wood borehole, indicate transmissivities ranging from 100 to 500 $m^2 d^{-1}$. Exceptionally high values of up to 12 000 $m^2 d^{-1}$ have been recorded locally in the Delamere area. Packer testing and CCTV logging has been used to confirm that most of the transmissivity is due to fissured or fractured zones. The Wilmslow Sandstone typically contains more fissures than the pebbly Helsby Sandstone because it is less well cemented. The large influence of fractures, fissures and faults makes bulk hydraulic conductivities in new boreholes difficult to predict.

A few metres of fluvio-glacial sands and gravels overlie the aquifer at the site of the borehole and to the east, although these give way to exposed Sherwood Sandstone within 100 m or so to the west. These deposits overlying the aquifer provide an important means of recharge, either directly or by providing continuity with surface waters. It is thought that most recharge to the Sherwood Sandstone aquifer of the Cheshire Basin is via drift deposits, although in the vicinity of the Abbey Arms Wood borehole it is probable that recharge moves directly into the aquifer where it outcrops. Drift deposits may in some places constitute a minor aquifer where they are thick enough, although limited storage and areal extent means that such supplies are vulnerable to long periods of dry weather. Chemical and bacteriological water quality may be variable.

Borehole yields from the Sherwood Sandstone are variable, although dry boreholes are virtually unknown. There is a 50% probability of boreholes in the Sherwood Sandstone yielding more than 2.3 L s^{-1} for the country as a whole. 50 L s^{-1} is a common yield, whilst large diameter boreholes may yield over 100 L s^{-1}. Running sand may be a problem in boreholes, in particular in the less well cemented Wilmslow Sandstone. Casing is generally considered unnecessary, although borehole sides can sometimes collapse.

The geometric mean of specific capacity measurements made on 29 sites in the Sherwood Sandstone of the Cheshire and South Lancashire region is 98 m^3 d^{-1} m^{-1}, and the median is 68 m^3 d^{-1} m^{-1}.

The water level in the borehole was 40.06 m below ground level in April 2002. The regional flow in the Cheshire Basin is towards the north and northwest, although it is probable that this is distorted locally by pumping from public supply boreholes, in particular the Delamere Pumping Station. Groundwater flow in the Delamere area is believed to be towards the west (see below). Groundwater residence times in the Sherwood Sandstone are relatively short, as shown by modern ^{14}C dates.

3.5 THE DELAMERE PUBLIC SUPPLY BOREHOLES

3.5.1 Borehole network

There are nine United Utilities' public supply boreholes within 3 km of the observation borehole at Abbey Arms wood and another, at Eaton, which is approximately 5 km distance that abstracts from the aquifer confined beneath the Tarporley Siltstones. These boreholes vary in age, construction and depth. Details of these are given in Table 3.2. Abstraction takes place from both the Helsby Sandstone and the underlying Wilmslow Sandstone. These are in hydraulic continuity in this area. Fractures are present in both the Helsby and Wilmslow Sandstones but given the friable nature of the Wilmslow Sandstone, these fractures may not stay open at depth.

3.5.2 Hydrogeology

During the 1980s, a series of pumping tests were carried out on the boreholes to assess their performance. These tests also identified differences in the hydraulic properties of the boreholes and provided information on the way the aquifer has responded to recent changes in groundwater abstraction since the 1970's.

In 1970, the average water level in the aquifer in this area was approximately 49 m AOD. During the period of the pumping tests during the late 1980s, average water levels were

recorded at approximately 34 m AOD; a drop of 15 m since 1970. This drop reflects the fact that in this part of the aquifer system, abstraction was exceeding recharge over this period.

Water levels in some Environment Agency observation boreholes in the Delamere area show minima in 1993/94, e.g. Organsdale SJ 56/50A shows a minimum of 27.9 m AOD in 1994. Since that time, water levels have generally increased across the aquifer and are now similar to their 1970 levels, e.g. at Cotebrook 40", recent rest water levels have been measured at approximately 48 m AOD and at Delamere No.4, recent rest water levels have been measured at approximately 45 m AOD. This regional increase in water levels reflects the fact that recharge is likely to be exceeding abstraction again in this area. Given the exceptional rainfall in the north-west region over the last few years, this is not unexpected.

A large range of transmissivities has been calculated for each borehole. The value largely depends on the number, size and distribution of fractures intercepted by the borehole and the degree of interconnectivity between these fractures. Eaton and Cotebrook 15” are the least efficient boreholes in the group. At high abstraction rates, there is a disproportionate increase in drawdown relative to flow in these boreholes. The boreholes at Eddisbury, Delamere and Organsdale show above-average transmissivities for the aquifer in this area. These values may be related to an increased zone of fracturing related to the proximity of the East Delamere Fault. Eddisbury is the nearest borehole to this fault line and shows the highest transmissivity.

Table 3.2 Details of United Utilities public supply boreholes in the Delamere area

Borehole name	WRB No.	Depth (m bgl)	Construction details	Aquifer	Transmissivity ($m^2 d^{-1}$)
Delamere No.3	SJ 56/11A	91	Drilled in 1905. Construction: 24" diameter borehole	Helsby Sst/Wilmslow Sst	742
Delamere No.4	SJ 56/35	243	Drilled in 1951. Construction: 0 to 22.9 m 40" plain casing; 22.9–122.2 m 36" slotted casing; 122.2–243 m 24" slotted casing.	Helsby Sst/Wilmslow Sst	866
Organsdale	SJ 56/49	123	Drilled in 1971. Construction: 0–30.5 m 36" plain casing; 30.5–123.45 m 30" slotted casing.	Helsby Sst/Wilmslow Sst	866
Sandyford	SJ 56/17A+B	60 and 91	Two boreholes 11 m apart, drilled in 1910. No.1: 59.6 m deep, lined to 29.6 m (24") lining tubes. No.2: 91.4 m deep, lined 0–36.58 m (30") plain casing; open hole to base.	Helsby Sst/Wilmslow Sst	158
Eddisbury	SJ 56/2	229	Drilled in 1935 and deepened in 1939. Construction: 0–152.4 m 24" diameter; 152.4-base 17" diameter.	Helsby Sst/Wilmslow Sst	924
Cotebrook 15”	SJ 56/36	126	Drilled in 1906. Construction: 61.0 m of 10" plain casing, 8" slotted PVC tube to bottom.	Helsby Sst/Wilmslow Sst	89
Cotebrook 40”	SJ 56/19	244	Drilled in 1951. Construction: 0–22.9 m 40" plain casing; 22.9–122 m 37.75" plain casing; 122–183 m 25" plain casing, 19" hole to base.	Helsby Sst/Wilmslow Sst	184
Eaton	SJ 56/26A+B	244 and 243	Drilled in 1938/39 15 m apart. Construction: Borehole A, 244 m deep, 0–35 m 40" plain casing; 35–base 15"" slotted casing. Borehole B 243 m deep, 0–35 m 40" plain casing; 35–83.8 m 36"; 83.8–131.1m 33"; 131.1–183 m 30"; 183–base 15".	Tarporley Siltstones/ Helsby Sst/Wilmslow Sst	31

4 Construction and properties of the project borehole

4.1 BOREHOLE CONSTRUCTION

The project borehole is situated in Abbey Arms wood near Oakmere [356418 368133] about 0.5 km from Delamere pumping station (Figures 4.1 and 4.2) and adjacent to the B4162 road (Figure 4.1 and Figure 4.2). It was constructed during February and March 2002 by BB Drilling (a division of British Drilling and Freezing). The borehole was constructed by rotary air-flush drilling using a Dando 250 drilling rig and a 980 cfm/360 psi Super Silenced compressor. Photographs taken at various stages of borehole construction are given in Figure 4.3.

The upper section of the borehole was drilled using a rock roller bit and the permanent steel casing (200 mm diameter) was installed and grouted at 9.55 m depth. The Helsby Sandstone was encountered at 6.35 m depth, beneath Quaternary sand and gravel deposits.

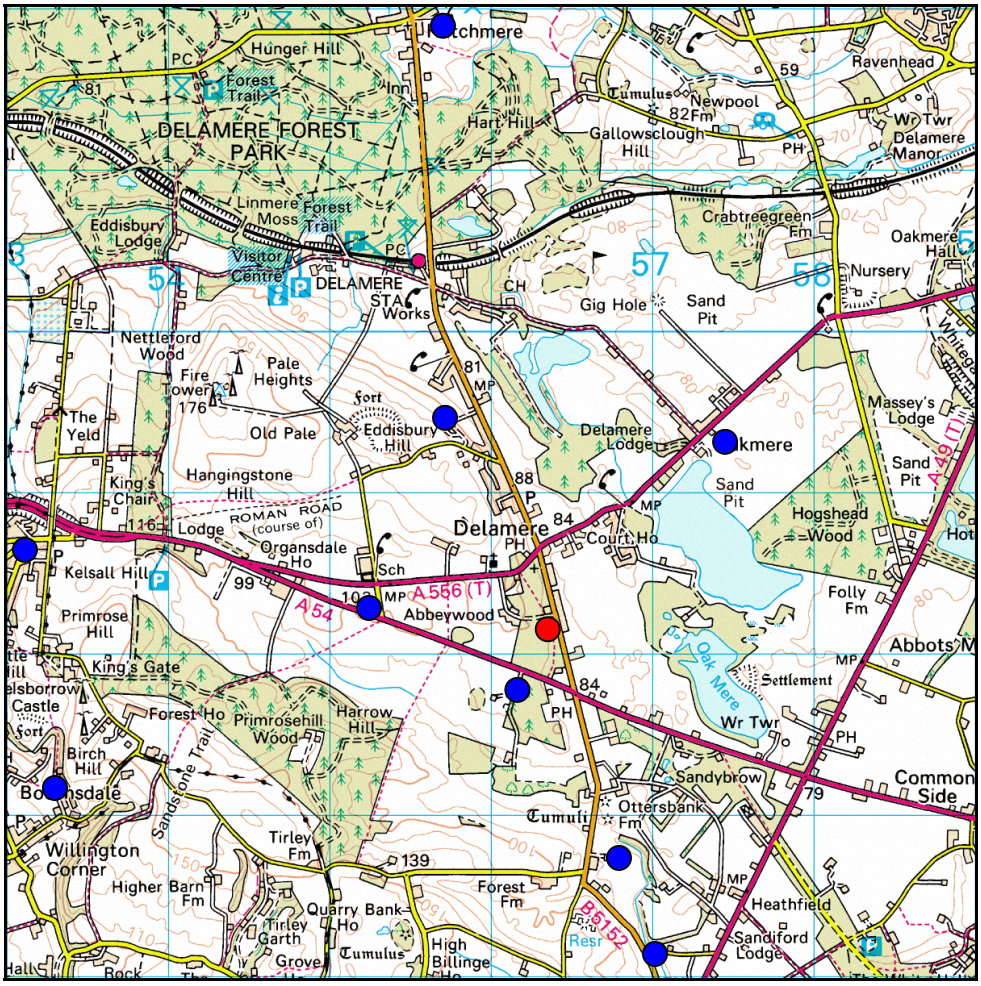

Figure 4.1 Location of the Delamere project borehole (red circle) and surrounding water-supply and observation boreholes (blue circles). The blue grid is made up from 1 km squares.

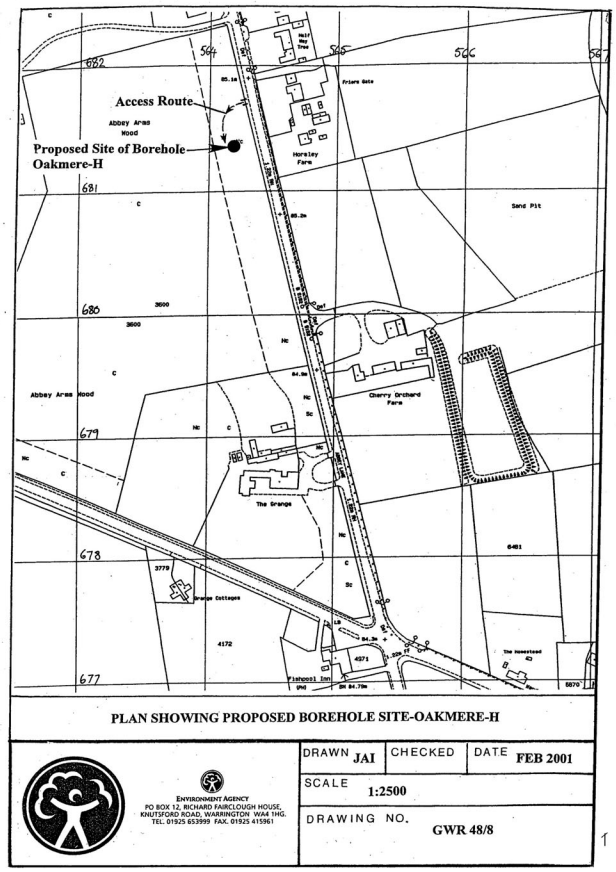

Figure 4.2 Location of the Abbey Arms Wood borehole

Figure 4.3 Aerial photograph showing the borehole location (white arrow) with Oak Mere to the east (black) with sand pit to the north of it (from Multimap©).

Below 9.55 m, the sandstone was cored using a SF diameter double core barrel with rigid plastic core lining tubes. This produced core of approximately 105 mm diameter. As each 3 m core run was completed, the core and liner were removed from the barrel and cut in half with a hacksaw. The core material in the plastic core liner was sealed at both ends with plastic caps and tape to reduce moisture loss, boxed and periodically transported to Wallingford.

Following coring to a depth of 150 m, the borehole was reamed out to 200 mm diameter and was finally flushed for five hours. Water samples were collected during this flushing. The borehole was completed as a groundwater level monitoring network observation borehole and equipped with a data-logger to record the water levels.

At Wallingford, the plastic liner was opened with two longitudinal cuts and a lithological log of the core was prepared. Sub-samples of core material about 10 cm long were then selected at approximately 2–3 m intervals from the core. The outer material was discarded, the material sealed in a plastic bag and then mixed thoroughly.

Porewater was extracted from this field-moist core material by high speed centrifugation using a Beckman J2-21C centrifuge. A custom-made set of 6 plastic liners was placed in a JA14 rotor and spun at 14000 rpm for ½ hr. These liners were sealed at both ends with O-rings and so were not open to the atmosphere. This minimised evaporation and degassing during centrifugation but was not designed to completely avoid access to the atmosphere and so some oxidation would be possible at this stage. Porewater extraction was carried out as quickly as practically possible after opening the core, normally within a day.

The porewater was filtered through a 0.45 μm Whatman membrane filter and split into sub-samples for chemical analysis (as for the pumped water samples). The upper horizons of the unsaturated zone were quite dry and required repeated spinning to obtain sufficient porewater for analysis, preferably 15–20 ml. A list of the 60 samples collected is given in Table 4.1. The moisture content in the upper part of the unsaturated zone was only about 1/3 of that in the saturated zone. The moisture content of the saturated Wilmslow Sandstone was somewhat greater than the Helsby Sandstone indicating a slightly greater porosity in the Wilmslow Sandstone.

Table 4.1 Core samples selected for porewater extraction and detailed chemical analysis

Sample ID	Top depth (m)	Bottom depth (m)	Lithology, saturation	Moisture content (g kg^{-1} dry)
S02-00606	10.74	10.92	Helsby sst, unsatd	15.7
S02-00607	13.30	13.55	Helsby sst, unsatd	21.1
S02-00608	16.30	16.45	Helsby sst, unsatd	18.9
S02-00609	20.40	20.55	Helsby sst, unsatd	19.9
S02-00610	23.07	23.17	Helsby sst, unsatd	15.1
S02-00611	26.26	26.36	Helsby sst, unsatd	41.2
S02-00612	28.50	28.62	Helsby sst, unsatd	25.4
S02-00613	32.03	32.13	Helsby sst, unsatd	16.3
S02-00614	34.70	34.80	Helsby sst, unsatd	37.8
S02-00615	37.49	37.61	Helsby sst, unsatd	42.0
S02-00616	40.80	40.90	Helsby sst, satd	58.8
S02-00617	43.50	43.60	Helsby sst, satd	61.6
S02-00618	45.92	46.02	Helsby sst, satd	50.4
S02-00619	48.18	48.30	Helsby sst, satd	54.3
S02-00620	50.77	50.87	Wilmslow sst, satd	59.7
S02-00621	53.47	53.57	Wilmslow sst, satd	76.7
S02-00622	55.40	55.47	Wilmslow sst, satd	77.3
S02-00623	58.56	58.64	Wilmslow sst, satd	85.3
S02-00624	60.16	60.26	Wilmslow sst, satd	88.1
S02-00625	63.55	63.66	Wilmslow sst, satd	88.2
S02-00626	65.42	65.50	Wilmslow sst, satd	88.2
S02-00627	68.50	68.60	Wilmslow sst, satd	82.8
S02-00628	71.25	71.35	Wilmslow sst, satd	87.0
S02-00629	74.56	74.70	Wilmslow sst, satd	82.8
S02-00630	77.60	77.70	Wilmslow sst, satd	76.2
S02-00631	76.03	76.14	Wilmslow sst, satd	98.2
S02-00632	80.77	80.88	Wilmslow sst, satd	90.7
S02-00633	81.79	81.88	Wilmslow sst, satd	80.0
S02-00634	84.08	84.18	Wilmslow sst, satd	75.6
S02-00635	86.53	86.65	Wilmslow sst, satd	89.7
S02-00636	88.35	88.42	Wilmslow sst, satd	78.6
S02-00637	89.32	89.44	Wilmslow sst, satd	89.2
S02-00638	91.47	91.59	Wilmslow sst, satd	82.9
S02-00639	92.49	92.58	Wilmslow sst, satd	84.4
S02-00640	94.60	94.70	Wilmslow sst, satd	85.3
S02-00641	96.14	96.24	Wilmslow sst, satd	103.7
S02-00642	98.02	98.12	Wilmslow sst, satd	104.3
S02-00643	100.00	100.10	Wilmslow sst, satd	102.2
S02-00644	101.45	101.56	Wilmslow sst, satd	84.7
S02-00645	104.08	104.20	Wilmslow sst, satd	93.2
S02-00646	104.38	104.47	Wilmslow sst, satd	92.1
S02-00647	105.78	105.89	Wilmslow sst, satd	89.9
S02-00648	109.89	110.00	Wilmslow sst, satd	101.4
S02-00649	113.58	113.68	Wilmslow sst, satd	86.8
S02-00650	117.17	117.25	Wilmslow sst, satd	80.8

Sample ID	Top depth (m)	Bottom depth (m)	Lithology, saturation	Moisture content (g kg^{-1} dry)
S02-00651	118.50	118.60	Wilmslow sst, satd	79.3
S02-00652	119.57	119.65	Wilmslow sst, satd	71.9
S02-00653	123.07	123.18	Wilmslow sst, satd	84.0
S02-00654	125.70	125.80	Wilmslow sst, satd	69.7
S02-00655	129.01	129.11	Wilmslow sst, satd	107.9
S02-00656	131.10	131.20	Wilmslow sst, satd	110.4
S02-00657	132.33	132.43	Wilmslow sst, satd	59.5
S02-00658	134.50	134.60	Wilmslow sst, satd	97.2
S02-00659	136.43	136.25	Wilmslow sst, satd	86.0
S02-00660	139.27	139.35	Wilmslow sst, satd	98.5
S02-00661	141.05	141.14	Wilmslow sst, satd	58.2
S02-00662	141.88	141.97	Wilmslow sst, satd	92.2
S02-00663	143.98	144.07	Wilmslow sst, satd	21.5
S02-00664	146.82	146.92	Wilmslow sst, satd	95.7
S02-00665	149.03	149.13	Wilmslow sst, satd	73.7

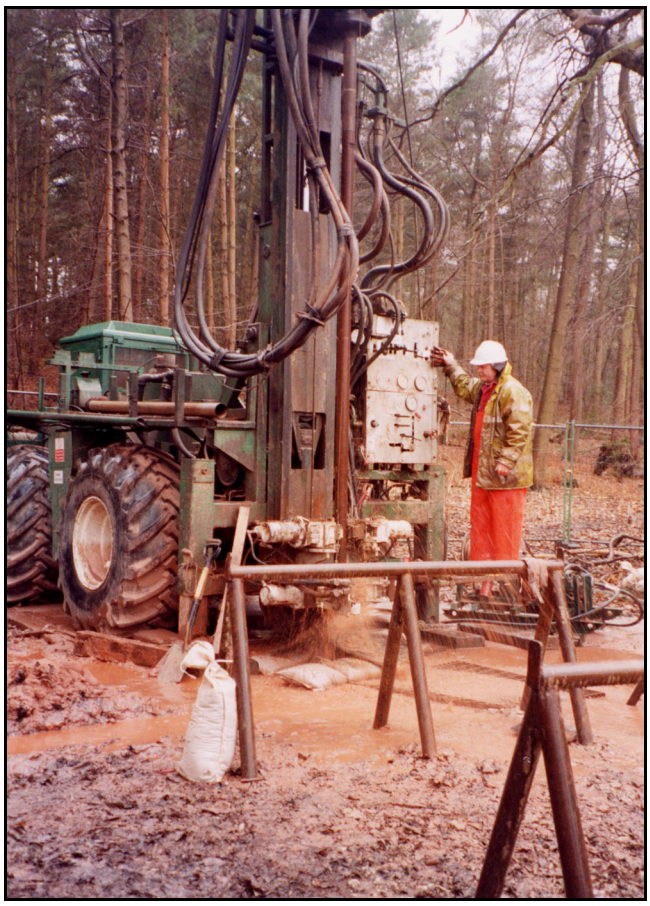

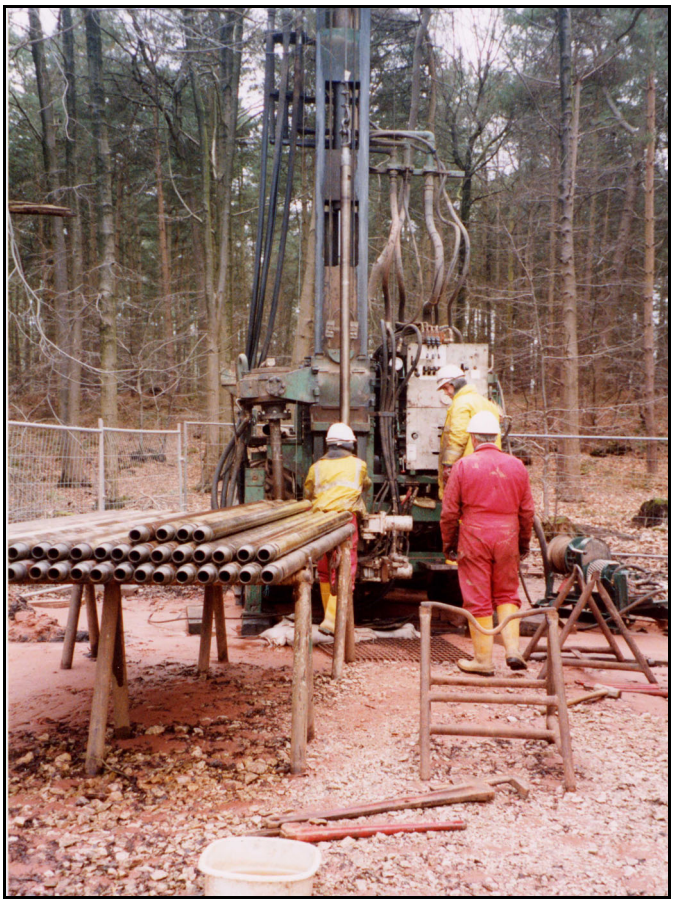


HEWDEN
Power
9505

Figure 4.4 Photographs showing the Abbey Arms Wood borehole during construction, including core processing and the borehole after completion (photographs by John Ingram, EA).

4.2 CORE LOGGING

The core material was logged at Wallingford. Visible features were noted including the presence of cements and any mineralization. A detailed descriptive core log is given in Appendix 2. A complete set of pictures of the core was recorded with a digital camera. Some typical views of the core sections are given in the photographs shown in Figure 4.5.

4.3 BOREHOLE LOGGING

4.3.1 Introduction

Borehole geophysical logging was carried out on 2 and 3 April 2002. The following details were recorded for the borehole:

Site Elevation:	85 m above Ordnance Datum (AOD)
Datum used for logs:	Casing flange, which was 0.34 m above ground level.
Water level:	40.40 m below datum.
Depth of logging:	149.01 m below datum.

Figure 4.5 (a) Delamere Borehole, core box 6, 22.15-22.55 m interval, Helsby Sandstone Formation.

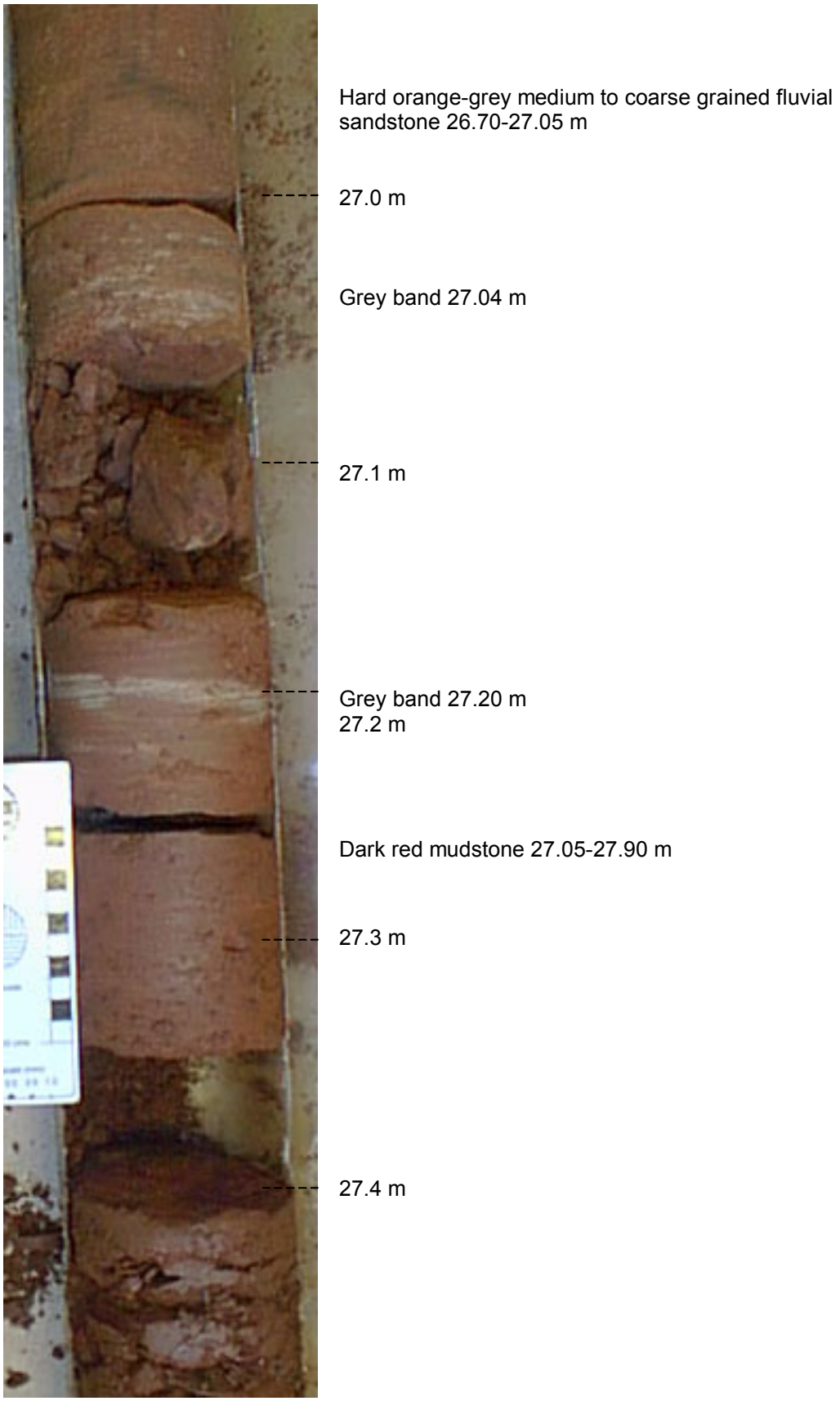

Figure 4.5(b) Delamere borehole, core box 8, 26.90-27.50 m interval, Helsby Sandstone Formation.

Figure 4.5(c) Delamere borehole, core box 31, 90.55-91.25 m interval, in Wilmslow Sandstone Formation.

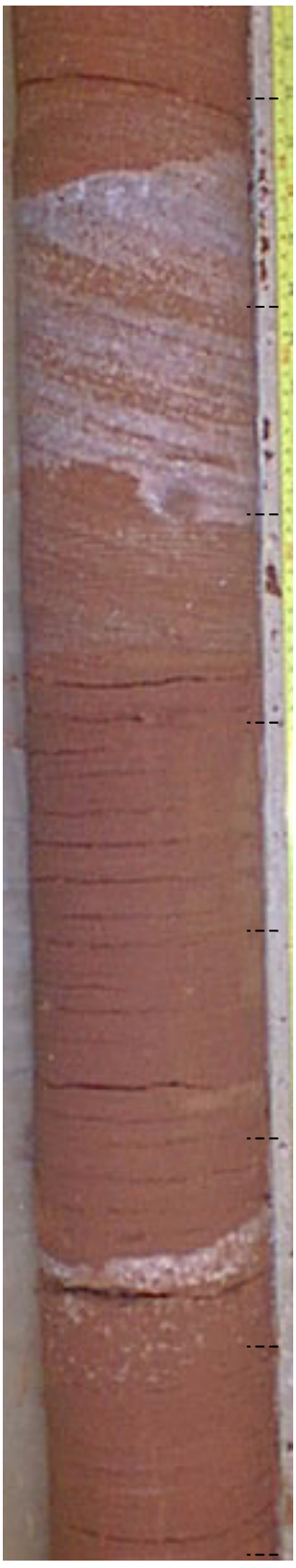

Figure 4.5(d) Delamere borehole, core box 48, 143.8-144.6 m interval in Wilmslow Sandstone Formation.

Figure 4.5. Photographs of various sections of the Delamere core.

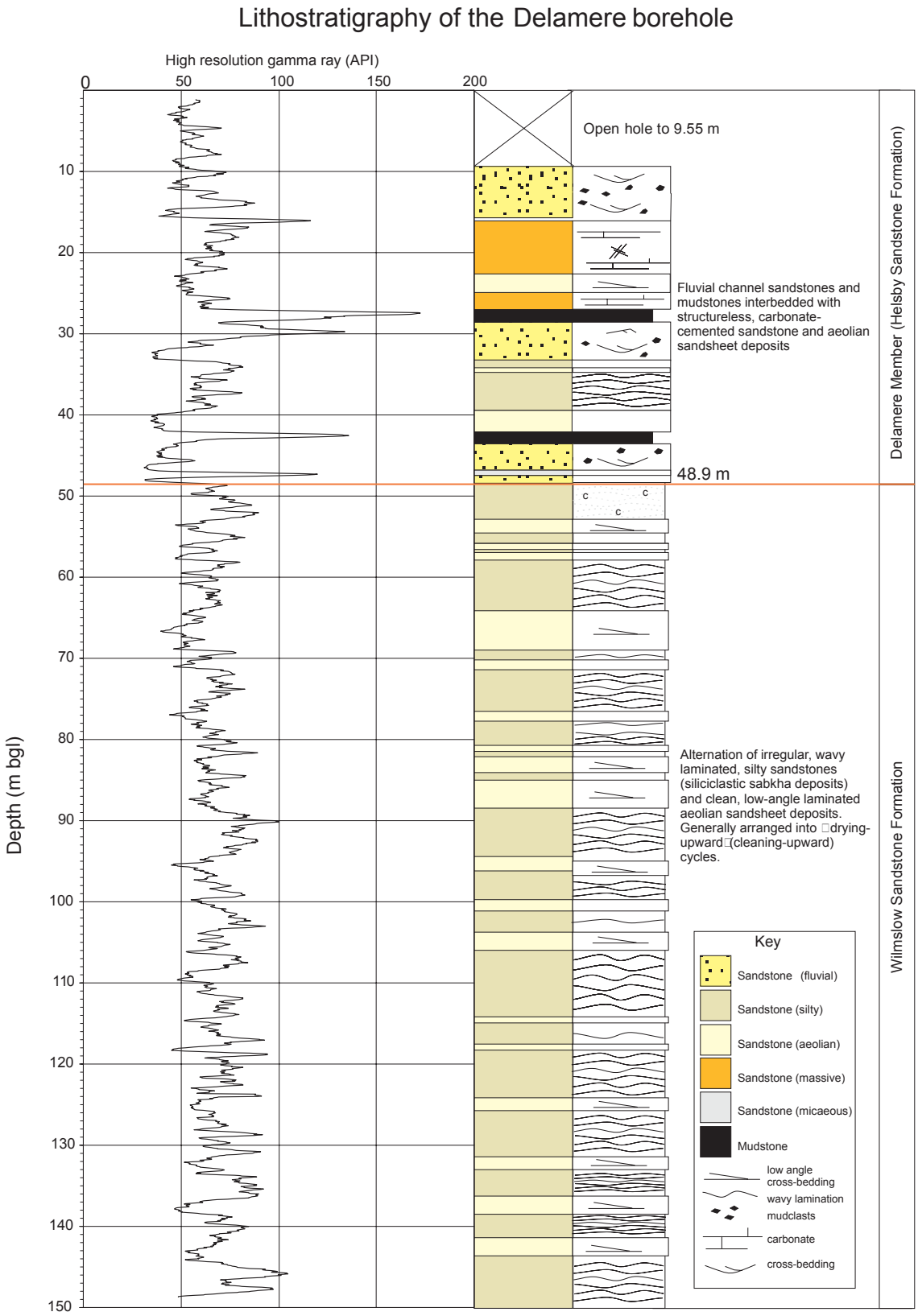

Figure 4.6 Lithostratigraphy of the Abbey Arms Wood borehole and the corresponding gamma-ray log.

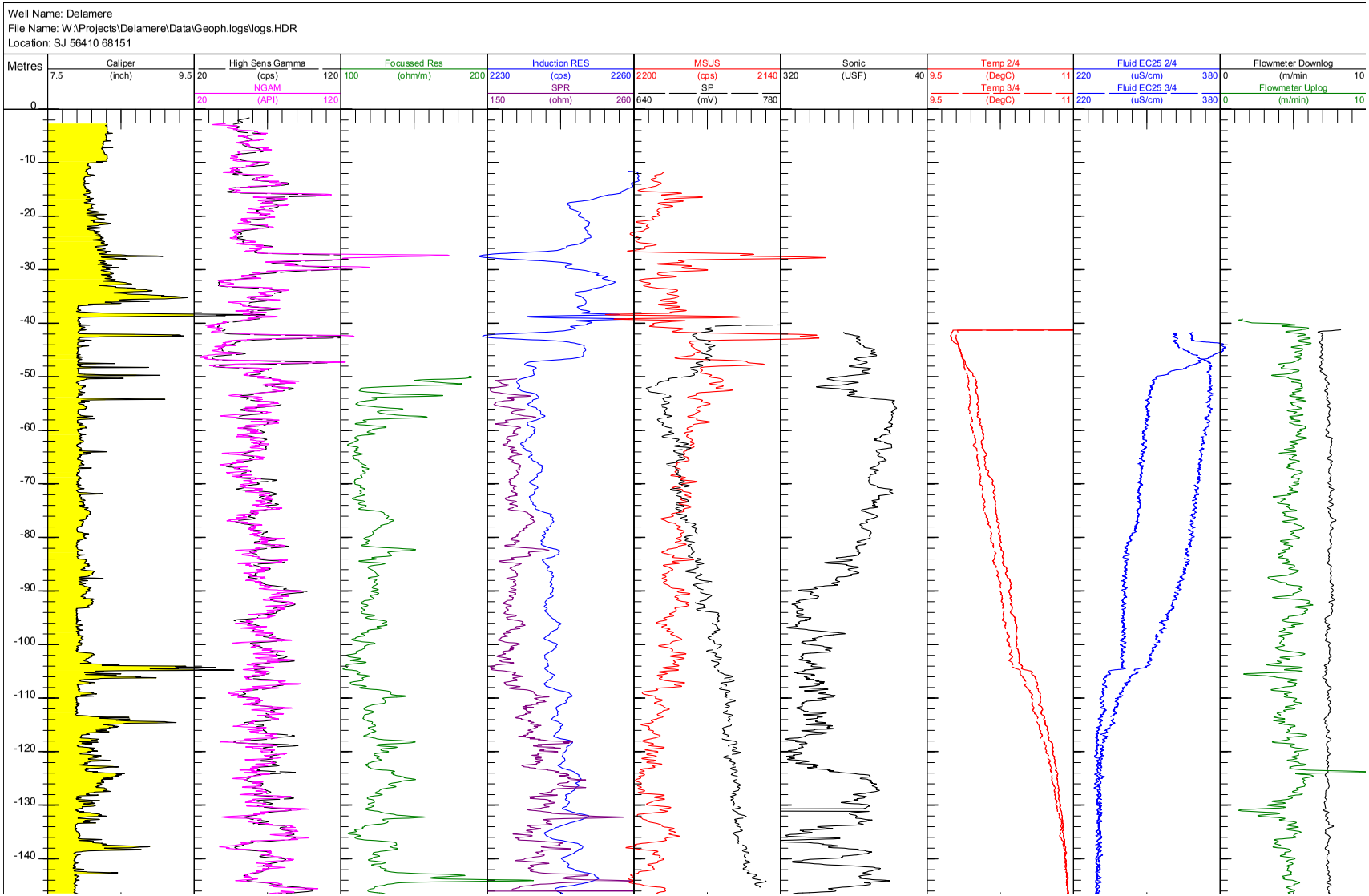

Figure 4.7 Geophysical logs of the Abbey Arms Wood borehole

A suite of formation logs including caliper, natural gamma, resistivity, self-potential, magnetic susceptibility and sonic logs was run to determine the formation properties. Fluid temperature and fluid conductivity logs were used to measure these properties of the water in the borehole, and an impeller flow-meter was used to determine the inflows within the borehole. Focused resistivity, self-potential, single-point resistivity, sonic and the fluid logs were recorded in the saturated part of the borehole.

The focused and single-point resistivity logs have been displayed up to a point ten metres below the water table, because the readings are affected when the cable insulation leaves the fluid above this point. The other logs were recorded for the full depth of the hole. Formation logs were recorded with the probes running up the hole, whilst the fluid logs were generally recorded running down the hole. A lithostratigraphy log was prepared and is shown alongside the gamma-ray log (Figure 4.6).

Logs were recorded using the BGS Landrover-based logging system, and printed in the field using a thermal printer. The digital data were later processed and plotted in VIEWLOG. The logs are shown in standard display format in Figure 4.7.

Four depth samples of the borehole water were taken for chemical analysis from 65, 96, 110 and 140 m below datum (m bgl) using a depth-sampler. Three samples were taken from each horizon; one for cation analysis (acidified with concentrated acid to 1% v/v HNO_3 final concentration), one for anions (no acidification) and a third for arsenic analysis (acidified with concentrated acid to 2% v/v HCl final concentration). The samples from each horizon were measured in the field for pH, Eh and electrical conductivity, and titrated against 1.6N H_2SO_4 to determine alkalinity.

4.3.2 Formation Logs

The caliper log (track 2, Figure 4.6) shows that the casing (approximately 8.3 inches or 210 mm diameter) has been installed to a depth of 10 metres below datum (m bgl), and the borehole is open hole below. The caliper log shows a gradual enlargement below the bottom of the casing to a maximum of about 9.4 inches at 35 m bgl, after which it narrows sharply to the drilled diameter of 7.89 inches (200 mm). Several enlargements, interpreted as fractures, are visible in the upper part of the borehole at 27, 35, 38, 42 and 48 m bgl. The lithology changes from the Delamere Member of the Helsby Sandstone to the less variable Wilmslow Sandstone at 49.24 m bgl, and the uneven nature of the caliper log above this horizon may be a reflection of the comparatively greater lithological differences in the Helsby Sandstone. Further significant enlargements of the borehole are visible at 105, 106, 114, 124 and 138 m bgl. There is a relatively even and less fractured part of the borehole between about 55 and 103 m bgl. Some of these enlargements may be induced by the drilling process, and may not therefore represent zones of increased permeability or horizons of fluid flow.

The gamma ray tool detects gamma ray emissions from minerals containing potassium-40 (^{40}K) and also uranium and thorium. Potassium is often concentrated in silts and clays and so ^{40}K values are typically higher in the fine-grained deposits. Gamma logs can indicate sand/clay ratios and thus relative permeabilities in the Sherwood Sandstones. The gamma logs (track 3) show local peaks in the Helsby Sandstone (above 49.24 m bgl) which is consistent with the presence of argillaceous horizons in this formation. Two large fractures in the Helsby Formation as shown on the caliper log, at 27 and 42 m bgl, coincide with gamma ray peaks (and low resistivity and high magnetic susceptibility) and indicate mudstone horizons. Below the Helsby Sandstone, the gamma ray emissions correspond with a series of cycles of deposition, with cleaner, aeolian sandstone horizons corresponding to gamma ray lows, for example at 109.5 and 118 m bgl.

The resistivity logs (tracks 4 and 5) display a considerable variation in the Helsby Sandstone Formation, reflecting its more variable lithology, and in particular it highlights the more

compact, resistive layers at 46.5 and 48 m bgl. Below the Helsby Sandstone the resistivity decreases generally, indicating softer rocks. The focused resistivity log shows increases at 82, 99.5, 109.5, 118 and 132 m bgl, all of which coincide with reduced gamma ray activity and indicate harder, cleaner sands. There is an increase in resistivity below about 104 m bgl, which corresponds with greater hole enlargement and lower magnetic susceptibility, and indicates a difference in lithology.

The magnetic susceptibility log (track 6) shows a gradual decrease in susceptibility with depth. It shows an inverse relationship with resistivity, with peaks at 54, 76.5, 82, 132, 138 and 144 m bgl, confirming that changes in lithology occur at these horizons. These also correspond with high gamma ray emissions, indicating a more clay-rich lithology. It has the advantage of being usable above the water table up to the base of the steel casing at about 10 m bgl.

4.3.3 Fluid Logs

The fluid temperature and fluid conductivity probe was run twice, first at 15:00 on 2 April and again at 09:30 on 3 April. These dates are indicated on the log tracks. These were carried out without pumping. The fluid temperature logs (track 8) show a gradual increase with depth, with a change in gradient at about 50 m bgl, and a significant shift towards warmer water at about 105 m bgl. When compared with the fluid conductivity logs (track 9) which show changes at similar depths, this has been interpreted as indicating a zone of cooler and higher conductivity water above 50 m bgl.

The fluid temperature and conductivity profiles suggest there may be cooler water of higher conductivity moving down the borehole to exit at the large fracture (see caliper log) at 105 m bgl. A steady increase in fluid temperature with depth would normally be expected, and the inflow and suspected downward movement of water to 105 m bgl has caused the temperature to remain relatively cool above the exit point. The temperature profile is not completely invariant with depth however, and there may be some outflow at other horizons or via the intergranular matrix. One possible outflow is probably at about 80 m bgl, and can be seen particularly on the fluid conductivity log run on 2 April which shows a change to fresher water at this horizon. This corresponds with a small caliper enlargement.

The higher conductivity cooler water entering the borehole above 50 m bgl may be due to surface contamination and more rapid shallow circulation, or to the differences in lithology above this horizon.

There is a difference in the fluid logs run on consecutive days (2 and 3 April) and this may indicate a change in the pumping regime at the nearby Abbey Arms Wood borehole. It is likely that this borehole was pumping at a greater rate on 3 April, causing greater downflow of the cooler temperature water and increasing the fluid conductivity above 105 m. It is possible that not all of the water that enters above 50 m bgl exits the borehole by 105 m bgl, and some of this water moves further down the hole to leave lower down. This is suggested by the divergence of the fluid logs down to 138 m bgl, again corresponding to a caliper enlargement.

An impeller flow-meter was run up and down the borehole at constant line speed and is presented as fluid velocity profiles in track 10. The logs have been displayed as flow velocities past the probe in m/min. The down log recorded an apparent higher velocity throughout which is at variance with the interpretation of the fluid conductivity and temperature logging. The difference between the downlog and the uplog flow-meter runs is due to the probe geometry, and the probe does not identify the suspected down-flow. For satisfactory flow-meter measurement in the borehole, a heat-pulse flow-meter could be used to determine the induced fluid movement and the impeller measurements should also be made whilst the borehole is pumping to determine the main inflow positions.

4.3.4 CCTV survey

A CCTV down-the-hole survey was undertaken on 20 June 2002. Copies of the videotape are available from BGS, EA or UU. These show the whole length of borehole. The CCTV shows the structure of the borehole better than the retrieved core since it shows fractures in a relatively undisturbed condition and includes those regions of the borehole where core recovery was poor or nil. These often-friable zones are important for understanding the hydrogeology.

The video clearly, and sometimes spectacularly, shows the position of mudstone beds, bleached zones where the iron oxide has been removed, and faults and fractures. A summary of some of the key features observed is given in Table 4.2. Depths refer to depths recorded on the video and are depths from the top of the flange. These correspond well with those given in the other logs.

A distinctly wet mudstone bed was observed in the unsaturated zone at about 26 m. This mudstone bed was also evident from the core logging (Figure 4.6) and from the gamma-ray log (Figure 4.7). This appeared to give rise to a perched water table. Various faults, fractures and cavities were observed which corresponded well with those recorded in the caliper log (Figure 4.7). The greatest of these was a double cavity at approximately 103–105 m. As discussed above, the fluid conductivity and temperature logs in this region suggested that this was where there was a significant outflow of warm, low conductivity water derived from deeper in the borehole.

A vertical fracture was observed running down much of the borehole below 105 m. This is believed to be an artefact arising from the drilling. The borehole was also enlarged at the base where the hole had been 'cleaned'.

Table 4.2 Key features noted in the CCTV video

Depth (m bgl)	Feature
27.00	50-cm thick wet marl band
27.50	Fracture and small cavity
32.30	Vertical fracture
33.95	Minor fault
37.70	High angle fracture, large fracture
39.77	Water level
41.70	Cavity
42.90	Minor fault
43.90	Minor fault
47.15	Bedding parallel fracture, enlarged
49.40	Bedding parallel fracture, enlarged
53.70	Small cavity
55.40	Subvertical fracture
57.40	Subvertical fracture
87.15	Bedding parallel cavity
103.67–104.60	Large cavity associated with fracture
104.90–105.20	Cavity
113.60	Bedding parallel fracture
117.90	Open joint
118.90	Open joint
120.00	Vertical fracture
136.70	Vertical fracture
147.90	Large cavity
148.33	Bottom of hole; enlarged by drilling

5 Physical properties

5.1 SAMPLE SELECTION AND PREPARATION

During hydrogeological logging, the core was sampled at approximately 2.7 m intervals for material for both physical properties testing and for pore water extraction. Two samples were taken immediately adjacent to each other at each sampling interval. This was to enable potential correlations between physical properties parameters and porewater chemistry to be investigated. Sampling intervals were selected by the hydrogeological logger to be representative of the full range of lithologies encountered in the core.

At each sampling interval, wherever possible, both a horizontal and a vertical core plug were prepared from the material sampled for physical properties testing. The core plugs were cut as right-cylindrical plugs of about 24.5 mm diameter and about 27.5 mm length. All samples were then oven dried at 60 degrees C for a minimum of 24 hours prior to any physical properties tests.

5.2 TESTING PROGRAMME

A total of 103 plugs from 51 sampling intervals were cut and tested for gas permeability. Fifty one of these were horizontally oriented plugs and 52 were vertically oriented plugs. The 51 horizontally oriented core plugs were also tested for porosity, bulk density and grain density.

In addition to the core plugs, the whole core was tested using a probe permeameter. This was used to provide a more detailed permeability profile along the length of the whole core. 386 probe permeameter measurements were made over a drilled length of core of 139.4 m. Given the small amount of core loss during drilling, this approximates one probe permeameter measurement every 0.36 m, *i.e*. almost an order of magnitude better sampling resolution than the core plug sampling. The probe permeameter was also used on the 103 core plugs. This calibrated the probe permeameter measurements and enabled the probe measurements made on the whole core to be compared with the standard gas permeability measurements on the sample plugs.

5.3 METHODS

A standard liquid resaturation method was used to determine effective porosity, bulk and grain density (Bloomfield *et al.* 1995). Gas permeability was determined using nitrogen under steady state conditions and an equivalent liquid permeability calculated on the basis of a previous empirical correlation (Bloomfield and Williams 1995). Probe permeametry was performed using nitrogen as the permeant under steady state flow conditions and assuming radial flow geometry. Details of each of the methods is given below.

5.3.1 Porosity

Effective porosity, bulk density and grain density were measured using a liquid resaturation method based on the Archimedes principle. The methodology is described in detail in Bloomfield *et al.* (1995). A sample to be tested is weighed and then placed in a resaturation jar. The jar is evacuated then flooded with propanol. Propanol is used as it is relatively inert with respect to the core and reduces the potential for swelling clays to modify the porosity during testing. The sample is allowed to saturate for at least 24 hr. The saturated sample is then weighed, firstly immersed in the propanol and then, still saturated with propanol, in air. For each sample, a record is made of dry weight (w), propanol saturated weight in air (S_1) and saturated weight immersed in propanol (S_2). The density of the propanol (ρ_f) is also noted. From these

values, sample dry bulk density (ρ_b), grain density (ρ_g) and effective porosity (ϕ) can be calculated as follows:

$$\rho_b = (w\rho_f)/(S_1\text{-}S_2) \quad (1)$$

$$\rho_g = (w\rho_f)/(w\text{-}S_2) \quad (2)$$

$$\phi = (S_1\text{-w})/(S_1\text{-}S_2) \quad (3)$$

The effective errors on the porosity measurements were approximately ±0.5%.

5.3.2 Permeability

Gas permeability tests were performed on samples under steady-state conditions. A full description of the methodology and discussion of the correlation between gas and liquid permeability in sandstones can be found in Bloomfield and Williams (1995). Samples were constrained in a core holder and a pressure-regulated supply of nitrogen gas was applied to one end of the sample (the downstream end of the sample was held at atmospheric pressure). A soap-foam flow meter was used to measure the outflow of nitrogen from the downstream end of the sample. Gas permeability was calculated using the measured sample dimensions, differential pressure, and the steady-state gas flow rate as follows:

$$k_g = \mu\, Q\, L\, P_o/[A\,(P_i^2\text{-}P_o^2)] \quad (4)$$

where k_g is gas permeability, μ is gas viscosity, Q is the volumetric gas flow rate measured at atmospheric pressure, L and A are the sample length and area respectively, P_o is the downstream (atmospheric) pressure, and P_i (absolute pressure) is given by $P_i = P_o + P_g$, where P_g is the gauge pressure of the regulated nitrogen permeant. The effective errors associated with the gas permeability measurements are about ± 2.5% of measured sample permeability.

5.3.3 Probe permeametry

Probe or mini-permeameters have become increasingly popular in recent years for differentiating lithofacies and for quantifying the effects of small-scale heterogeneities on permeability. The probe samples a small volume of rock and works by forcing nitrogen gas through a small injection tip which is sealed against an otherwise unconfined sample. The gas flows radially through the tested region and out through the free surface. Probe permeability is calculated using a modified form of Darcy's law from the known injection pressure and flow rate and the geometry of the tip and the rock as follows:

$$k_a = \frac{2\mu Q_b P_b T_{act}}{aG_0(P_1^2 - P_2^2)T_{ref}} \quad (5)$$

where G_0 is a dimensionless geometrical shape factor, μ is viscosity, Q_b is volumetric flow rate, P_b is a reference pressure, T_{act} and T_{ref} are actual and reference temperatures, a is the internal radius of the probe tip and P_1 and P_2 are the upstream and downstream pressures, respectively.

A Temco Inc. MP-402 probe permeameter was used. Measurements were made on the circumference of the core at about 30 to 40 cm intervals along its length. Consequently, the measurements are analogous to horizontal permeability measurements on sample plugs. Probe permeametry measurements were only made on unfractured consolidated core of at least 4 cm in length. Between 5 and 10 measurements were made at each sampling point and an average value was calculated. Measurements were attempted at 386 sampling points. However, at 21 sampling points the permeability was below the effective resolution of the probe permeameter (about 1 mD) and no measurement was obtained.

On the plug samples, 10 probe permeameter measurements were made at each end of the plug and an average was calculated.

5.4 RESULTS

A full listing of the results is given in the Appendix 1. Table A1 shows the porosity, bulk density, and grain density measurements for the core samples, Table A2 lists the results of gas permeability tests on the sample plugs and Table A3 presents the results of the permeability measurements on the whole core using the probe permeameter. This last table includes both the measured values and the calibrated values based on the data in Table A2.

The physical properties measurements are summarized in Table 5.1 and Table 5.2 below. Table 5.1 summarizes the porosity and density data and Table 5.2 summarizes the gas permeability data. Figure 5.1 is a probability plot of the porosity data. Figure 5.2 is a cross-plot showing the correlation between porosity and horizontal permeability based on standard permeability measurements on the plugs. Figure 5.3 shows the correlation between plug permeability using the standard method and results on the same samples obtained using probe permeametry. On the basis of this cross plot a calibration has been established for the probe permeametry measurements on the whole core. Figure 5.4 presents a series of probability plots of the permeability data including the calibrated whole core data. Figure 5.5 shows depth trends in the porosity and density data and Figure 5.6 shows depth trends in the permeability data.

Table 5.1 Summary statistics for the porosity and density data.

Statistic	Porosity	Bulk Density	Grain Density
	(%)	(g/cm^3)	(g/cm^3)
n	51	51	51
Minimum	5.90	1.94	2.63
Maximum	26.60	2.51	2.67
Arithmetic mean	20.33	2.11	2.65
Std.Dev.	3.54	0.10	0.01
Skewness	-1.79	1.76	0.03

Table 5.2 Summary statistics for the gas permeability data.

Statistic	Plug gas permeability (mD)			Probe gas permeability (mD)			
				On Plugs			Corrected
	All samples	Horizontal samples	Vertical samples	All samples	Horizontal samples	Vertical samples	permeability on whole core
n	103	52	52	103	52	52	365
Minimum (mD)	0.1	0.8	0.1	1.4	1.4	13.5	20.6
Maximum (mD)	7916.8	7916.8	7585.8	5168.8	5168.8	4417.2	1786.2
Arithmetic mean (mD)	790.6	981.1	603.6	727.8	678.4	776.3	473.0
Geometric mean (mD)	187.9	314.1	113.5	313.0	286.4	341.5	334.1
Std Dev. (mD)	1310.7	1406.1	1193.9	912.1	867.9	959.4	352.7
Skewness	3.4	2.9	4.3	2.4	3.1	1.9	1.0

5.4.1 Porosity and density data

Table 5.1 shows that porosity, bulk density and grain density are in the ranges 5.9 % to 26.6 %, 1.94 to 2.51, and 2.63 to 2.67 respectively with a mean porosity of 20.3%. These values are consistent with those previously reported for the Triassic sandstones of the central and north-west England (Allen *et al.* 1997 reported porosity varying in the range 2% to 35% with a median value of 26%). The porosity data are approximately normally distributed (Figure 5.2), and show a relatively good correlation with the permeability data (Figure 5.3).

Figure 5.5 shows that porosity is generally more variable in the top 50 m but that there is no significant trend with depth. Grain density decreases slightly with depth.

5.4.2 Permeability data

Table 5.2 shows that plug permeability varies over almost five orders of magnitude, between 0.1 mD and 7916.8 mD with a geometric mean of 187.9 mD. These values are broadly consistent with permeabilities for the Permo-Triassic sandstones. Allen *et al.* (1997) reported permeability varying by just over six orders of magnitude from 0.01 to about 20,000 mD for the sandstones, with a median permeability of the order of 1000 mD. Table 5.2 shows that the vertical perm abilities are on average only slightly lower than the horizontal permeabilities (the geometric mean horizontal permeability is 314.1 mD while the corresponding vertical permeability is 113.5 mD) suggesting that the sandstones intercepted by the Abbey Arms Wood borehole are generally isotropic at the matrix scale. The normal probability plot for plug permeability data (Figure 5.4) also confirms this observation.

Table 5.2 shows that the probe permeability measurements on the plug samples generally overestimate permeability compared to the standard gas permeability tests. In addition, and contrary to normal expectations, the vertical probe permeability measurements on the plug samples are generally higher than the corresponding horizontal measurements. It is thought that it is due to a combination of factors including sample geometry and test configuration.

The diameter of the plugs is of the same order of size as, or a little smaller, than the theoretical diameter of the tested volume for the tip size of the probe permeameter used in the experiments. Consequently, gas flow lines in the sample plugs may be shorter than expected and may contribute to higher than expected apparent probe permeabilities. If sub-horizontal laminations or hydraulic heterogeneities at the scale of the plugs are present, this effect would be enhanced for vertically oriented plugs but suppressed for horizontally oriented plugs. Consequently, it is inferred that the probe permeametry measurements on the sample plugs are more reliable for horizontal samples than for vertically oriented samples.

Figure 5.4 shows correlations between plug permeability using the standard method and results on the same samples obtained using probe permeametry for both horizontally and vertically oriented samples. A linear regression of the $\log_{10}$ of the standard gas permeability data on the probe permeability data for the horizontally oriented plug samples has the form:

$$\log_{10} k_{standard} = 0.8304 \times \log_{10} k_{probe} + 0.4568 \qquad (6)$$

with an r^2 value of 0.5. This correlation has been used to calibrate the probe measurements (made in a horizontal direction) on the whole core, see Tables 5.2 and A2.

Figure 5.6 shows depth trends in horizontal and vertical permeability based on plug measurements, the k_h/k_v ratio based on plug measurements, and the calibrated probe permeametry measurements for the whole core.

Overall there does not appear to be a significant depth trend in matrix permeability or any significant variation in matrix anisotropy with depth. Between about 20 and 40 m bgl there appear to be three fining upwards sequences associated with an increase in permeability with depth. In addition, there appears to be a larger fining upward sequence between about 50 m bgl

and 65 m bgl with a coarsening upward sequence immediately below between 65 m bgl and 75 m bgl. Other fining upwards sequences may be present below 65 m bgl but these are poorly defined.

Above about 45 m bgl, the probe permeametry and plug permeability measurements indicate more small-scale variability in permeability than in the interval 45 to 110 m bgl. Below about 110 m bgl, there is again an increased small-scale variability in permeability. The 45 m bgl depth interval broadly corresponds with the inferred Helsby Sandstone Formation–Wilmslow Sandstone Formation boundary at about 49 m. Towards the base of the borehole, the sandstones become more friable and less cohesive. It was difficult to make permeability measurements and so it became more difficult to track small-scale changes in the sequence.

Figure 5.6 shows good agreement between trends in the calibrated probe permeametry data and the horizontal gas permeability measurements on the plugs. The probe permeametry does not characterize the occasional low permeability units where permeability is less than about 1 mD. It should be noted that where it was not possible to obtain a probe measurement because of the low permeability of the core this data has not been include in the figure.

5.5 DISCUSSION

The permeability profile shows some correlation with the gamma log (Figure 4.7). High gamma log values are associated with high clay contents and hence lower permeabilities. In the top 50 m of the borehole, changes in permeability with depth appear to be inversely related to changes in the gamma log, however, below about 50 m the gamma log and the permeametry profile became noisy and less easy to interpret.

Correlations between either porosity or permeability and either porewater or rock chemistry are generally weak. There weak are inverse correlations between Sr, Al, Fe, K, Mg, Na, and P in the rock and permeability. It is inferred that lower values of Sr are associated with calcite cement removal, and lower values of the other elements are associated with removal of feldspars and some clays – hence the inverse correlation with permeability. Both the Cl content and the Ca/Mg ratio of the porewaters show a small positive correlation with permeability and there is a small negative correlation between pH and permeability.

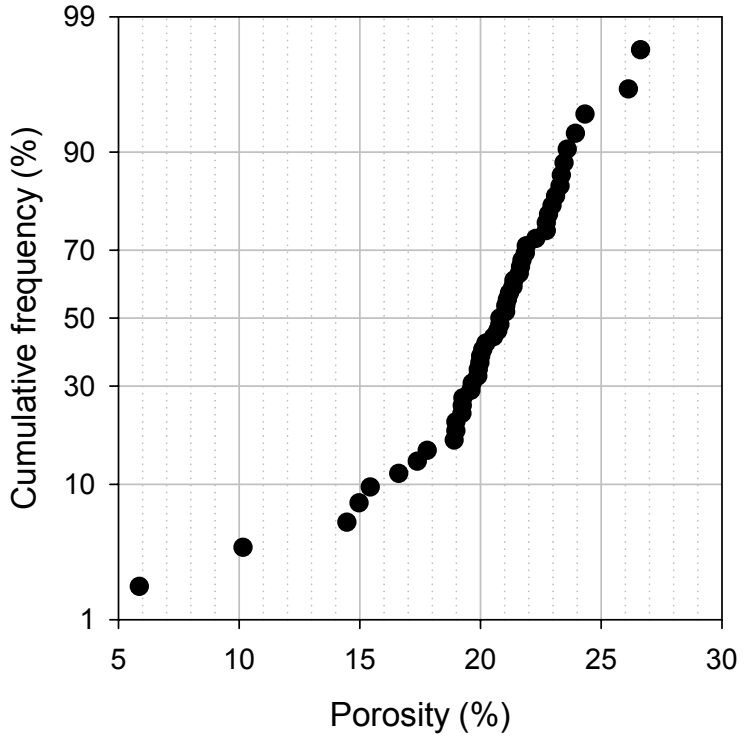

Figure 5.1 Probability plot of the porosity data.

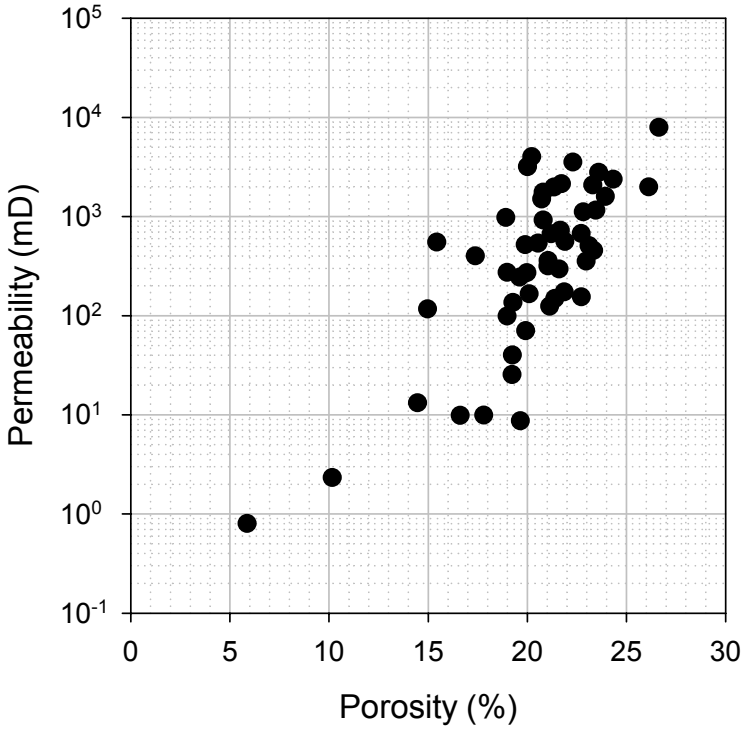

Figure 5.2 Correlation between porosity and permeability.

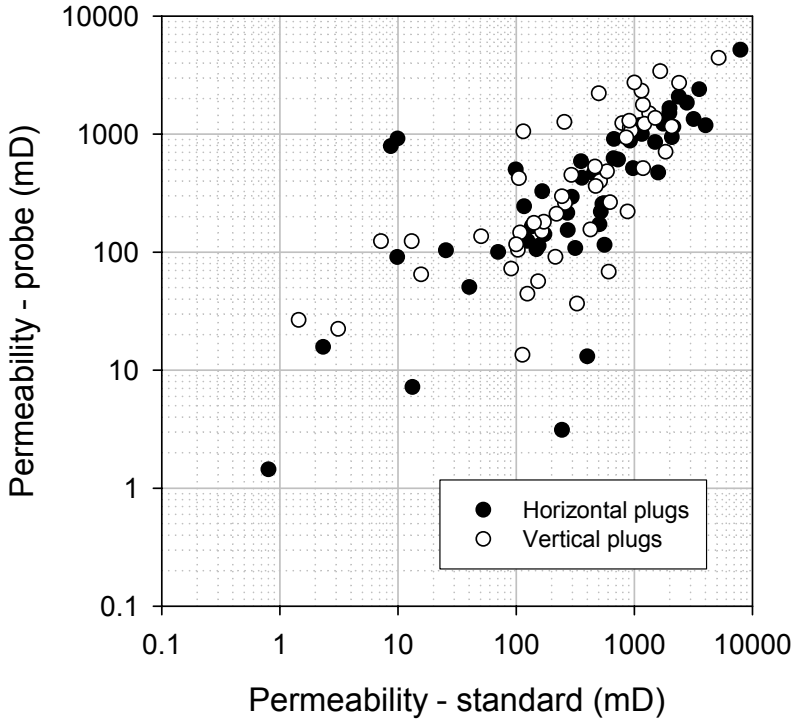

Figure 5.3 **Correlation between plug permeability using the standard method and results on the same samples obtained using probe permeametry.**

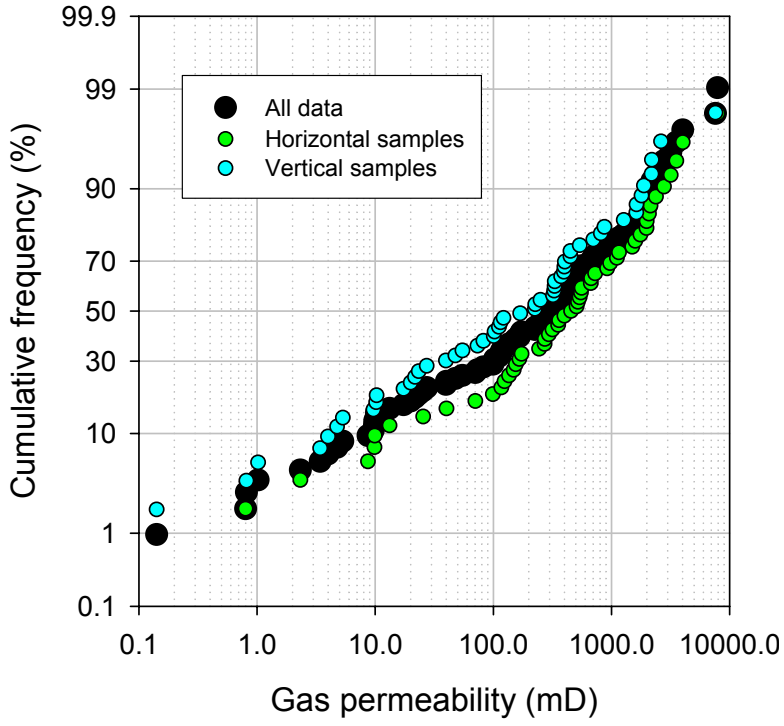

Figure 5.4 **Probability plots of the plug permeability data.**

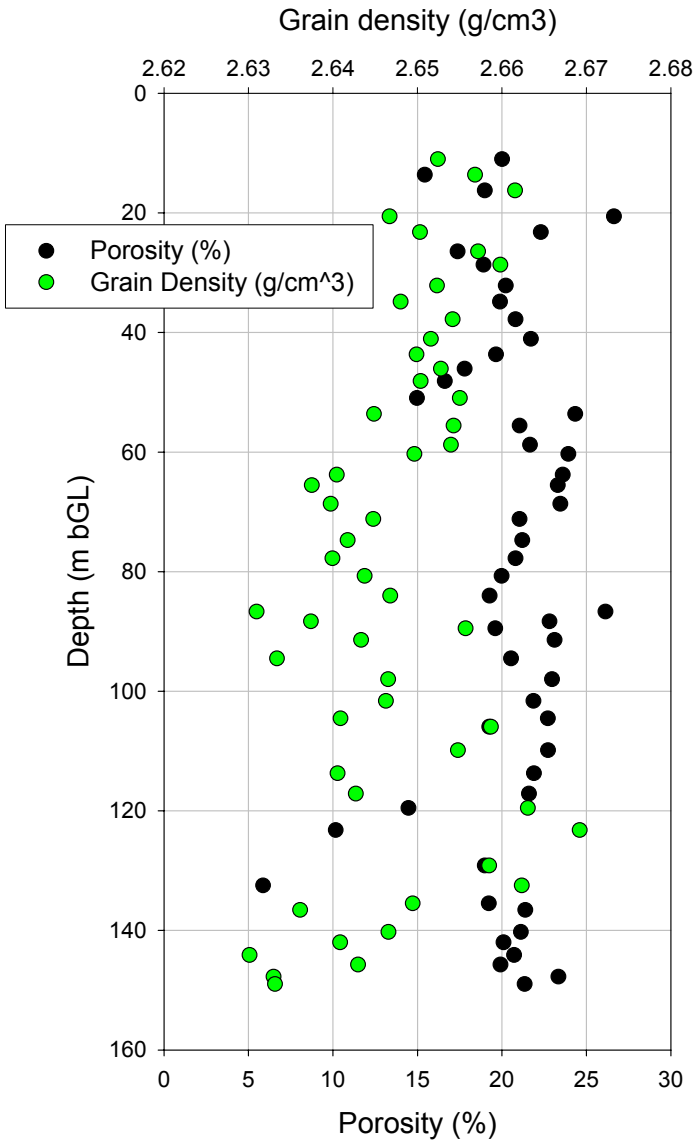

Figure 5.5 Depth profiles in the porosity and density data.

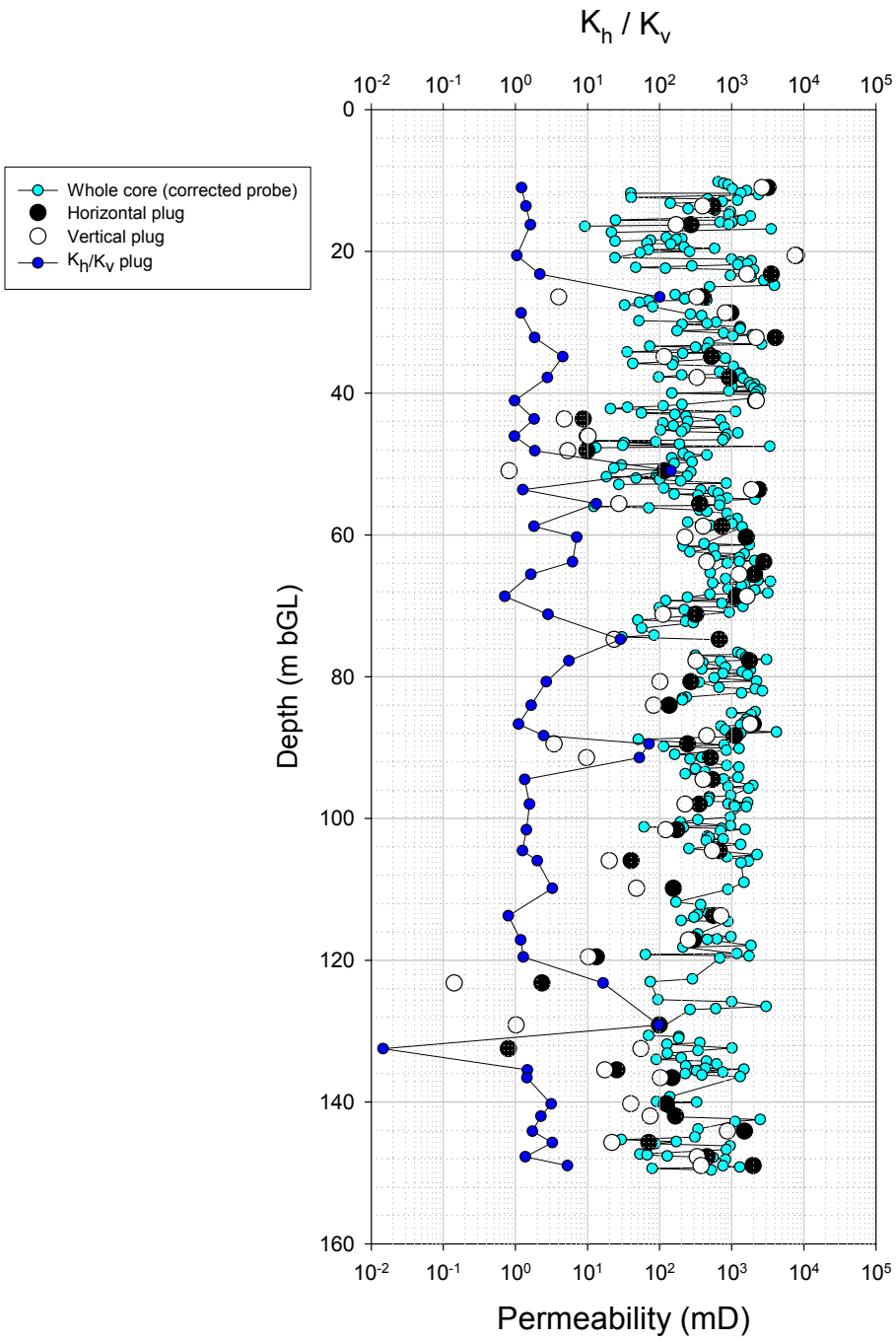

Figure 5.6 Depth profiles in the permeability data.

6 Water quality

6.1 REGIONAL SCALE

6.1.1 General features

It is not intended to review the groundwater quality in the North-West region in any detail but it is useful to take a brief look at the data to put the present results in context. A more detailed analysis of the data from the Wirral Peninsula-Cheshire Basin area is currently being undertaken as part of the BGS-EA 'Baseline' project (Griffiths *et al.*, 2002).

At the time of reporting, the EA North-West region groundwater quality database contained data for some 2137 samples from 672 individual groundwater sources. Not all parameters were recorded for each sample. The major water quality parameters were mapped to provide an insight into the variation within the region (Figure 6.1 and Figure 6.2). The data were not processed in any way, e.g. to average data for a particular source. Therefore, because of the high density of data, the maps tend to be dominated by the higher concentration classes since the data were plotted from the lowest concentration class upwards. Nevertheless, the maps show the major features, in particular the low concentrations of many of the sources from the Lake District reflecting the low weathering rates there. The absence of sources to the east of Delamere reflects the lack of a suitable aquifer in this area.

The aquifers are dominated by the Triassic sandstones and the groundwaters tend to be typically Ca-Mg-HCO_3-type waters with relatively high Mg/Ca ratios indicative of dolomitic sources. Calcite, gypsum and anhydrite cements also contribute to the water quality. Chloride concentrations are typically less than 40 mg L^{-1} but not infrequently exceed that expected from atmospheric inputs reflecting saline intrusion near the coast (in places, induced by excessive pumping) and mixing with deeper Na-Cl brines further inland.

Low nitrate sources (<2 mg L^{-1} NO_3-N) are common throughout much of the area. Nevertheless, nitrate concentrations are strongly influenced by fertiliser leaching and are particularly high in the fertile Vale of Eden to the north and the Cheshire plains to the south, often exceeding the MAC of 11.3 mg L^{-1} NO_3-N.

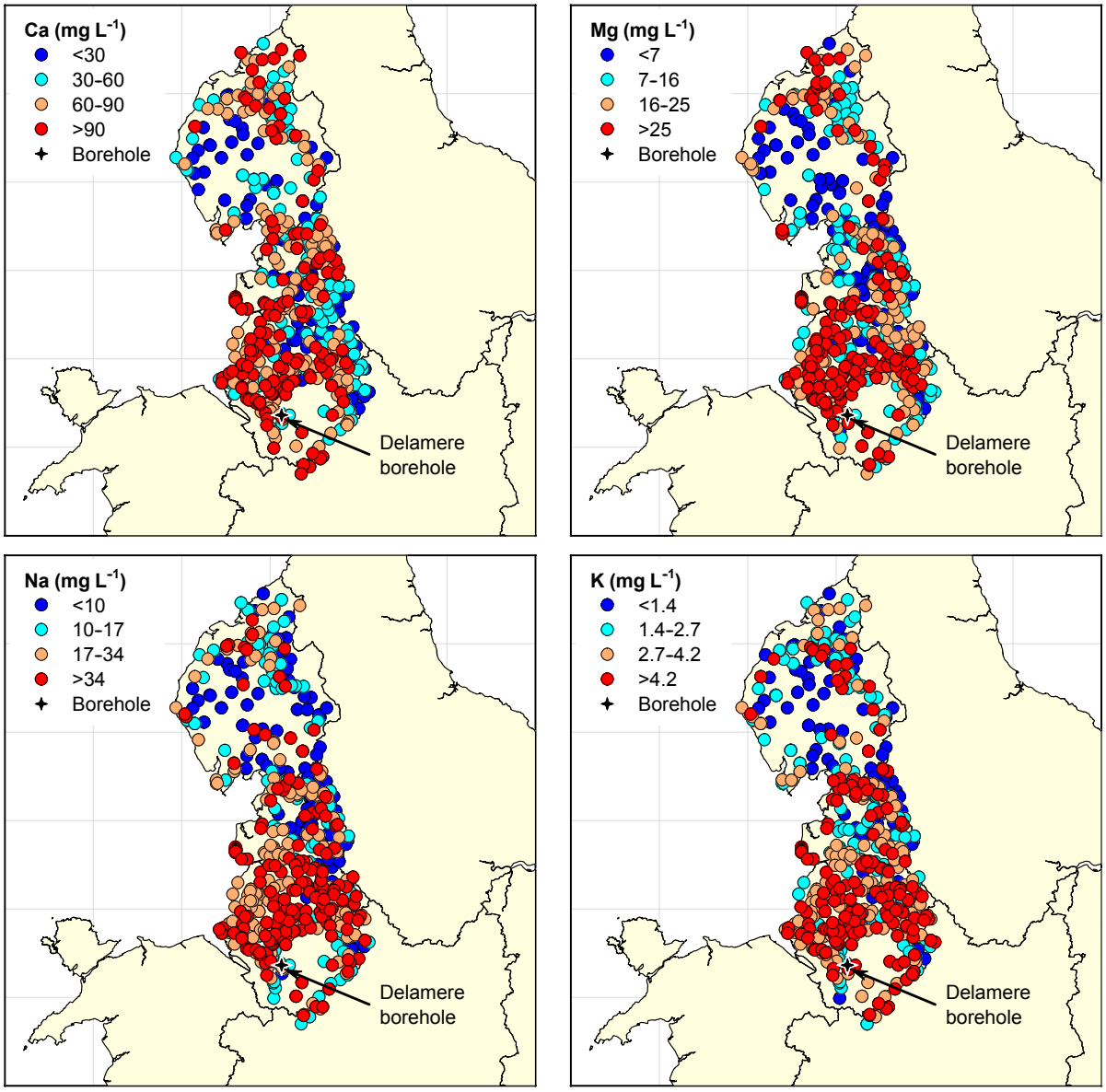

Figure 6.1 Regional water quality in the EA North-West region for calcium, magnesium, sodium and potassium (EA monitoring data).

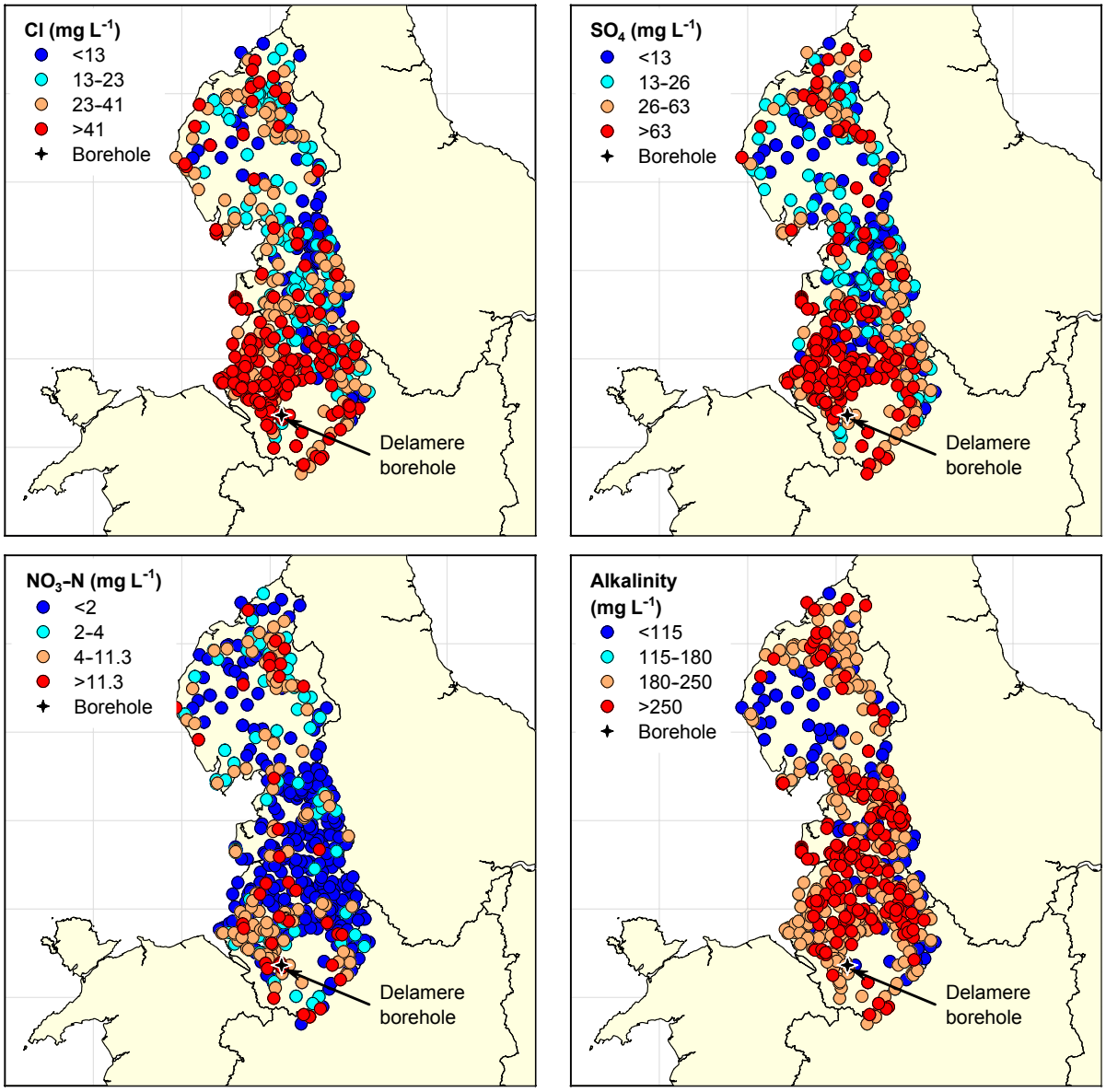

Figure 6.2 Regional water quality in the EA North-West region for chloride, sulphate, nitrate and alkalinity (EA monitoring data).

6.1.2 Arsenic

The map of arsenic (Figure 6.3) for the region indicates that nearly 60% of groundwater samples fell below the reporting limit for As (normally 1 µg L^{-1} but sometimes 5 µg L^{-1}). 11.5% of samples exceeded 10 µg L^{-1}, the recently revised UK drinking-water limit. 1.6% of samples exceeded 50 µg L^{-1} but these were mostly from farm and industrial sources. The highest concentrations observed in public supply sources (raw water) averaged 81 µg L^{-1}, 54 µg L^{-1} and 44 µg L^{-1} at individual boreholes, all from the Delamere area. Several other sources in the Delamere area exceeded 10 µg L^{-1}. About 79 distinct sources had exceeded 10 µg L^{-1} As at some time. The highest recorded As concentration was 261 µg L^{-1} from near Irlam between Manchester and Warrington.

Several other high-As groundwater sources can be seen from the map including the Beckermet mine shaft in the Lake District, a small cluster west of Manchester and a cluster near Ormskirk.

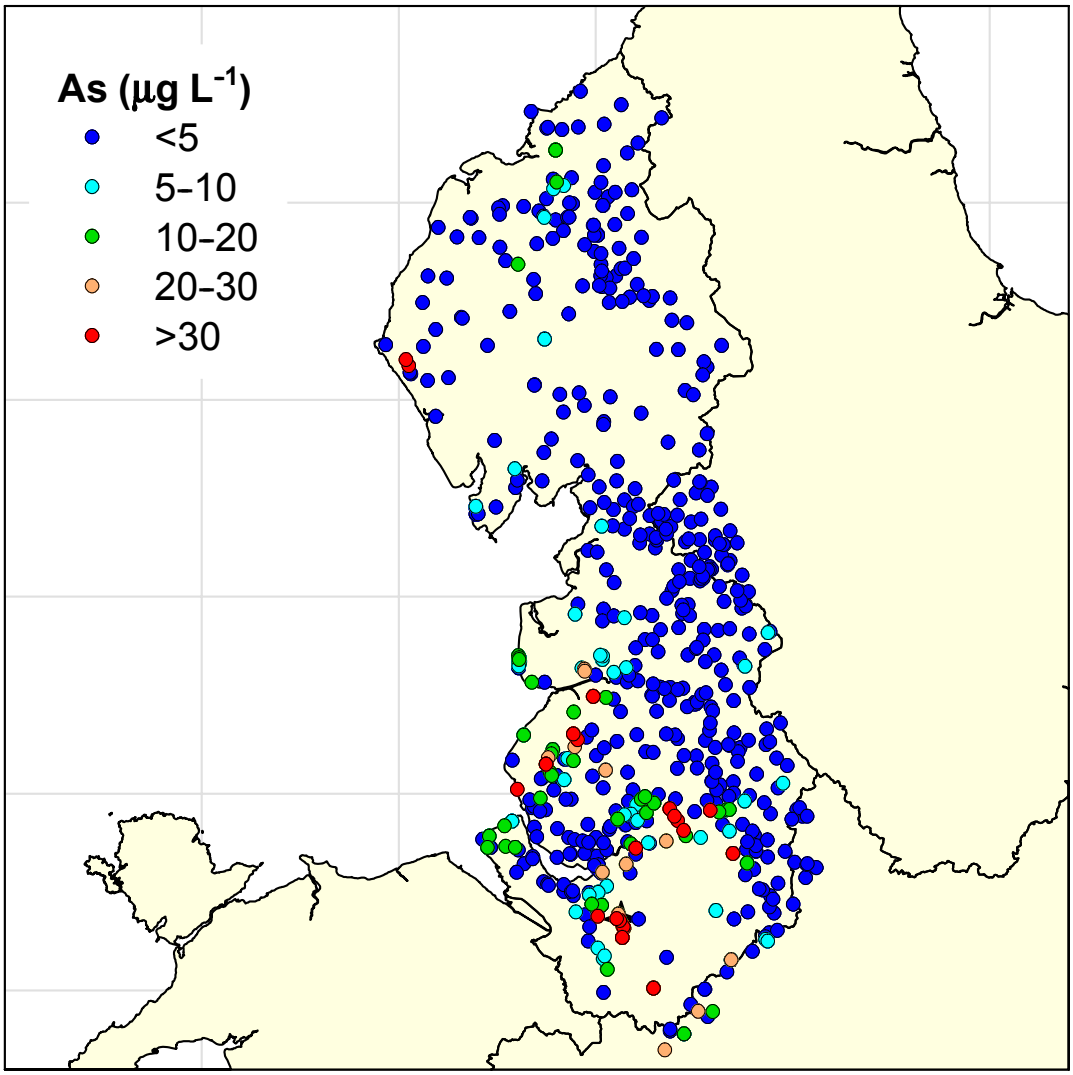

Figure 6.3 Distribution of arsenic in groundwater in the EA North-West region (EA data).

6.2 BOREHOLES IN THE DELAMERE REGION

The locations of public supply boreholes within a few km of the project borehole are shown in Figure 6.4. Delamere pumping station is about 0.4 km south-west of the project borehole and Organsdale PS is about 1 km due east. The East Delamere Fault lies about 0.5 km east of the project borehole and follows a north-south direction. The Overton and Primrose Hill Faults are also within 2 km of the site. The geological map shows that boreholes are situated on the Helsby Sandstone Formation although as the drilling showed, this is overlain by up to 6 m of unconsolidated sand and gravel. Unlike the data in Table 6.1, arsenic concentrations indicated in Figure 6.4 are average concentrations derived solely from EA data and sampled between August 1986 and December 2000. In order to comply with the new arsenic standard of 10 µg L^{-1}, United Utilities has invested significantly in water treatment plants for arsenic removal in the Delamere area.

Table 6.1 Water chemistry from public water supply boreholes in the Delamere area*

Source and number	Cotebrook 40″	Cotebrook 15″	Delamere BH 3	Delamere BH 4	Eaton BH 2	Eddisbury SJ56/2	Organsdale SJ56/49	Sandyford
Lab id	S00-00972	S00-00971	S00-00969	S00-00968	S00-00973	88006805	88006811	S00-00970
Field no.	CH 10	CH 9	CH 7	CH 6	CH 11	88006805	88006811	CH 8
Depth of bh (m)	244	126	91	243	243	229	123	57
Lab used	BGS	BGS	BGS	BGS	BGS	EA	EA	BGS
Easting	357150	357000	356150	356020	356690	355775	355310	356740
Northing	365760	366110	367780	367720	363410	369425	368230	366720
Date sampled	24-Oct-00	24-Oct-00	24-Oct-00	24-Oct-00	24-Oct-00	12-Jan-00	12-Jan-00	24-Oct-00
Time sampled	14:00	13:40	12:30	11:45	14:30	9:40	9:30	13:15
Temperature	10.9	10.6	10.1	10.1	12.1	9.4	10.1	10.8
pH	7.51	7.53	7.58	7.58	7.8	7.81	7.63	7.35
Eh (mV)	521	428	362	443	521			417
DO	6	8.6	10.9	7.7	1.7	8.2	8.8	7.9
SEC (µS cm^{-1})	582	546	554	484	331	515	584	736
Ca	75.7	74.3	82.5	72.4	37.2	54.5	89.2	94.3
Mg	18.9	19.8	6.16	5.43	16.6	23.6	8.47	14.7
Na	20.7	14.6	19.2	14.1	8.4	12.3	15.9	28.5
K	3.9	2.2	2	1.6	2.5	2.45	1.99	4.4
Cl	35.2	30	37.4	29.4	1.1	26.8	41.4	47.2
SO_4	41.6	34.9	30.8	21.7	24.7	30.3	25.2	37.2
Alk (as HCO_3)	201	227	157	158	153			218
NO_3 as N	8.36	7.13	14.5	10.2	0.47	15.1	17.5	17.7
Si	5.59	5.45	5	5.09	7.15	9.51	9.9	5.27
NO_2 as N	<0.001	<0.001	0.024	0.012	<0.001	<0.004	<0.004	0.008
NH_4 as N	0.005	0.008	<0.003	<0.004	0.004	<0.5	<0.5	<0.003
P	0.04	0.05	0.13	0.10	<0.02	<0.5	<0.5	0.10
TOC	1.4	2.3	3.5	1.7	1.1			2.9
DOC	2.9	4.3	1.9	1.7	2.5			4.9
F (µg L^{-1})	110	90	90	100	140	61	55	130
Br (µg L^{-1})	80	80	110	70	40	<50	83	100
I (µg L^{-1})	4	4	4	3	3			6
Al (µg L^{-1})	6	1	27	2	2		<10	4
As (µg L^{-1})	**26**	**23**	**15**	**30**	**53**	**13.5**	**28.3**	**19**
Ba (µg L^{-1})	122	135	499	624	125			299
Cu (µg L^{-1})	7.6	6.3	7.4	10.1	2.7	111	14.8	14.5
Fe (µg L^{-1})	<5	<5	7	<5	<5	<30	<30	<5
Li (µg L^{-1})	8	5	5	5	12			5
Mn (µg L^{-1})	<2	<2	<2	<2	<2	<10	<10	<2
Mo (µg L^{-1})	0.5	0.2	< .1	0.1	3			<0.1
Rb (µg L^{-1})	3.2	2.3	2.0	1.8	2.1			3.6
Sb (µg L^{-1})	0.2	0.15	0.13	0.17	0.1			0.1
Sc (µg L^{-1})	1.66	1.65	1.39	1.5	2.16			1.71
Se (µg L^{-1})	0.7	< .5	<0 .5	<0.5	<0.5			<5
U (µg L^{-1})	2.5	1.5	0.2	0.9	7.5			0.5
V (µg L^{-1})	< 1	< 1	< 1	< 1	< 1			<1
Zn (µg L^{-1})	11	15	11	8	8	150	12	10
Zr (µg L^{-1})	< 0.5	< 0.5	< 0.5	< 0.5	< 0.5			<5

* All data are in units of mg L^{-1} unless otherwise indicated. Data are either from the current BGS/EA 'Baseline' project or from EA archives.

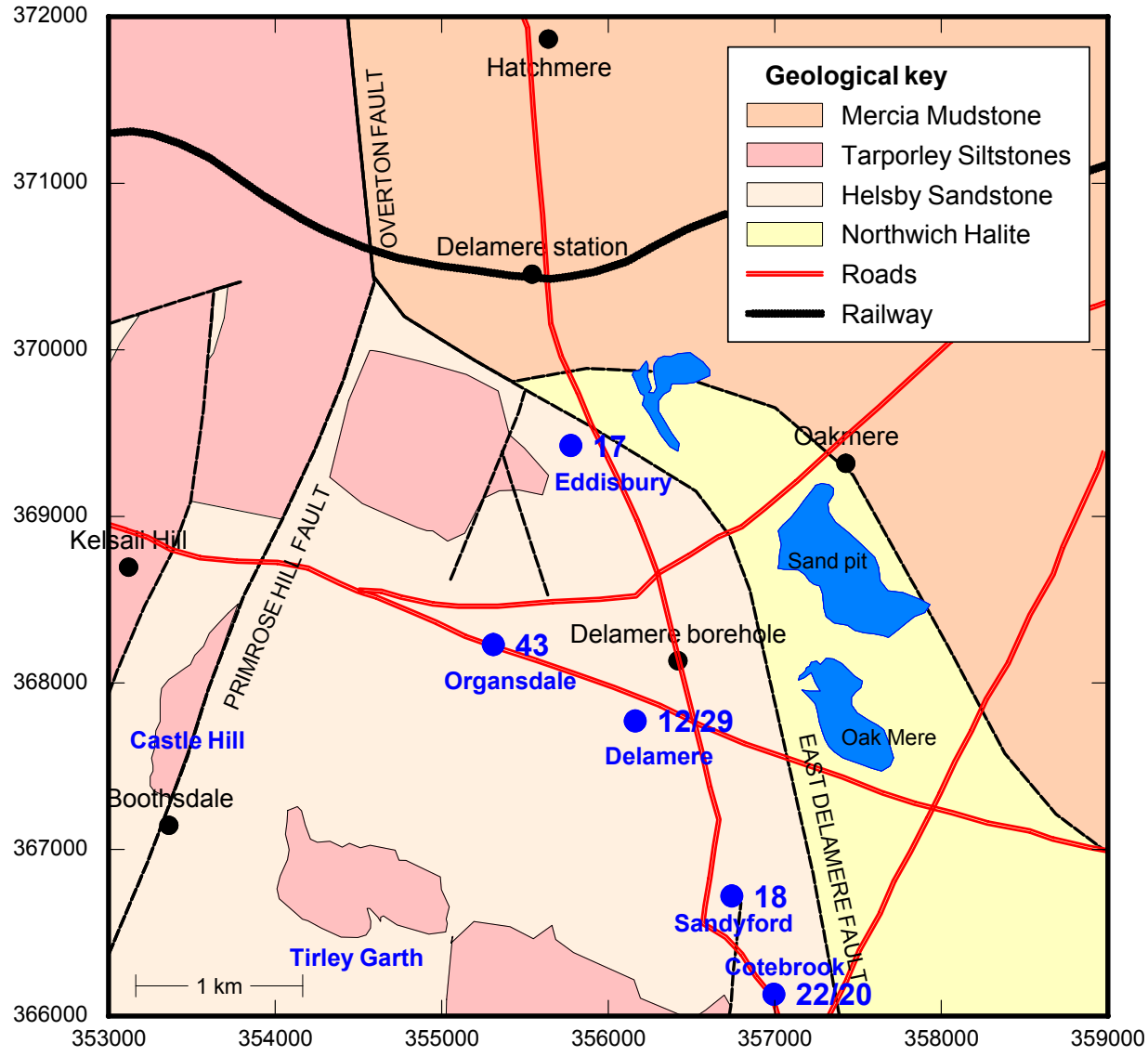

Figure 6.4 **Location of public supply boreholes in the Delamere area with the average arsenic concentrations shown in blue (in µg L^{-1}) (from EA data). Where two numbers are shown for a site, these are for two different boreholes. Eaton is about 6 km to the south of Delamere.**

A summary of the water quality in some of the Delamere water supply boreholes is given in Table 6.1. These data are from the ongoing 'Baseline' re-survey of the area (BGS data) and from EA archives (Griffiths *et al.*, 2002). The data show that the waters are mostly near-neutral and oxidising, despite their considerable depth, with high concentrations of DO, high Eh and sulphate, and low concentrations of ammonium, iron and manganese. Nitrate concentrations are mostly high (7–18 mg L^{-1} NO_3-N). The exception to this is the Eaton 2 borehole, which has a very low concentration of nitrate (0.47 mg L^{-1}) and Cl (1.1 mg L^{-1}) but is the source with the greatest As concentration. It is the only borehole which partially penetrates the Tarporley Siltstone (Table 3.2) and is the 'freshest' in terms of salt content although it does have a lower DO than the other waters. It is probably 'old' water and has a slightly higher temperature.

There is a relatively large variation in Mg concentration, greater than for Ca, probably reflecting the varying abundance of dolomite/calcite cements in the sandstones. Uranium concentrations are high, in two cases exceeding the provisional WHO guideline value for drinking water. No other trace elements are present in 'unusual' concentrations.

Arsenic concentrations exceed 10 µg L^{-1} in the raw water from all of the boreholes. There is not a clear relationship between As concentration and depth (Table 6.2, Figure 6.5) but the relationship with temperature is perhaps clearer. The 'depth of borehole' is not necessarily a good guide to the depth of the major inflows. Temperature is probably a better guide to this given the steady rise of temperature with depth (Figure 4.7). It appears from these data that, if anything, the As concentration increases with depth although the Eaton data are having an undue influence on the perceived relationship. Curiously the temperature of the two Delamere borehole sources is the same, suggesting a common, shallow source. By contrast, the As and other data point to different sources (the shallower source has a somewhat greater SEC which is consistent with the geophysical logging, Figure 4.7). No speciation of the As is available for these data.

Table 6.2 Average arsenic concentrations in public supply sources in the Delamere area and the depth of the boreholes

Source	Depth (m)	Temp (ºC)	Avg As (µg L^{-1})
Delamere 3	91	10.1	12
Delamere 4	243	10.1	29
Eaton 1	244		29
Eaton 2	243	12.1	51
Eddisbury	229	9.4	17
Cotebrook 15"	126	10.6	22
Cotebrook 40"	244	10.9	20
Organsdale	123	10.1	43
Sandyford 1	59.6	10.8	18

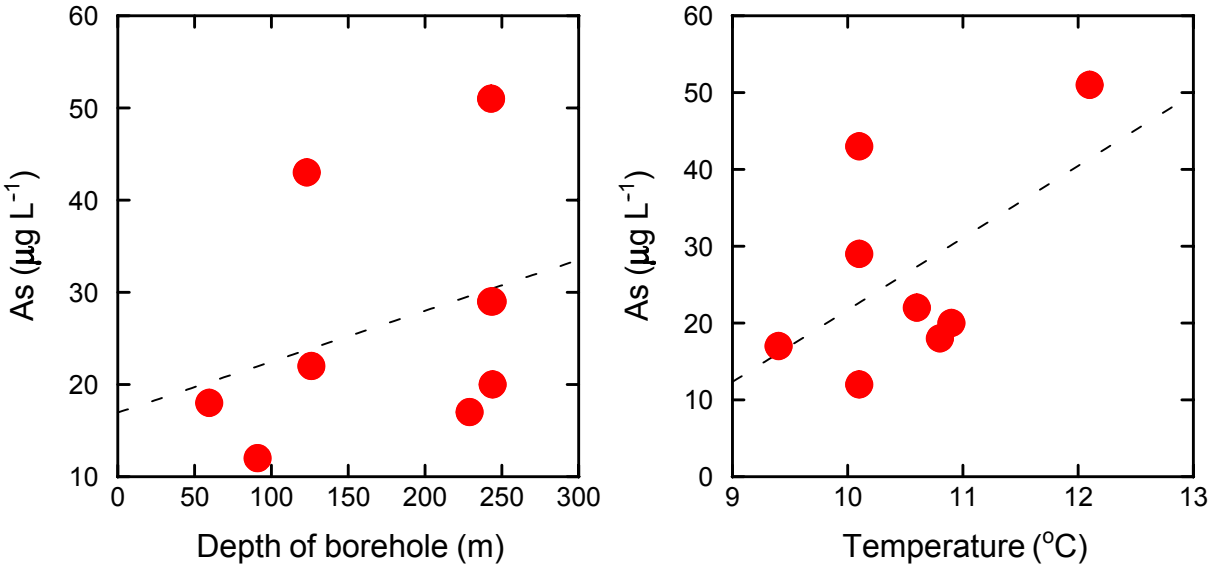

Figure 6.5 Variation in the average arsenic concentration of various public supply boreholes in the Delamere area as a function of borehole depth and pumped water temperature. Best-fitting linear trends are shown.

6.3 THE PROJECT BOREHOLE

6.3.1 Moisture content profile from the retrieved core material

As part of the porewater extraction procedure, the moisture content of each sample horizon was measured by drying overnight in an oven at 110 ºC. The moisture content is expressed as g H_2O per kg dry soil.

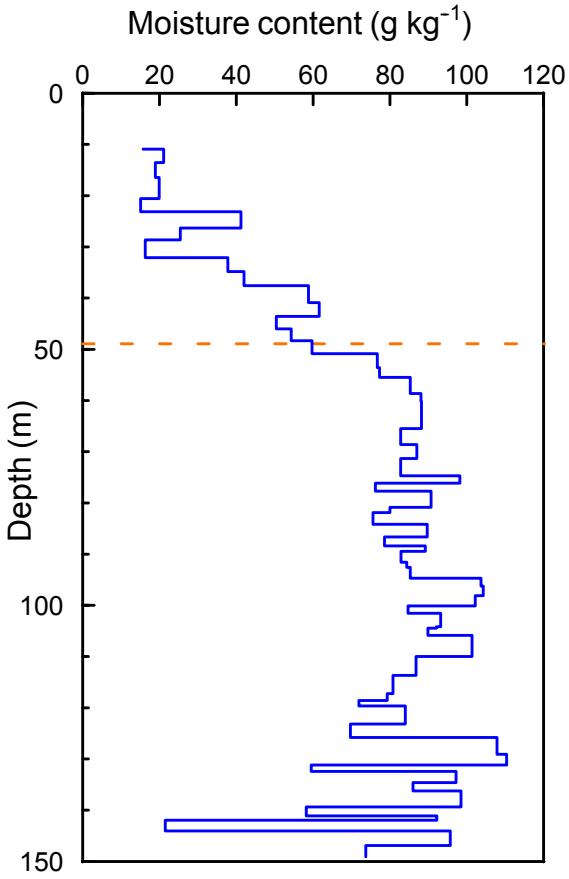

Figure 6.6 Moisture content profile of the project borehole measured gravimetrically.

The moisture content profile (Figure 6.6) shows a steady increase from 20 g kg^{-1} at 10 m to about 60 g kg^{-1} at the water table. There is an intermediate peak at 26 m which corresponds to the perched water table at the top of the 26 m marl band.

In the saturated zone, the moisture content fluctuates around an average of about 80 g kg^{-1}. Given an average crystal density equivalent to that of quartz (2650 kg m^{-3}), this corresponds to a moisture-filled porosity of 21%. This is in good agreement with independent measurements (Figure 5.5).

6.3.2 Depth samples

Once the borehole had been completed and cleaned, four samples were taken at different depths using a depth sampler. This sampling was carried out on 2–3 April 2002, just before the geophysical logging was undertaken. The depths chosen were at 65 m, 96 m, 110 m and 140 m based on observed zones of inflow. The sampled horizons selected were fairly uniformly spaced

within the saturated zone. The results of the field measurements and chemical analyses are given in Table 6.3. On-site temperature and dissolved oxygen were not measured.

The data show a decline in SEC with depth, at least down to 110 m, which is similar trend to that shown by the conductivity log (Figure 4.6). Eh, Ca, Mg, Cl, NO_3-N, SO_4, alkalinity, As(III), As(V) and Zn also decrease with depth. Only Mg increases with depth, possibly reflecting dolomite dissolution, and Si shows no change.

The 110 m and 140 m samples are very similar in terms of major-element chemistry and are consistent with an upward movement of water to the large fracture at 103 m. The 96 m sample is substantially different in several respects and supports a discontinuity in flow around 100 m.

Table 6.3 Chemical analysis of depth samples taken from the project borehole at the time of logging.

Parameter	Units	65 m	96 m	110 m	140 m
Sample id		S02-00777	S02-00778	S02-00779	S02-00780
pH		7.82	7.87	7.95	7.98
Eh	mV	388	403	174	159
SEC	µS cm^{-1}	425	357	270	280
Mg	mg L^{-1}	6.7	7.3	8.5	8.9
Ca	mg L^{-1}	63.6	52.3	34.5	34.0
Na	mg L^{-1}	14.7	11.9	9.0	9.0
K	mg L^{-1}	1.77	1.70	1.61	1.62
Cl	mg L^{-1}	38.3	29.1	16.5	16.1
NO_3-N	mg L^{-1}	7.0	5.8	3.8	3.7
SO_4	mg L^{-1}	15.7	11.8	7.8	7.7
Alkalinity	mg L^{-1}	141	135	119	111
Si	mg L^{-1}	5.3	5.3	5.4	5.4
AsT	µg L^{-1}	10.6	17.7	35.8	35.6
As(III)	µg L^{-1}	6.7	11.4	22.8	24.3
As(V)*	µg L^{-1}	3.9	6.3	13.0	11.2
Ba	µg L^{-1}	522	492	427	439
Cu	µg L^{-1}	1.2	1.8	0.4	1.3
Fe	µg L^{-1}	0.2	1.2	0.3	1.0
Li	µg L^{-1}	4.3	3.8	3.4	3.3
Mn	µg L^{-1}	1.4	0.4	<0.2	<0.2
Mo	µg L^{-1}	2.8	3.5	2.9	2.9
NO_2-N	µg L^{-1}	<3	<3	<3	<3
P	µg L^{-1}	82	78	66	59
Sr	µg L^{-1}	63	59	46	46
Zn	µg L^{-1}	67	135	27	14

* By difference: As_T–As(III)

The concentrations of As_T observed are at the levels expected for the area (Table 6.2), lying between the concentrations found at the Delamere and Organsdale pumping stations. The speciation suggests that the majority of the As, about 2/3, is present as As(III). This is the reduced form of As which is normally only found in quite strongly reducing groundwaters. Therefore this finding is somewhat surprising given the redox and chemical measurements found regionally and in these depth samples. These point to essentially oxidising groundwaters, although a decline in Eh with depth was noted in the depth samples. While the BGS method for As speciation has proven reliable in the past, the method is not certified and we therefore suggest that the speciation results are treated with caution at this stage.

6.3.3 Porewater quality

The porewater extracted from the fresh core by centrifugation was analysed using standard BGS methods, notably ICP-AES and HG-AFS for As. The full results are given in Table 6.4. The pH data, while measured soon after pore water extraction, have been omitted because it is not possible to guarantee that there was no degassing of CO_2 during extraction. The measured pH's were mostly in the range pH 7.8–8.2 which is within the range found during borehole logging (Table 6.3).

ARSENIC

The variation of As_T, As(III), SO_4, Ca, Mg and NO_3 concentrations in the porewater extracted by centrifugation from the core material obtained from the project borehole is shown in Figure 6.2. As(III) was not measured in all of the samples.

Selected porewater chemistry profiles are shown in Figure 6.7. The As profile shows a rising background with three significant 'spikes', the greatest being 125 μg L^{-1} at 89.4 m. The other spikes were at 96.2 m (89 μg L^{-1}) and 118.5 m (47 μg L^{-1}). Most of the As was present as As(III) in those samples having the background concentration of As but was predominantly As(V) in the two spikes for which speciation was carried out. The measured Fe concentration in samples from these depths were less than 5 μg L^{-1} but these samples were based on different aliquots from those in which the As were measured.

We were suspicious of these spikes because they are quite discrete (only spanning a single contiguous sample) and are very different from the underlying trend. Therefore these samples were reanalysed (Table 6.5). One sample had already been repeated as a check on the stability of As in solution but was also reanalysed along with the other two. All QCs and proficiency samples analysed with these samples were within limits, indicating that the analyses were correct. As can be seen, all three samples have increased with time, two noticeably so. This should not occur and suggests some kind of problem with these samples. The most obvious explanation is that a small amount of As-rich colloid past through the filter (or otherwise contaminated the sample) and has subsequently slowly dissolved in the acidic solution in which the As samples were preserved (2% HCl). An Fe-rich colloid is the most likely suspect given the affinity of As for iron oxides and the abundance of iron oxides in the sandstones. It is therefore likely that the spikes are anomalous and that the true As depth profile is a steadily increasing concentration with depth from about 8 μg L^{-1} at the water table to about 25–30 μg L^{-1} at 150 m. These results are consistent with those from the depth samples apart from the 110 m depth sample which appears higher than the pore water (Figure 6.6).

OTHER WATER QUALITY PARAMETERS

Sulphate – this shows some erratic behaviour in the unsaturated Helsby Sandstone with some spikes exceeding 20 mg L^{-1} but in the Wilmslow Sandstone (and with saturation) there is a steady decline to about 90 m and then a constant concentration of about 10 mg L^{-1}. The erratic behaviour in the unsaturated zone could be due to small and highly localised amounts of barite ($BaSO_4$) mineralization. There was a very strong correlation between SO_4 and Ba in the sediments (see Figure 7.2). The depth samples agree. Sulphate is not correlated with NO_3.

Calcium and magnesium – calcium shows a steady decline in the Helsby Sandstone, a small increase between 50–70 m in the Wilmslow Sandstone and then a steady decline between 70–100 m, after which it is constant at about 40 mg L^{-1}. Magnesium, on the other hand, shows a low concentration in the Helsby Sandstone and steadily increases with depth in the Wilmslow Sandstone. There is a particularly sharp rise from 4 to 7 mg L^{-1} at 88.4 m possibly related to the cavity observed at 87.15 m depth (Table 4.2).

Table 6.4 Porewater chemistry from the project borehole (all concentrations in units of mg L^{-1}).

Sample	Top	Bottom	M C	Alk	As_T	As(III)	B	Ba	Be	Ca	Cd	Cl	Cr	Cu	Fe	K	Mg	Mn	Na	NO_2-N	P	Si	SO_4	Sr	TON	Zn
S02-00606	10.74	10.92	15.7	89.6	23.1		1	1.87	<0.002	94.7	<0.001	149	0.004	0.097	0.099	5.5	5.46	0.058	52.4	0.14	<0.1	7.83	16.2	0.126	11	0.229
S02-00607	13.30	13.55	21.1	73.2	<3.00		1	2.38	<0.002	92.2	0.002	155	<0.002	0.066	<0.005	6.3	4.2	0.043	45.1	0.055	<0.1	7.74	14	0.136	16	0.321
S02-00608	16.30	16.45	18.9	429	<3.00		1.8	2.51	<0.002	92.2	0.003	128	<0.002	0.049	<0.005	4.3	4.51	0.006	58.7	0.079	0.1	7.85	24.1	0.113	17	0.309
S02-00609	20.40	20.55	19.9	109	<4.00		1.7	2.14	<0.002	70.4	<0.001	103	<0.002	0.034	<0.005	2.8	3.34	0.002	43.9	0.05	<0.1	5.79	15.1	0.084	6	0.074
S02-00610	23.07	23.17	15.1	96	<10.0		2.5	2.07	<0.002	71.5	<0.001	117	<0.002	0.048	<0.005	2.3	3.13	0.002	58.3	0.08	<0.1	4.76	15.5	0.084	7	0.071
S02-00611	26.26	26.36	41.2	114	3.0		0.3	1.95	<0.002	77.0	0.004	65.6	<0.002	0.025	<0.005	2.4	2.91	0.017	23.7	0.083	0.1	5.49	16.6	0.0906	12.8	0.527
S02-00612	28.50	28.62	25.4	106	4.4		0.6	1.22	<0.002	64.9	<0.001	97.1	<0.002	0.016	<0.005	4.6	4.19	0.011	33.2	0.026	0.3	7.71	16.7	0.099	1	0.138
S02-00613	32.03	32.13	16.3	108	<12.0		0.3	0.707	<0.002	61.1	<0.001	62	<0.002	0.065	0.017	2.4	4.15	0.008	28.4	<0.03	0.3	5.54	30.7	0.0845	<7	0.083
S02-00614	34.70	34.80	37.8	116	5.0		0.5	0.917	<0.002	48.9	<0.001	54.9	0.003	0.028	<0.005	1.8	3.39	0.005	24.6	0.037	<0.1	6.11	11.6	0.0614	0.9	0.109
S02-00615	37.49	37.61	42.0	111	5.8		0.3	0.894	<0.002	48.1	<0.001	50.9	<0.002	0.023	<0.005	2	3.33	0.004	21.4	0.029	<0.1	6.15	11.3	0.0578	0.9	0.095
S02-00616	40.80	40.90	58.8	116	5.4		0.1	0.463	<0.002	47.5	<0.001	44.9	<0.002	0.01	<0.005	1.8	3.52	0.002	18.2	0.02	<0.1	4.92	8.9	0.0495	0.6	0.06
S02-00617	43.50	43.60	61.6	118	5.1		0.1	0.729	<0.002	62.6	<0.001	49	<0.002	0.013	<0.005	2.2	7.17	0.005	22.1	0.007	<0.1	5.18	48.6	0.0884	5.2	0.082
S02-00618	45.92	46.02	50.4	121	6.1		0.2	0.86	<0.002	56.0	<0.001	46.8	<0.002	0.013	<0.005	2.4	6.44	0.003	21.9	0.021	<0.1	5.98	18.3	0.082	5.8	0.062
S02-00619	48.18	48.30	54.3	103	9.5		0.4	0.882	<0.002	53.5	<0.001	55.3	<0.002	0.019	<0.005	2.9	2.73	0.003	22.8	0.016	<0.1	6.25	13.8	0.0593	3.2	0.102
S02-00620	50.77	50.87	59.7	115	7.5		0.2	0.885	<0.002	60.2	<0.001	51.8	<0.002	0.016	<0.005	2.3	3.17	0.002	19.6	0.018	<0.1	5.61	16.9	0.0644	7.5	0.093
S02-00621	53.47	53.57	76.7	132	7.9		0.2	1.15	<0.002	61.6	<0.001	47.5	<0.002	0.015	<0.005	1.8	3.77	<0.002	18.3	<0.003	<0.1	5.72	14.9	0.0665	6.8	0.072
S02-00622	55.40	55.47	77.3	141	8.6	7	0.1	0.999	<0.002	62.7	<0.001	47.9	<0.002	0.015	<0.005	2.2	3.87	<0.002	19.5	0.013	<0.1	5.81	16.1	0.0678	7.1	0.091
S02-00623	58.56	58.64	85.3	127	6.3		0.2	1.04	<0.002	64.2	<0.001	58	<0.002	<0.008	<0.005	2.5	3.68	<0.002	22.3	0.026	<0.1	5.97	15.6	0.07	7	0.093
S02-00624	60.16	60.26	88.1	134	5.1	4	0.1	1.04	<0.002	69.9	<0.001	55.1	<0.002	0.008	<0.005	2.8	3.91	<0.002	21.7	0.043	<0.1	5.04	24.1	0.07	7	0.078
S02-00625	63.55	63.66	88.2	139	6.9	5.4	0.1	1.04	<0.002	70.3	<0.001	53.9	<0.002	0.015	<0.005	2.2	3.68	<0.002	20.5	0.035	<0.1	5.01	19.3	0.0685	7.7	0.088
S02-00626	65.42	65.50	88.2	128	6.4	4.8	0.1	1	<0.002	67.4	<0.001	52.6	<0.002	0.014	<0.005	1.9	3.62	<0.002	19.5	0.017	<0.1	4.91	18.4	0.0652	7	0.095
S02-00627	68.50	68.60	82.8	133	7.3	5.5	0.1	0.907	<0.002	70.3	<0.001	50.4	<0.002	0.013	<0.005	2.3	3.73	<0.002	21.7	0.008	<0.1	5.52	19.7	0.0695	8.5	0.074
S02-00628	71.25	71.35	87.0	135	6.7	5.2	0.1	0.963	<0.002	72.4	<0.001	52	<0.002	0.011	0.007	2.4	3.83	<0.002	21.5	0.005	<0.1	5.63	19.2	0.0711	8.1	0.099
S02-00629	74.56	74.70	82.8	129	7.1		0.2	1.05	<0.002	59.4	<0.001	43.6	<0.002	<0.008	<0.005	2.3	3.28	<0.002	19.2	0.012	<0.1	5.42	12.7	0.0609	5.4	0.106
S02-00631	76.03	76.14	98.2	133	7.8	6	<0.1	0.799	<0.002	63.6	<0.001	45.7	<0.002	<0.008	<0.005	1.7	3.46	<0.002	16.4	0.007	<0.1	5.14	15.3	0.0592	5.6	0.068
S02-00630	77.60	77.70	76.2	121	6.7	5.1	<0.1	0.778	<0.002	62.4	<0.001	49.4	<0.002	0.01	<0.005	2.1	3.48	<0.002	17.9	0.018	<0.1	5.59	14.7	0.0623		0.075
S02-00632	80.77	80.88	90.7	133	6.1	4.9	<0.1	0.986	<0.002	57.9	<0.001	41.6	<0.002	<0.008	<0.005	1.8	3.38	<0.002	15.9	0.024	<0.1	5.38	13	0.0579	5.2	0.088
S02-00633	81.79	81.88	80.0	133	6.4	4.8	0.1	0.889	<0.002	57.9	<0.001	40.6	<0.002	0.011	<0.005	1.8	3.31	<0.002	17.3	0.007	<0.1	5.28	12.8	0.0575	4.6	0.065
S02-00634	84.08	84.18	75.6	123	7.9		0.2	1.01	<0.002	54.2	<0.001	43.3	<0.002	<0.008	<0.005	2.2	3.61	<0.002	19.3	0.037	<0.1	5.67	11.7	0.062	4.9	0.062
S02-00635	86.53	86.65	89.7	123	6.6	4.8	<0.1	0.729	<0.002	53.8	<0.001	37.3	<0.002	<0.008	<0.005	1.7	4.03	<0.002	16	0.004	<0.1	5.35	13.7	0.058	4.7	0.075

Sample	Top	Bottom	M C	Alk	As_T	As(III)	B	Ba	Be	Ca	Cd	Cl	Cr	Cu	Fe	K	Mg	Mn	Na	NO_2-N	P	Si	SO_4	Sr	TON	Zn
S02-00636	88.35	88.42	78.6	126	15	11.7	0.2	0.846	<0.002	45.3	<0.001	40.6	<0.002	<0.008	<0.005	2.3	7.05	<0.002	17.6	0.016	<0.1	5.65	12.2	0.0808	4.7	0.063
S02-00637	89.32	89.44	89.2	136	125.3	12.4	0.1	0.947	<0.002	45.3	<0.001	39.8	<0.002	0.008	<0.005	2.6	7.99	<0.002	17.3	0.009	<0.1	5.86	11.7	0.0871	4.7	0.072
S02-00638	91.47	91.59	82.9	128	16.3	11.7	0.2	0.904	<0.002	41.8	<0.001	39	<0.002	<0.008	<0.005	2.4	7.62	<0.002	18.4	0.008	<0.1	5.83	10.9	0.0858	4.3	0.078
S02-00639	92.49	92.58	84.	132	18.2		0.2	0.884	<0.002	42	<0.001	36.7	<0.002	<0.008	<0.005	2.3	8.14	<0.002	18.5	0.009	<0.1	5.82	10.2	0.0872	4.1	0.071
S02-00640	94.60	94.70	85	134	16.7	12.6	0.1	0.822	<0.002	42.5	<0.001	39.2	<0.002	<0.008	<0.005	2	8.19	<0.002	17.2	<0.003	<0.1	5.17	11.6	0.0849	4.6	0.058
S02-00641	96.14	96.24	104	137	89.1	13.9	<0.1	0.848	<0.002	42	<0.001	36.4	<0.002	<0.008	<0.005	1.8	7.86	<0.002	14.4	0.009	<0.1	4.86	11.3	0.079	4.6	0.066
S02-00642	98.02	98.12	104	130	18.7	14.4	<0.1	0.747	<0.002	39.4	<0.001	34.5	<0.002	<0.008	<0.005	1.8	7.67	<0.002	14.6	0.007	<0.1	4.89	10.1	0.0775	4.2	0.05
S02-00643	100.00	100.10	102	130	17.9	13	<0.1	0.783	<0.002	38	<0.001	31.3	<0.002	<0.008	<0.005	2.1	7.78	<0.002	13.8	0.013	<0.1	5.53	9.9	0.0755	4.2	0.059
S02-00644	101.45	101.56	85	119	18.9		0.2	0.816	<0.002	37	<0.001	33.9	<0.002	0.011	<0.005	2.8	7.54	<0.002	16.8	0.046	<0.1	6.42	9.5	0.0803	4.0	0.037
S02-00645	104.08	104.20	93	121	10.1	7.5	0.1	0.81	<0.002	47.8	<0.001	42.4	<0.002	0.011	<0.005	2.4	6.16	<0.002	17.8	0.031	<0.1	5.46	12.9	0.0713	4.5	0.042
S02-00646	104.38	104.47	92	117	12.4	10.3	0.2	0.851	<0.002	47.3	<0.001	39.4	<0.002	<0.008	0.049	2.3	5.19	0.003	18.4	0.023	<0.1	5.91	12.8	0.0673	5.1	0.063
S02-00647	105.78	105.89	90	120	14.4		0.2	0.909	<0.002	43.4	<0.001	34.7	<0.002	<0.008	<0.005	2.5	5.54	<0.002	18.3	0.015	<0.1	5.53	10.5	0.0728	4.2	0.048
S02-00648	109.89	110.00	101	125	18.2	14.6	0.2	0.91	<0.002	42.6	<0.001	35.6	<0.002	<0.008	<0.005	2.4	7.84	<0.002	18.2	0.013	<0.1	6.12	11.5	0.074	4.4	0.03
S02-00649	113.58	113.68	87	137	21		0.2	0.856	<0.002	40.6	<0.001	33.4	<0.002	<0.008	<0.005	2.5	8.75	<0.002	17.5	0.015	<0.1	6.26	11.1	0.0735	4.1	0.052
S02-00650	117.17	117.25	81	127	14.4		0.2	0.912	<0.002	45.8	<0.001	36.1	<0.002	<0.008	<0.005	3	6.42	<0.002	19.5	0.023	<0.1	6.05	11.8	0.073	4.4	0.05
S02-00651	118.50	118.60	79	129	47.4	13.3	<0.1	0.867	<0.002	44.2	<0.001	33.8	<0.002	<0.008	<0.005	2.6	7.76	<0.002	17.9	0.015	<0.1	5.84	11.3	0.0712	4.1	0.066
S02-00652	119.57	119.65	72	117	15.4		0.2	0.863	<0.002	41.2	<0.001	33.4	<0.002	<0.008	<0.005	2.6	6.25	<0.002	19.4	0.013	<0.1	5.93	10.7	0.0707	3.8	0.047
S02-00653	123.07	123.18	84	114	18.3		0.2	0.772	<0.002	37.5	<0.001	26.3	0.002	<0.008	<0.005	2.6	5.95	<0.002	16.8	0.015	<0.1	6.18	10	0.0586	3.4	0.052
S02-00654	125.70	125.80	70	119	14.3		<0.1	0.73	<0.002	41.6	<0.001	31.3	<0.002	<0.008	<0.005	2.3	6.35	<0.002	15.6	0.016	<0.1	5.53	11	0.0612	3.8	0.047
S02-00655	129.01	129.11	108	119	18.1	14.1	0.1	0.709	<0.002	39.1	<0.001	24.1	<0.002	<0.008	<0.005	2.1	5.83	0.003	13.5	0.011	<0.1	5.09	10.4	0.0566	3.7	0.055
S02-00656	131.10	131.20	110	119	16.4	12.7	<0.1	0.636	<0.002	38	<0.001	24.1	<0.002	<0.008	<0.005	1.9	5.89	<0.002	13.4	0.012	<0.1	5.61	10.3	0.0545	3.7	0.05
S02-00657	132.33	132.43	60	117	14.3		0.1	0.689	<0.002	40.4	<0.001	30.5	0.002	<0.008	<0.005	3.2	5.65	<0.002	16.1	0.021	<0.1	5.87	11.3	0.0583	3.7	0.063
S02-00658	134.50	134.60	97	121	18.5	14.6	0.1	0.621	<0.002	39.3	<0.001	27.1	<0.002	<0.008	<0.005	2.4	6.35	<0.002	14.1	0.023	<0.1	5.52	10.8	0.0595	3.8	0.066
S02-00659	136.43	136.25	86	120	28.4		0.2	0.787	<0.002	40.5	<0.001	29.4	0.003	0.01	<0.005	3.5	6.62	<0.002	16.9	0.038	<0.1	6.11	9.9	0.063	3.8	0.037
S02-00660	139.27	139.35	99	117	20.2	14.8	<0.1	0.591	<0.002	35.4	<0.001	24.1	<0.002	<0.008	0.007	2.4	7.11	<0.002	13.5	0.042	<0.1	6.27	10.9	0.0592	3.4	0.042
S02-00661	141.05	141.14	58	101	19.8		0.2	0.603	<0.002	37.4	<0.001	31.1	0.004	<0.008	<0.005	2.8	7.34	<0.002	16.1	0.016	<0.1	6.41	10.8	0.0636		0.05
S02-00662	141.88	141.97	92	116	24.4	19	0.1	0.598	<0.002	34.4	<0.001	21.3	<0.002	<0.008	<0.005	2.2	6.73	<0.002	13.4	0.009	<0.1	5.85	9.6	0.0569	3.2	0.036
S02-00663	143.98	144.07	22	96.4	9.2		<0.1	0.59	<0.002	35	<0.001	39	<0.002	<0.008	<0.005	1.9	7.1	<0.002	12.9	0.004	<0.1	6.4	9.4	0.059	1.3	0.012
S02-00664	146.82	146.92	96	115	32.6	25.5	0.1	0.577	<0.002	33.3	<0.001	20.3	<0.002	<0.008	<0.005	1.8	6.65	<0.002	12.6	0.008	<0.1	5.95	8.6	0.0558	2.8	0.025
S02-00665	149.03	149.13	74	128	26.9	19.8	0.2	0.644	<0.002	34.7	<0.001	21.7	<0.002	<0.008	<0.005	2	7.9	<0.002	12.7	0.007	<0.1	5.7	8.4	0.0578	3.1	0.06

M.C. = moisture content in g kg^{-1} dry wt; Alk = alkalinity as HCO_3. Top and Bottom are depths in m bgl. No pH data are included because of possible CO_2 degassing.

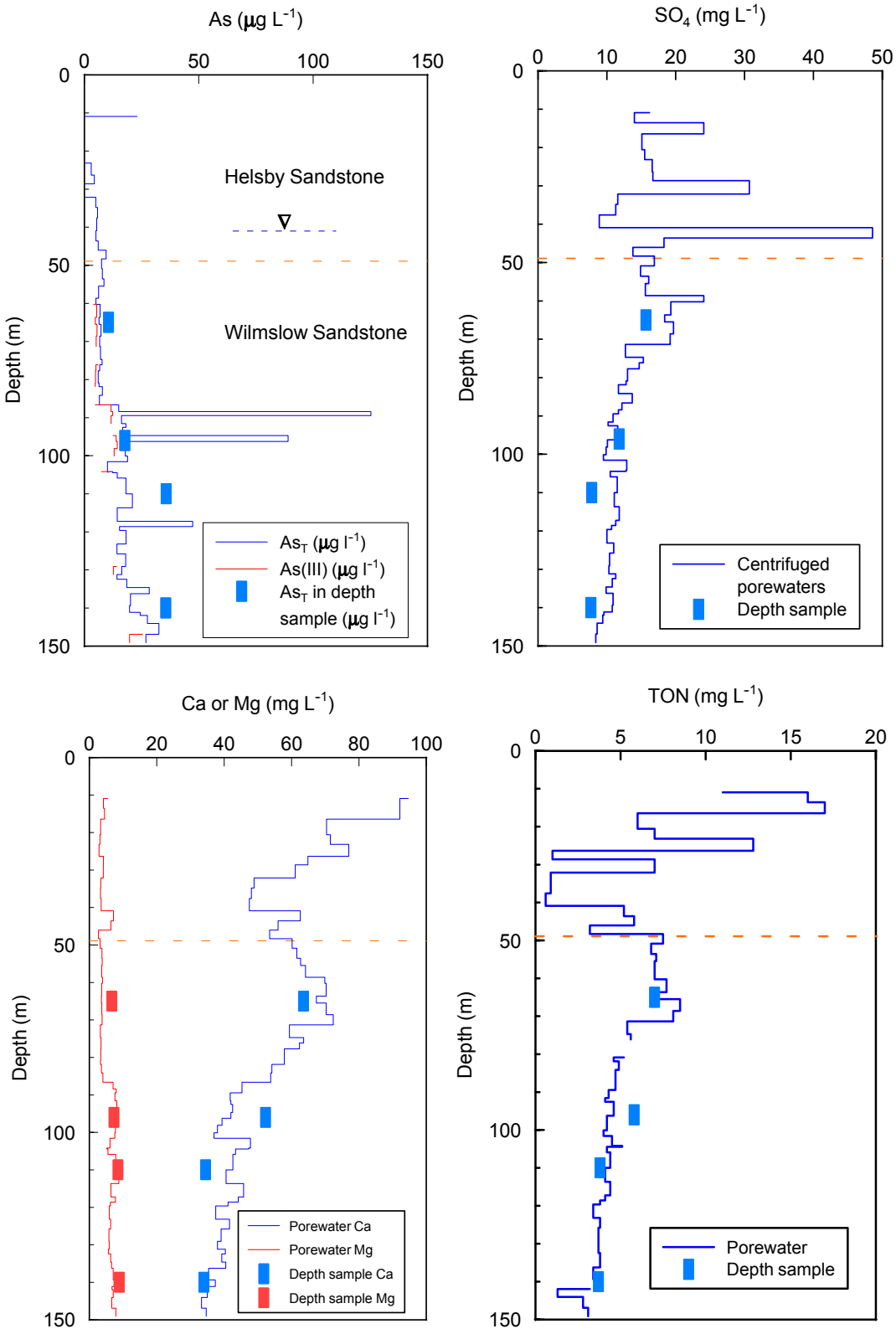

Figure 6.7 **Total arsenic, arsenic(III), sulphate, calcium, magnesium and nitrate concentrations versus depth in the porewater extracted from the project borehole. The orange dashed line marks the boundary between the Helsby and Wilmslow Sandstone Formations.**

There is also a jump in porewater Mg concentration from 3 to 7 mg L^{-1} close to the water table. This goes back to 'background' after a few metres. The centrifuged porewater and depth samples are consistent with each other.

Table 6.5 Arsenic concentration in the three porewaters with the largest arsenic concentrations reanalysed at different times

Analysis ID	BGS sample ID	Date		
		27/03/02	18/06/02	16/10/02
10265-0061	S02-00637-04	125		164
10265-0065	S02-00641-04	89		100
10265-0075	S02-00651-04	47	63	107

Nitrate – the top 30 m of the unsaturated zone shows high and erratic concentrations of nitrate ranging from 1–17 mg NO_3-N L^{-1}. The upper part of the saturated zone contained approximately 7 mg L^{-1} NO_3-N. There is a tendency for concentrations to decrease with depth. These data point to erratic inputs of nitrogen. Given that the site was forested, the variation could be related to either atmospheric variations in input (particularly of dry deposition of ammonia) or to variations in uptake by the trees. Forests are known to be more spatially-variable than arable land in terms of nitrate leaching (Kinniburgh and Trafford, 1996). There was no evidence for extensive denitrification in the profile. The environment is not sufficiently reducing. The trees could also scavenge sulphate aerosols and may explain the relatively high SO_4 concentrations seen in parts of the unsaturated zone.

The nitrate-N concentration at depth (greater than 100 m) is about 3–4 mg L^{-1} which probably reflects inputs a century or more ago. These concentrations are considerably lower than currently pumped from nearby boreholes from an equivalent depth (e.g. Delamere 3) which points to the possibility of some drawdown of nitrate-rich groundwater at the pumping stations. Although woodland is often regarded as benign as far as nitrate leaching is concerned, the high concentrations of nitrate presently in the upper unsaturated zone, often exceeding the current drinking water limit, indicate that 'nitrogen saturation' may currently exist within the forest. Again the depth samples are consistent with the porewater samples.

Since nitrate concentrations in aerobic groundwaters are strongly controlled by past land use, the results of the present borehole cannot be used as a guide to nitrate concentrations in surrounding arable land. Nevertheless, since the surrounding area is predominantly arable, relatively high concentrations of nitrate can be expected in the upper part of the unsaturated zone.

7 Mineralogy and sediment chemistry

7.1 SEDIMENT CHEMISTRY

7.1.1 Analytical methods

Subsamples of the sediments were thoroughly mixed, air-dried, ground in a Tema mill and then subjected to a nitric-perchloric acid dissolution. The extracts were analysed by ICP-AES for major and minor elements. Although arsenic was analysed by ICP-AES, this method is not very sensitive and so arsenic was also analysed using the more sensitive hydride generation-atomic fluorescence spectrometry (HG-AFS) method. This involved a pre-reduction with KI-ascorbic acid and so it measured total As.

7.1.2 Arsenic content

The two methods outlined above agreed well (Figure 7.1) and therefore it appears that direct aspiration ICP-AES is sufficiently accurate for determining As contents of rocks. The results showed that the As content was 5–15 mg kg^{-1}. This is an average content for sandstones (Smedley and Kinniburgh, 2002) and not atypical of UK red bed sandstones (Haslam and Sandon, 1991).

There is no obvious trend of As content in the sediments with depth nor a clear difference between the Helsby and Wilmslow Sandstones. Nevertheless, there is some apparently random variation. Arsenic does not correlate strongly with any of the other elements. The mean As content was 8 mg kg^{-1} overall with a slightly lower concentration in the Wilmslow Sandstone compared with the Helsby sandstone (7.5 and 8.5 mg kg^{-1}, respectively).

7.1.3 Other elements

Data for the concentrations of a wide range of major and minor elements in the selected subsamples of sediments are given in Table 7.1 and average concentrations for the Helsby and Wilmslow Formations are given in Table 7.2. A selection of sediment chemistry profile plots is given in Figure 7.2.

The were some strong positive correlations ($r>0.9$) between element pairs: Al vs K, Al vs Mg, Al vs Na, Al vs P, K vs Na, K vs P, Mn vs Ca, Mg vs Fe and Ba vs SO_4. These are consistent with the overall mineralogy (see below) especially the presence of feldspars and metal-rich coatings although the source of many of the minor elements (e.g. P) is not clear. There was a weak negative correlation between Ca and Mg indicating that the presence of dolomite is unlikely. It is also clear from the profile plots (Figure 7.2) that calcite is probably rare or absent in the upper part of the Wilmslow formation (50–100 m) but is likely to be present erratically above and below that interval. There is significantly more Na and K in the Wilmslow Sandstone Formation than in the Helsby Sandstone Formation perhaps reflecting a higher concentration of feldspars in the Wilmslow Formation.

There is considerably more Al in the Wilmslow Sandstone, as well as more Fe and less Mn. The strongest correlation was Ba vs SO_4 and clearly points to the occasional presence of barite ($BaSO_4$) in the Helsby Sandstone. The molar ratio in the high Ba-SO_4 horizons is close to one which supports this observation.

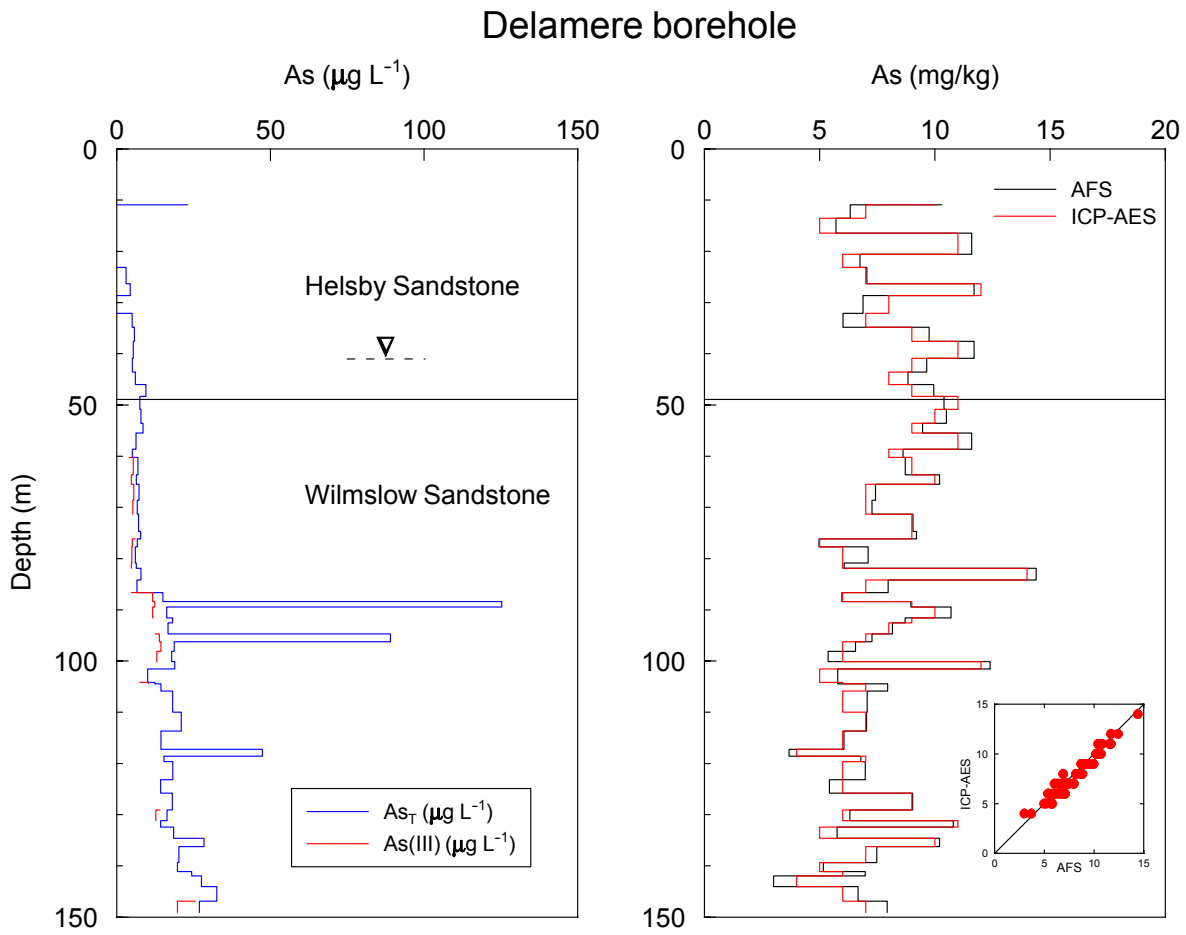

Figure 7.1 Arsenic concentration in porewater and sediments from the project borehole. Results of sediment analysis by both ICP-AES and HG-AFS are given. The inset shows the correlation between the two methods.

A stepwise multiple regression model was run on the data in Table 7.1 (excluding those trace metals which were sometimes below the detection limit) to see which of the observed variables best predicted the As concentration of the sediment. The output (from S-Plus) was as follows:

```
     *** Linear Model ***

Call: lm(formula = As ~ Bottom + Li + Mg + Mn + Na + SO4 + Sr, data = SolidMajors,
na.action = na.exclude)

Residuals:
     Min       1Q  Median      3Q     Max
 -3.0277 -0.75946 -0.2253 0.63121 3.1654

Coefficients:
              Value Std. Error  t value Pr(>|t|)
(Intercept) -1.42096  3.07820   -0.46162  0.64628
     Bottom -0.01787  0.00629   -2.84036  0.00642
         Li  0.76124  0.30676    2.48155  0.01635
         Mg  0.00419  0.00100    4.20604  0.00010
         Mn -0.00788  0.00456   -1.72771  0.08997
         Na -0.00241  0.00054   -4.47938  0.00004
        SO4 -0.00134  0.00086   -1.55095  0.12698
         Sr  0.09472  0.04731    2.00231  0.05048

Residual standard error: 1.4976 on 52 degrees of freedom
Multiple R-Squared: 0.58308
F-statistic: 10.389 on 7 and 52 degrees of freedom, the p-value is 4.4769e-008
```

Overall the fit was highly significant in a statistical sense. With the 7 variables: –bottom depth, +Li, +Mg, –Mn, –Na, –SO_4, +Sr (sign indicates direction of influence), it is possible to explain 58% of the variation in As concentrations. The three most significant factors were a large Mg concentration, a small Na concentration and a shallow depth. Iron was not selected as a significant factor even though there was a weak positive correlation between Fe and As.

Note that despite the significant negative correlation with depth, there is not a clear decrease of As with depth. This presumably is due to compensating trends such as that of Mg or SO_4. The positive correlations with Li and Mg may point to a clay control on the As concentration. The negative correlations are harder to explain and may reflect other unexplored factors.

Table 7.1 Sediment chemistry of samples from the project borehole from a total dissolution (units of mg kg^{-1} unless otherwise indicated)

Top depth (m)	Bottom depth (m)	%Al	%Fe	%Ca	%Mg	%K	%Na	As AFS	As ICP	Ba	Cu	Li	Mn	P	Pb	SO_4	Sr	Zn
10.74	10.92	1.00	0.31	3.07	0.06	0.86	0.10	10.3	10	1306	1	11	147	113	<7	935	49	8
13.3	13.55	1.90	0.47	3.99	0.09	1.58	0.26	6.3	7	347	<1	10	169	202	<7	147	60	5
16.3	16.45	0.90	0.37	2.17	0.05	0.77	0.09	5.7	5	367	2	11	129	109	<7	242	31	3
20.4	20.55	0.88	0.27	0.06	0.05	0.74	0.07	11.6	11	309	1	11	14	112	<7	169	23	4
23.07	23.17	0.73	0.23	0.57	0.05	0.58	0.06	6.8	6	1542	1	10	37	112	<7	1058	27	5
26.26	26.36	1.54	0.39	2.74	0.10	1.20	0.20	7.1	7	378	1	11	136	192	<7	122	50	5
28.5	28.62	1.96	0.47	2.67	0.11	1.49	0.30	11.7	12	3931	1	16	156	180	8	2871	97	6
32.03	32.13	0.61	0.18	1.02	0.04	0.50	0.05	6.9	8	903	2	11	47	96	<7	646	26	3
34.7	34.8	1.99	0.51	1.42	0.12	1.58	0.25	6.0	7	331	2	11	78	268	<7	103	47	7
37.49	37.61	2.24	0.62	2.07	0.14	1.66	0.30	9.8	9	347	2	12	111	287	<7	78	54	6
40.8	40.9	1.19	0.27	2.90	0.06	1.11	0.12	11.7	11	222	<1	11	120	164	<7	85	40	3
43.5	43.6	1.31	0.30	2.11	0.06	1.18	0.13	9.7	9	236	1	10	101	163	<7	78	37	3
45.92	46.02	0.66	0.19	1.54	0.03	0.63	0.05	8.8	8	134	<1	10	78	111	<7	19	21	2
48.18	48.3	3.06	0.54	0.11	0.16	2.13	0.46	10.0	9	396	1	14	31	278	<7	74	61	7
50.77	50.87	2.25	0.58	3.27	0.13	1.71	0.33	10.4	11	317	1	12	148	163	<7	106	61	5
53.47	53.57	2.57	0.53	0.09	0.12	1.98	0.42	10.5	10	384	2	12	29	274	8	23	58	5
55.4	55.47	2.45	0.54	0.09	0.11	1.86	0.40	9.5	9	355	2	13	28	257	10	47	56	5
58.56	58.64	2.76	0.80	0.11	0.17	1.97	0.36	11.6	11	356	2	13	42	303	11	64	59	7
60.16	60.26	2.46	0.58	0.68	0.12	1.86	0.40	8.6	8	361	2	13	49	264	7	48	58	5
63.55	63.66	2.15	0.43	0.10	0.09	1.74	0.30	8.7	9	336	2	13	30	226	12	35	52	4
65.42	65.5	2.33	0.43	0.07	0.10	1.89	0.33	10.2	10	359	2	12	24	193	11	41	56	4
68.5	68.6	2.63	0.56	0.10	0.11	2.09	0.39	7.4	7	391	2	12	38	297	11	126	61	4
71.25	71.35	2.64	0.62	0.09	0.13	2.00	0.42	7.3	7	363	2	13	37	269	9	49	58	5
74.56	74.7	2.89	0.73	0.12	0.15	2.18	0.43	9.1	9	393	2	13	32	354	8	<10	63	10
76.03	76.14	1.91	0.30	0.07	0.07	1.72	0.24	9.2	9	344	1	11	18	228	12	52	51	3
77.6	77.7	1.89	0.37	0.09	0.07	1.65	0.24	5.0	5	326	1	12	28	221	10	68	48	3

Top depth (m)	Bottom depth (m)	%Al	%Fe	%Ca	%Mg	%K	%Na	As AFS	As ICP	Ba	Cu	Li	Mn	P	Pb	SO_4	Sr	Zn
80.77	80.88	2.61	0.50	0.09	0.11	2.08	0.40	7.1	6	387	2	12	32	285	8	51	60	5
81.79	81.88	1.79	0.26	0.06	0.06	1.67	0.22	6.1	6	363	2	13	26	219	11	68	48	3
84.08	84.18	2.78	0.86	0.11	0.17	2.02	0.34	14.4	14	348	2	13	40	336	11	60	61	7
86.53	86.65	2.02	0.34	0.18	0.07	1.80	0.25	8.0	7	382	1	11	35	246	8	54	52	3
88.35	88.42	2.60	0.40	0.10	0.10	2.15	0.38	6.0	6	417	2	12	26	312	9	50	62	4
89.32	89.44	3.01	0.75	0.12	0.16	2.24	0.44	9.0	9	377	2	14	44	390	9	57	62	6
91.47	91.59	3.07	0.85	0.12	0.18	2.22	0.44	10.7	10	380	2	14	44	402	10	80	65	6
92.49	92.58	3.05	0.64	0.12	0.16	2.30	0.44	8.7	9	413	2	13	37	384	9	69	66	5
94.6	94.7	1.88	0.32	0.09	0.09	1.50	0.23	8.2	8	282	1	12	27	279	<7	47	46	5
96.14	96.24	2.52	0.47	0.09	0.11	2.03	0.37	7.3	7	367	2	12	25	275	11	76	59	4
98.02	98.12	2.60	0.47	0.09	0.11	2.07	0.40	6.6	6	364	2	12	33	315	9	66	58	5
100	100.1	2.31	0.44	0.10	0.10	1.88	0.34	5.4	6	342	1	11	29	270	8	53	55	4
101.45	101.56	3.19	1.12	0.12	0.22	2.22	0.37	12.4	12	369	2	14	49	392	9	82	66	8
104.08	104.2	2.43	0.53	1.97	0.12	2.01	0.37	5.8	5	375	1	12	100	286	<7	94	59	5
104.38	104.47	2.68	0.53	0.11	0.12	2.11	0.41	5.8	6	378	2	12	34	309	10	122	60	5
105.78	105.89	3.50	1.00	0.15	0.20	2.45	0.57	8.0	7	413	2	14	45	461	10	80	69	10
109.89	110	2.92	0.69	0.11	0.14	2.20	0.45	7.1	6	385	2	13	36	332	9	66	64	7
113.58	113.68	2.84	0.69	0.11	0.14	2.18	0.44	7.0	7	376	2	13	37	354	8	57	61	7
117.17	117.25	2.83	0.52	0.92	0.14	2.22	0.48	6.1	6	411	2	12	59	318	10	119	65	5
118.5	118.6	1.40	0.31	5.38	0.07	1.23	0.18	3.7	4	287	<1	10	234	186	<7	114	52	4
119.57	119.65	2.45	0.61	2.34	0.14	1.87	0.39	6.8	7	328	1	12	131	329	7	119	62	5
123.07	123.18	3.06	0.65	0.13	0.16	2.22	0.49	7.0	6	393	2	13	38	394	9	73	68	8
125.7	125.8	1.62	0.36	3.35	0.08	1.41	0.20	5.4	6	454	1	11	205	210	<7	200	50	4
129.01	129.11	3.14	0.93	0.14	0.17	2.29	0.49	9.0	9	388	2	14	44	410	9	51	65	6
131.1	131.2	2.27	0.48	0.27	0.10	1.89	0.31	6.3	6	448	1	12	35	265	7	106	55	5
132.33	132.43	1.76	0.50	5.44	0.11	1.44	0.21	10.8	11	248	1	12	273	220	<7	79	54	7
134.5	134.6	2.29	0.47	0.09	0.11	1.85	0.32	5.8	5	342	2	12	29	269	9	45	56	4
136.43	136.25	2.78	0.79	0.13	0.17	2.01	0.38	10.2	10	344	2	13	39	381	8	53	63	6
139.27	139.35	2.98	0.71	0.14	0.15	2.25	0.46	7.5	7	386	2	13	40	360	9	33	63	6

Top depth (m)	Bottom depth (m)	%Al	%Fe	%Ca	%Mg	%K	%Na	As AFS	As ICP	Ba	Cu	Li	Mn	P	Pb	SO_4	Sr	Zn
141.05	141.14	2.36	0.44	3.05	0.11	1.95	0.35	5.2	5	353	1	11	135	293	8	104	63	4
141.88	141.97	2.64	0.56	0.12	0.13	2.08	0.38	7.0	6	368	2	12	38	303	9	24	59	11
143.98	144.07	1.07	0.17	8.53	0.04	1.07	0.15	3.0	4	190	<1	11	305	130	<7	95	57	11
146.82	146.92	2.38	0.47	0.08	0.10	1.96	0.33	6.7	6	358	2	12	32	271	11	59	57	4
149.03	149.13	2.02	0.47	0.10	0.09	1.68	0.28	7.9	7	309	1	11	38	254	8	52	49	10

Element*	Helsby Formation	Wilmslow Formation
n	14	46
%Al	1.43	2.47
%Fe	0.37	0.56
%Ca	1.89	0.85
%Mg	0.08	0.12
%K	1.14	1.94
%Na	0.17	0.36
As (ICP-AES)	8.5	7.5
Ba	768	361
Cu	0.9	1.6
Li	11.4	12.3
Mn	96.7	62.5
P	171	293
Pb	<10	<10
SO_4	473	70
Sr	45	59
Zn	4.8	5.6

*Concentrations in mg kg^{-1} except where indicated as wt%.

Table 7.2 Average concentration of various major and minor elements in the sediments subdivided by formation.

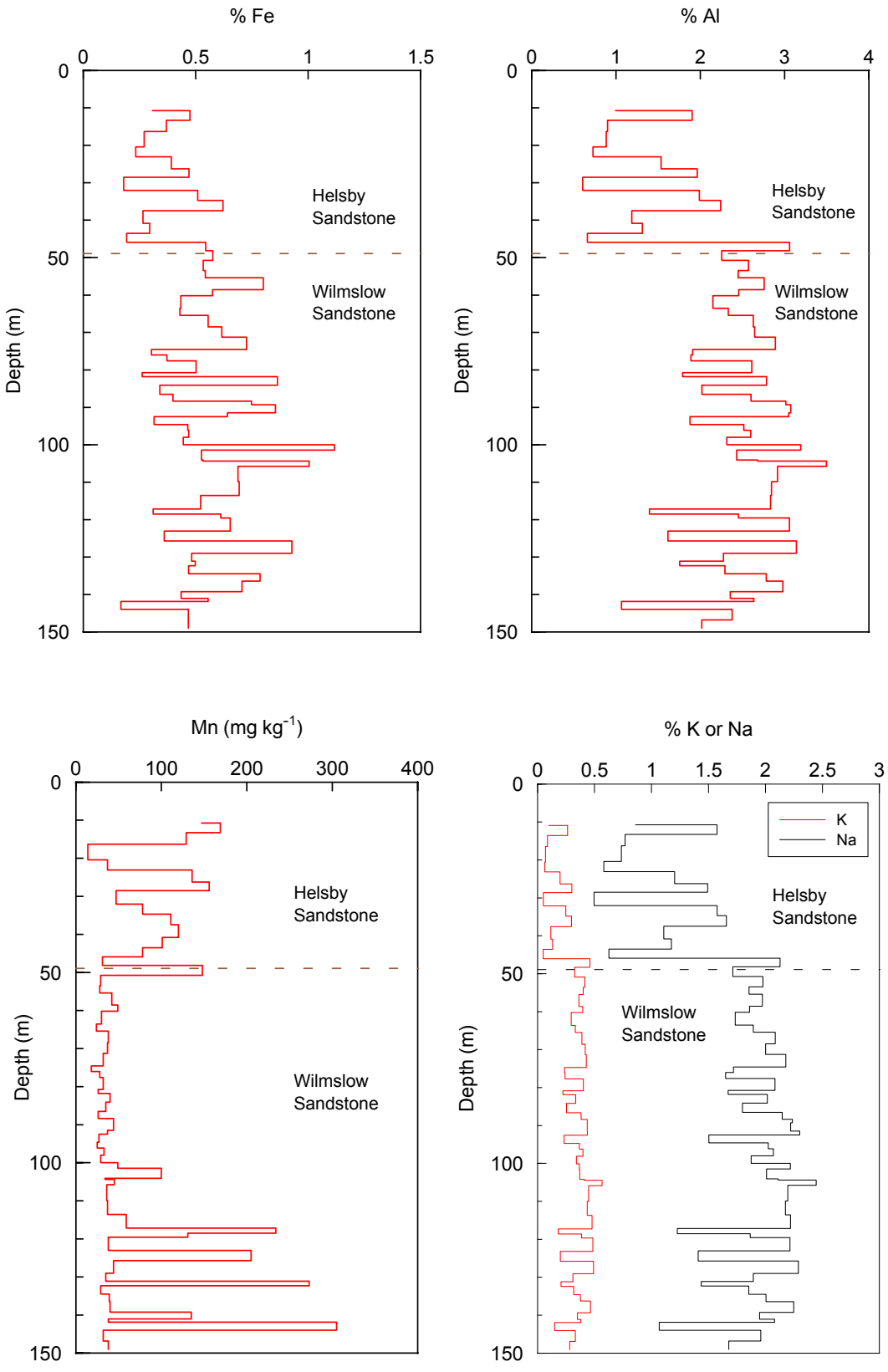

Figure 7.2 **Sediment chemistry profiles for the project borehole: iron, aluminium, manganese, sodium and potassium.**

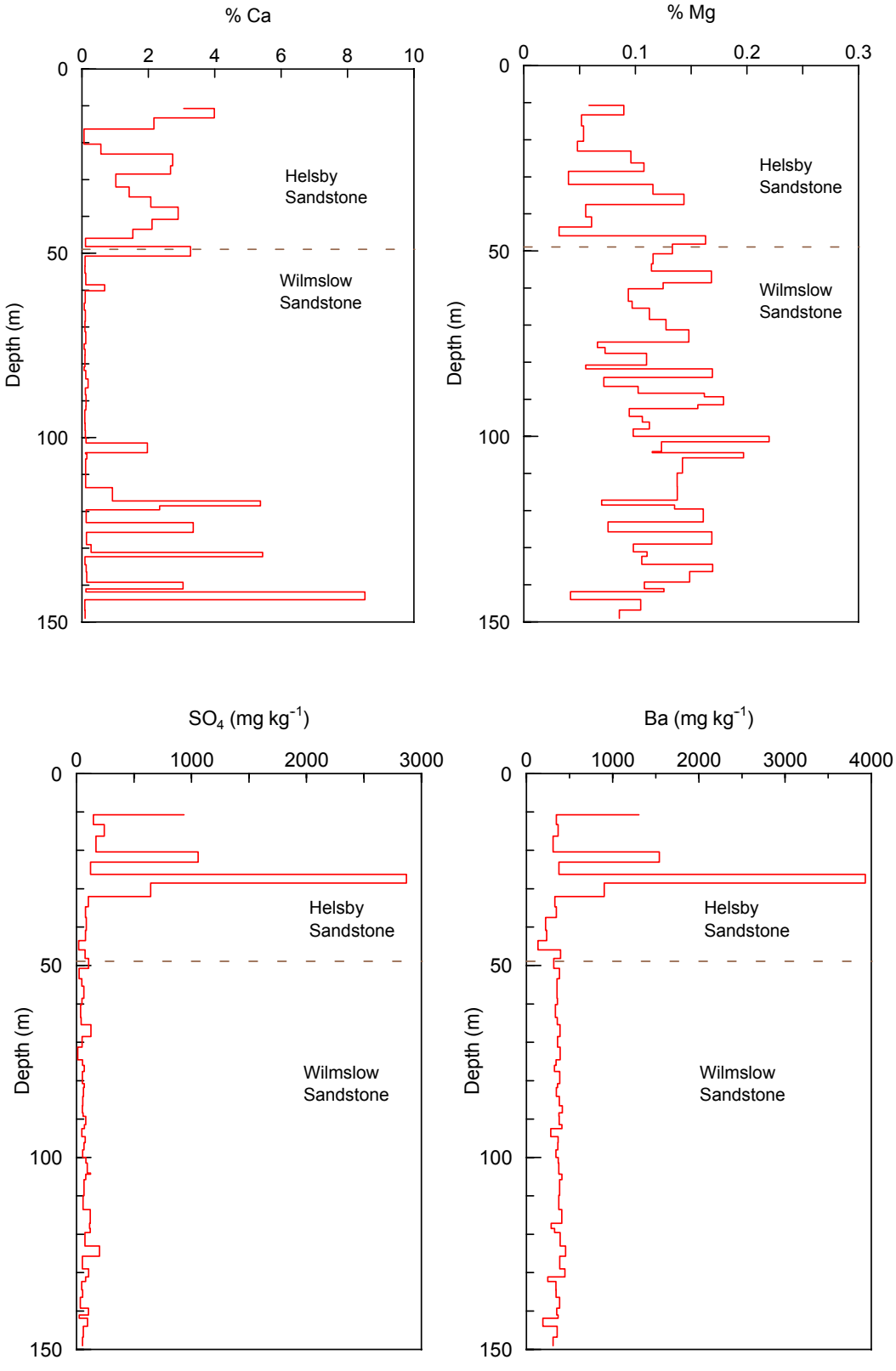

Figure 7.2 (contd) Sediment chemistry profiles for the project borehole: calcium, magnesium, sulphur (as sulphate) and barium.

7.2 PETROGRAPHIC ANALYSIS

7.2.1 Selection of samples

Twelve samples of sandstone from the project borehole were submitted for petrographic analysis (Table 7.3). The samples represent material from the Helsby and Wilmslow Sandstone Formations and were selected to compare horizons in which high porewater arsenic concentrations had been identified with horizons containing background porewater arsenic concentrations (Figure 7.1). Three of the samples, H675P1, H676P1 and H677P1, were untreated (i.e. not centrifuged) samples of sandstone from the three horizons which showed anomalously high porewater arsenic concentrations. Samples H682P1, H683P1 and H684P1 were taken from horizons immediately adjacent to zones in which high arsenic concentrations had been identified in the porewater. The remaining six samples were selected to represent horizons corresponding to background arsenic porewater concentrations.

Table 7.3 List of samples examined for petrographic analysis

Sample no.	Depth (m)	Formation	Comment
H678P1	29.50	Helsby Sandstone	Centrifuge residue from horizon with background porewater As concentration
H679P1	38.10	Helsby Sandstone	Centrifuge residue from horizon with background porewater As concentration
H680P1	49.50	Wilmslow Sandstone	Centrifuge residue from horizon with background porewater As concentration
H681P1	76.00	Wilmslow Sandstone	Centrifuge residue from horizon with background porewater As concentration
H685P1	129.50	Wilmslow Sandstone	Centrifuge residue from adjacent to low As porewater horizon
H686P1	135.00	Wilmslow Sandstone	Centrifuge residue from adjacent to low As porewater horizon
H682P1	89.30–89.32	Wilmslow Sandstone	Centrifuge residue from adjacent to high As porewater horizon
H675P1	89.34–89.44	Wilmslow Sandstone	Untreated sandstone from which high As porewaters had been extracted
H683P1	96.12–96.14	Wilmslow Sandstone	Centrifuge residue from adjacent to high As porewater horizon
H676P1	96.14–96.24	Wilmslow Sandstone	Untreated sandstone from which high As porewaters had been extracted
H677P1	118.50–118.60	Wilmslow Sandstone	Untreated sandstone from which high As porewaters had been extracted
H684P1	118.60–118.62	Wilmslow Sandstone	Centrifuge residue from adjacent to high As porewater horizon

7.2.2 Objectives of analysis

Hydrothermal and diagenetic arsenic mineralisation is known to occur in the Sherwood Sandstone Formation and overlying Tarporley Siltstone Formation (Mercia Mudstone Group) in the Cheshire Basin (Plant *et al*., 1999). It is principally hosted in the upper parts of the Sherwood Sandstone Group, within the Helsby and Wilmslow Sandstone Formations. It is closely associated with copper, iron, lead, zinc, cobalt, nickel, bismuth, silver, molybdenum, mercury and selenium sulphides and barite. This has been described in detail in the recently published study by Plant *et al.* (1999) and other references cited therein. Barite and copper, iron, lead, zinc and arsenic minerals dominate the hydrothermal assemblage, and the mineralisation is most

extensively developed near Alderley Edge (Cheshire) and Clive (Shropshire) where it was formerly exploited economically.

However, hydrothermal mineralisation, hosted within the Sherwood Sandstone Group, is also known from the nearby areas of Bickerton Hill and Peckforton Hill in Cheshire. Most of the major primary sulphide mineralisation in these areas has been altered to a complex secondary assemblage of copper, lead, cobalt and zinc carbonate, silicate, phosphate, oxide and oxyhydroxide minerals associated with iron and manganese oxyhydroxides. Similar arsenic mineralisation might be anticipated to be present in the Abbey Arms Wood borehole.

The objective of the petrographic analysis was therefore to examine the samples for any evidence of specific arsenic mineralisation and for other minerals which may potentially contain arsenic or which provide evidence of mineralization.

7.2.3 Analytical methods

The samples were air-dried and vacuum impregnated with epoxy resin to stabilise the friable sandstones prior to thin sectioning. A blue dye was added to the epoxy resin in order to make the porosity more readily visible during optical microscopic observation of the thin sections. The samples were then cut and prepared as polished thin sections. These were briefly examined with an optical petrographic microscope before more detailed characterisation under the scanning electron microscope (SEM).

SEM observations were undertaken using a Leo 435VP variable-pressure digital SEM instrument fitted with a four-element solid-state backscattered electron detector and an Oxford Instruments ISIS 300 digital energy-dispersive X-ray microanalysis (EDXA) system. Petrographic observations of the polished thin sections were made using the backscattered electron imaging (BSEM) mode. This produces images in which the contrast between the different minerals is dependent upon the difference in average atomic number (Goldstein *et al.*, 1981). Phases that have a high average atomic number (e.g. sulphides, heavy metal phases etc.) appear bright whilst low average atomic number phases (e.g. organic matter, quartz, or epoxy resin filling pores) appear dark. Thus, because arsenic has a moderately high atomic number, minerals which contain arsenic as a major component show up as bright phases in BSEM images.

The BSEM imaging technique provides a very good method for searching for such heavy element phases. Mineral identifications were based on the evaluation of semi-qualitative microchemical information obtained from EDXA spectra recorded simultaneously during BSEM observation. The SEM instrument was operated in the low vacuum mode (0.3–0.4 torr), using a beam accelerating potential of 15–20 kV, probe current of 200–700 pA, and a working distance of 19–25 mm. Low vacuum operation was used so that the polished sections could be observed without the need to coat them with an electrically-conductive layer. Although, this results in a lower resolution than conventional high vacuum SEM (which requires the samples to be made electrically conductive by coating them with gold or carbon), it allows the samples to be prepared much more quickly and to be observed under a conventional optical microscope without any obscuring of the detail by a conductive coating.

In addition to BSEM imaging, representative areas of the thin sections of samples corresponding to the high arsenic porewater horizons were ‘mapped’ for the distribution of As, Na, Mg, Al, Si, P, S, K, Ti, Mn and Fe, using the Oxford Instruments ISIS 300 ‘Speedmap©’ EDXA X-ray element mapping software. This was carried out to try to detect discrete arsenic minerals and determine their association with other major elements/minerals. The limit of detection by EDXA for most of the major elements is of the order of 0.2 to 0.5 weight percent, and the detection limit for arsenic is probably of a similar order.

7.2.4 Petrography and mineralogy

The twelve sandstones were mineralogically very similar with respect to their detrital components. They are subfeldspathic arenites to sublitharenites. Monocrystalline quartz is the major detrital component, with subordinate to minor amounts of polycrystalline quartz, lithic grains (which may include fine quartzite, schistose grains, fine siliceous volcanic grains, siltstone, fine sandstone), chert, and K-feldspar (orthoclase and microcline). Plagioclase (albitic) is present in most samples as a very minor to trace component. Other accessory detrital minerals include very minor muscovite, ilmenite and magnetite and traces of rutile, tourmaline, apatite, zircon and monazite.

All of the sandstones show the presence of thin coatings or pellicles of very fine illitic clay on the surfaces of detrital grains (e.g. Plate 7.1). These are impregnated with very fine-grained disseminated hematite or other iron oxide (Plate 7.2). The iron oxide is responsible for the red coloration of the rocks. The hematite is absent where reduction by later diagenetic mineralising fluids has produced late calcite-cemented bleached bands (e.g. sample H680P1). These clay pellicles are present between compacted grain surfaces. They are considered to be early diagenetic products and probably represent clay that infiltrated through the sediment shortly after deposition (cf. also Plant *et al.*, 1999 and references therein). Calcite is present as a major cement in some of the sandstones but absent from others (see more detailed sample descriptions given below). The calcite forms spherulitic micronodular concretions, which are often finely banded with thin layers of clay and hematite (Plate 7.3 and Plate 7.4). These nodules may coalesce to form irregular cemented patches.

The calcite cement preserves an ‘expanded’ or uncompacted grain fabric, and therefore pre-dates sediment compaction. It is similar to early diagenetic nodular non-ferroan calcite and dolomite cements described elsewhere from the Sherwood Sandstone Group in the Cheshire Basin and other Permo-Triassic basins in the United Kingdom (see Plant *et al.*, 1999 and references therein), and is interpreted as calcrete. Minor weakly ferroan calcite cement also occurs as later diagenetic overgrowths seeded on the earlier calcite cement in some of the sandstones. The calcite cement appears to be undergoing corrosion and dissolution. Traces of authigenic quartz and K-feldspar are present locally as weak overgrowths on some detrital grains. Detrital iron and titanium oxides are sometimes partially altered to fine-grained authigenic titanium oxides. The titanium oxide occasionally crystallised into coarser box-like crystals, which may be anatase or brookite.

In addition to secondary porosity formation caused by calcite cement dissolution, there is also evidence for the dissolution of detrital plagioclase, K-feldspar and lithic grains (feldspathic fragments and chert grains). This results in oversized pores, often containing the relict clay pellicles that originally surrounded the detrital grains that have been removed. This secondary framework grain dissolution porosity contributes significantly to the overall porosity of some of the sandstones.

No discrete arsenic minerals, sulphide minerals, or other hydrothermal or diagenetic mineralisation was observed in any of the sandstones. In addition, arsenic could not be detected as a minor component by EDXA in any of the minerals observed, either by point analysis or by the more systematic searching employed using EDXA X-ray mapping techniques (e.g. Plate 7. 5).

More detailed descriptions of individual samples are provided below.

7.2.5 Clay mineralogy and cation exchange capacity

Additional mineralogical and chemical analyses were undertaken on selected samples of the borehole core by Bellis (2002) which should be consulted for details of the methodology and results. Briefly, Bellis (2002) undertook whole rock XRD, clay fraction XRD, thin section

analysis, SEM, laser granulometry and cation exchange capacity measurements on 10 selected samples of the Delamere core. The samples used were (depth intervals in m): 10.74–10.92, 26.26–26.36, 40.80–40.90, 55.40–55.47, 68.50–68.60, 84.08–84.18, 100.00–11.10, 113.58–113.68, 129.01–129.11, 143.98–144.07). The principal results relating to the mineralogy of the samples are summarised below.

WHOLE ROCK ANALYSIS

Quartz is the main component with calcite detected in four of the ten samples, three of which were from the Helsby Sandstone Formation and contained about 5% calcite by XRD analysis. Only the 143.98–144.07 sample from the Wilmslow Sandstone Formation contained detectable calcite and this sample was found to contain 26% calcite. All of the samples contained small amounts of feldspar.

CLAY FRACTION XRD ANALYSIS

XRD analysis of the clay fraction indicated that the clays were predominantly illite and expanding clays (possibly a randomly layered illite-smectite mixture) with a minor amount of chlorite. Illite-smectite mixtures were also observed in sediments from the Cheshire Basin by Plant *et al.* (1999). An alternative explanation is that the expanding clay was a hydrated illite with a small amount of smectite.

TOTAL ORGANIC CARBON

The samples only contained trace quantities (about 0.1%) of organic carbon.

THIN SECTIONS

Five samples were prepared as thin sections and observed by light microscopy. The individual grains all had a red-orange coating of iron oxide and clays as expected. Calcite, where present, appeared as a patchy cement. There were no quartz overgrowths where calcite was present. The 143.98–144.07 m sample was the most extensively cemented sample with no porosity in much of the sample. The grain-size distribution, degree of sorting, degree of weathering and porosity varied between the samples. The Wilmslow Sandstone Formation samples showed a greater amount of clay/oxide matter and a lower porosity than the Helsby Sandstone Formation samples. Detrital mica was observed in some of the samples.

SCANNING ELECTRON MICROSCOPY

The shallowest sample (10.74–10.92 m) showed clear evidence of a quartz overgrowth on the rough surface of the original grain. Clays appear as a 3-dimensional network of whispery flakes. Energy-dispersive X-ray analysis of the clay confirmed an illitic composition. The SEM analysis of the heavily-cemented 143.98–144.07 m sample showed that the calcite cement completely filled the pore spaces between the grains.

LASER GRANULOMETRY

The particle size distributions of the <2 mm fraction of the ten samples after disaggregation were estimated by laser granulometry (in practice, no particles were actually >2 mm). Modal particle sizes were in the range 100–300 μm (fine to medium sand). The cemented horizons tended to be in the medium sand range while uncemented samples tended to be in the fine sand range. Some samples were strongly unimodal while others showed a much broader peak.

CATION EXCHANGE CAPACITY

The cation exchange capacity (CEC) of the ten samples was uniformly low from 2–13 meq kg^{-1}. The lowest CEC was in the heavily-cemented 143.98–144.07 m sample. The variation in the CEC of the remaining samples was not obviously correlated with any other measured sample property.

7.2.6 Summary of individual sample descriptions

H675P1 (89.34–89.44 M)

Laminated ferruginous siltstone with laminae, up to 3 mm thick, of very fine sandstone, and irregular ripple lenses of fine to medium sandstone. Composed mainly of angular monocrystalline detrital quartz, with very minor to trace amounts of polycrystalline quartz, plagioclase and K-feldspar. The siltstone laminae are compacted with low intergranular porosity. The sandstone laminae are very porous. Grains are coated with ferruginous clay rims. Calcite cements are absent.

H676P1 (96.14–96.24 M)

Finely parallel-laminated fine sandstone with thin laminae of siltstone and moderately sorted sandstone laminae 0.1 to 3 mm thick. The siltstone laminae are close-packed and strongly compacted with low intergranular porosity. The sandstone laminae are moderately well compacted and have high intergranular porosity. Composed of major monocrystalline detrital quartz, with minor polycrystalline quartz, K-feldspar and lithic grains, and traces of detrital Ti-Fe oxides, muscovite and plagioclase. Siltstone laminae have a ferruginous illitic detrital clay matrix, impregnated by fine hematite, and fine rims of ferruginous illitic clay coating detrital grains. Calcite cements are absent.

H677P1 (118.50–118.60 M)

Moderately well-sorted medium-grained calcite-cemented sandstone with well-rounded grains of medium sand in a matrix of sub-angular fine sand. The rock has very high intergranular porosity with a moderately uncompacted grain framework. Detrital mineralogy comprises major monocrystalline quartz, subordinate polycrystalline quartz and K-feldspar, minor plagioclase and trace amounts of ilmenite, magnetite, apatite, monazite, zircon and rutile. Detrital grains are coated by thin rims of illitic clay impregnated by very fine hematite. Fine authigenic titanium oxides (probably anatase or brookite) are present as minor alteration products of detrital Ti-Fe oxide grains. Major non-ferroan calcite cement is present in irregular patches of isolated and coalescing spherulitic or micronodular calcrete nodules. The calcite cement is corroded and shows evidence of dissolution.

H678P1 (29.50 M)

Moderately well-sorted fine-grained calcite-cemented sandstone with angular grains. Detrital mineralogy comprises major monocrystalline quartz, subordinate polycrystalline quartz and K-feldspar, minor plagioclase and trace amounts of ilmenite, magnetite. Detrital grains are coated by thin rims of illitic clay impregnated by very fine hematite. Minor non-ferroan calcite cement is present in irregular patches of isolated and coalescing spherulitic or micronodular calcrete nodules. Very minor later pore-filling weakly ferroan calcite cement is also present, occurring as localised overgrowths on the earlier calcrete micronodules. The calcite cements are corroded and show evidence of dissolution.

H679P1 (38.10 M)

Finely parallel-laminated medium and very fine sandstone, with thin siltstone laminae. Medium sandstone grains are well-rounded spherical grains of aeolian sand. The finer sandstone and siltstone grains are angular to sub-angular. Detrital mineralogy comprises major monocrystalline quartz, subordinate polycrystalline quartz and K-feldspar, minor plagioclase and trace amounts of ilmenite and magnetite. Detrital grains are coated by thin rims of illitic clay impregnated by very fine hematite. Very minor to trace amounts of non-ferroan calcite are present as rare micronodular calcrete.

H680P1 (49.50 M)

Moderate to poorly-sorted fine to medium compacted-sandstone with dominantly sub-angular grains, and rare well-rounded aeolian sand grains. The sandstone is generally red-brown but has a thin green-grey band calcite-cemented band of fine sandstone to coarse siltstone up to 12 mm thick. The uncemented sandstone is porous but the calcite-cemented sandstone has no intergranular porosity. The calcite is weakly ferroan, pore filling and post-dates compaction of the detrital grains. Traces of authigenic hematite occur as platy crystals in the intergranular porosity. Detrital ilmenite and magnetite are sometimes partially altered to fine authigenic titanium oxide (possibly anatase).

H681P1 (76.00 M)

Moderately compacted fine to medium laminated sandstone, with 0.1 to 2 mm laminae of ferruginous siltstone. The sandstone laminae are moderately well-sorted. Detrital mineralogy comprises mainly monocrystalline quartz, with very minor polycrystalline quartz and K-feldspar, and trace amounts of plagioclase, ilmenite, magnetite, tourmaline, zircon and monazite. Detrital grains are coated by thin rims of illitic clay impregnated by very fine hematite. Calcite cement is absent.

H682P1 (89.30–89.32 M)

Finely laminated fine to medium sandstone and very fine sandstone, with laminae 1-2 mm thick. The sand grains are dominantly angular to subangular, and laminae are generally moderately well sorted. Detrital mineralogy comprises major monocrystalline quartz, subordinate polycrystalline quartz and K-feldspar, very minor plagioclase and muscovite, and trace amounts of ilmenite, magnetite and zircon. Detrital grains are coated by thin rims of illitic clay impregnated by very fine hematite. Authigenic anatase replaces some detrital Ti-Fe oxides. Calcite cements are absent.

H683P1 (96.12–96.14 M)

Finely parallel laminated or sub-parallel laminated sandstone, with 1 to 2 mm laminae of fine sandstone in medium sandstone. The sand grains are dominantly angular to subangular, and laminae are generally moderately well-sorted. Detrital mineralogy comprises mainly monocrystalline quartz, with minor polycrystalline quartz and K-feldspar, and very minor to trace plagioclase, ilmenite, magnetite and zircon. Detrital grains are coated by thin rims of illitic clay impregnated by very fine hematite. Calcite cement is absent.

H684P1 (118.60–18.62 M)

Moderately-compacted to weakly compacted calcite-cemented medium sandstone. The sand grains are sub-rounded, and laminae are generally moderately well sorted. Detrital mineralogy comprises mainly monocrystalline quartz, with minor polycrystalline quartz and K-feldspar, very

minor plagioclase, and traces of ilmenite, magnetite, apatite and zircon. Detrital grains are coated by thin rims of illitic clay impregnated by very fine hematite. Major non-ferroan calcite cement is present in irregular patches of isolated and coalescing spherulitic or micronodular calcrete nodules. Very minor later pore-filling weakly ferroan calcite cement is also present, occurring as localised overgrowths on the earlier calcrete micronodules. The calcite cements are corroded and show evidence of dissolution. Rare authigenic K-feldspar and quartz are present as small or localised euhedral overgrowths on some detrital grains.

H685P1 (129.50 M)

Finely parallel laminated or sub-parallel laminated sandstone, with 1 to 2 mm laminae of very fine sandstone to siltstone in medium sandstone. The very fine sandstone/siltstone laminae are tightly compacted, with low porosity. The medium sandstone laminae are very porous, and are only moderately compacted. The sand grains are dominantly angular to subangular, and laminae are generally moderately well-sorted. Detrital mineralogy comprises mainly monocrystalline quartz, with minor polycrystalline quartz and K-feldspar, and very minor plagioclase and traces of muscovite, ilmenite, magnetite and zircon. Detrital grains are coated by thin rims of illitic clay impregnated by very fine hematite. Calcite cements are absent.

H686P1 (135.00 M)

Very fine sandstone to siltstone with thin laminae of siltstone up to 2 mm thick. The rock is porous but has a very compacted grain framework of angular grains. Detrital mineralogy comprises mainly monocrystalline quartz, with minor polycrystalline quartz and K-feldspar, and very minor plagioclase and traces of muscovite, ilmenite, magnetite and zircon. Detrital grains are coated by thin rims of illitic clay impregnated by very fine hematite. Calcite cements are absent.

7.2.7 Discussion and conclusions

No discrete arsenic minerals or other minerals containing arsenic in significant quantity were identified in any of the samples. However, it should be borne in mind that the analytical detection limits of the EDXA system used in this study are unlikely to detect arsenic present in minerals as a minor or trace element at concentrations below about 0.5 weight percent.

There is no evidence of any hydrothermal or diagenetic sulphide mineralisation similar to that which, elsewhere in the Helsby and Wilmslow Sandstone Formation of the Cheshire Basin, is closely associated with arsenic mineralisation as part of the red-bed type copper, iron, lead, zinc, cobalt, nickel, bismuth, silver, molybdenum, mercury and selenium sulphides and barite mineralisation (Plant *et al.*, 1999). It was initially thought that this type of mineralisation might account for the relatively high concentrations of arsenic encountered in groundwaters from boreholes in the Delamere area. However, this type mineralisation is not present within the sequence seen in the Abbey Arms Wood borehole.

If the arsenic found in the pore waters from the Abbey Arms Wood borehole is sourced from the sandstone host rocks, possible source minerals include Ti-Fe oxides (magnetite, ilmenite). EDXA detected minor amounts of copper and possibly zinc in some of these grains, and it might be possible for these minerals to contain trace amounts of other heavy elements, including arsenic. The early diagenetic fine iron oxide (probably hematite) associated with the ferruginous clay coatings on detrital grains might also conceivably be another potential source of arsenic. Iron oxides have a strong affinity for arsenic and adsorbed concentrations can exceed 1000 mg kg^{-1} As. The early diagenetic hematite encountered in red-bed sandstones is considered to be a potential source of metals for red-bed type mineralisation similar to that encountered elsewhere in the Cheshire Basin. This also includes arsenic (see Plant *et al.*, 1999 for a detailed

discussion). However, a more detailed analysis using a more sensitive microanalytical technique is needed to prove that these iron oxides are a potential source of arsenic.

Desorption of As from Fe oxides (hematite) was also suggested as the cause of relatively high As concentrations (up to 14 $\mu g\ L^{-1}$) in the East Midlands Triassic Sandstone aquifer together with ageing and diagenesis (Smedley and Edmunds, 2002).

Finally, the petrographic study has shown that there are no significant differences in mineralogy between horizons containing high arsenic porewaters and the horizons with background levels of arsenic. Consequently, there would appear to be no obvious mineralogical feature that controls the distribution of relatively high arsenic porewater in the Abbey Arms Wood borehole.

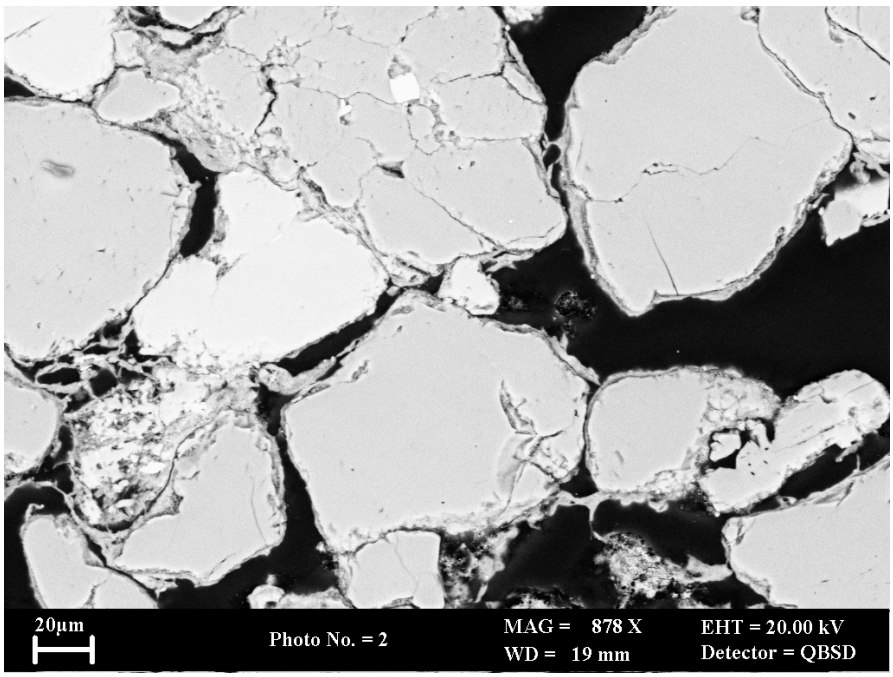

Plate 7.1 BSEM photomicrograph showing early diagenetic, thin illitic clay pellicles coating detrital grains. Dissolution of unstable detrital grains has produced oversized intergranular porosity containing relicts of the grain coating clay. Sample H685P1 (129.50 m).

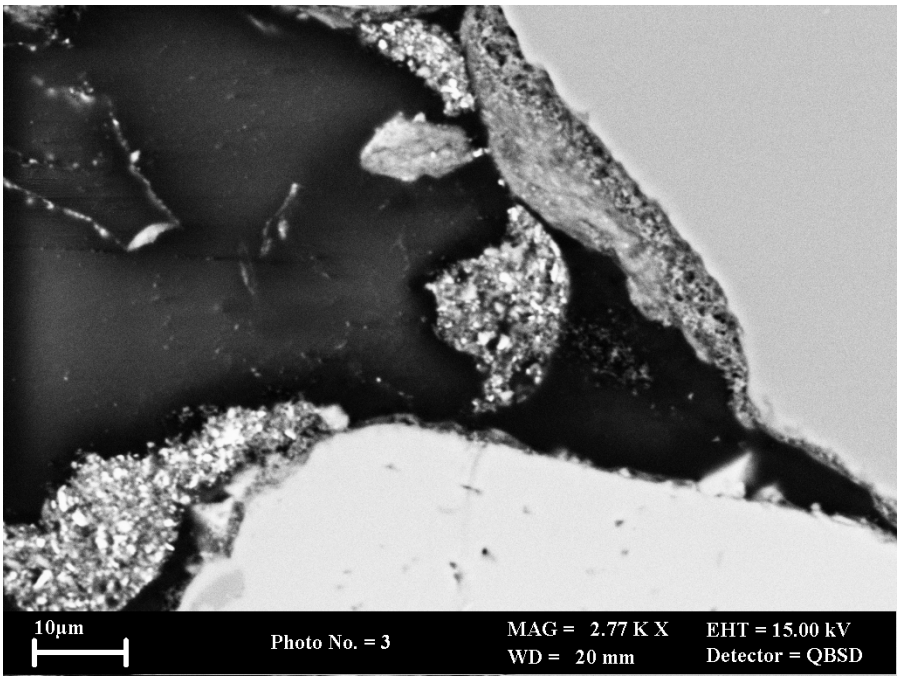

Plate 7.2 BSEM photomicrograph showing fine hematite (bright specs) disseminated through the illitic clay rim coating detrital grains. Sample H683P1 (96.12–96.14 m).

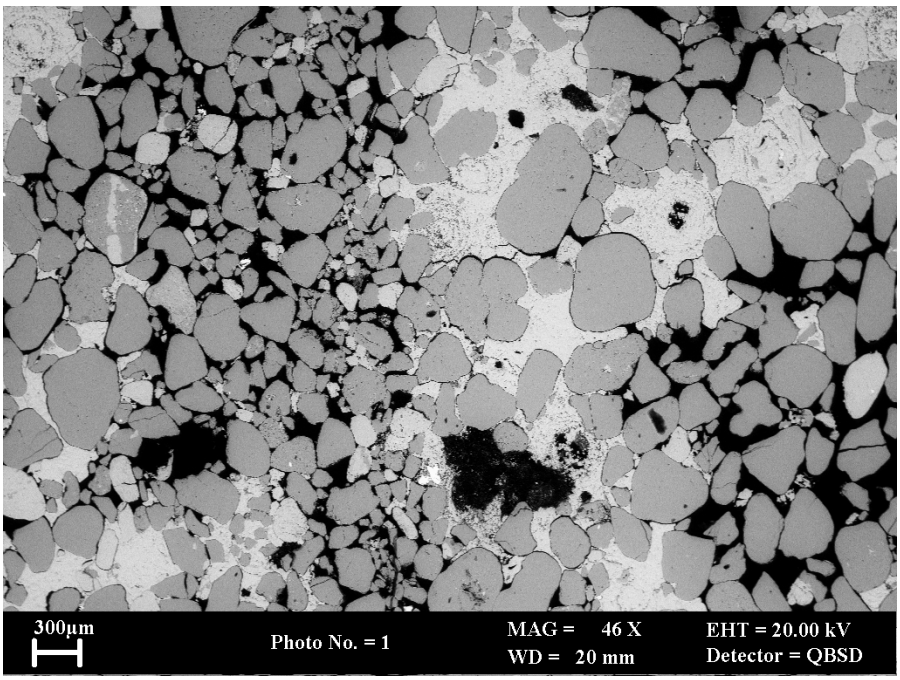

Plate 7.3 BSEM photomicrograph showing patchy distribution of expansive micronodular non-ferroan calcrete calcite cement (light grey) within and supported a very porous weakly compacted/uncompacted sandstone grain framework. Sample H677P1 (118.50–118.52 m).

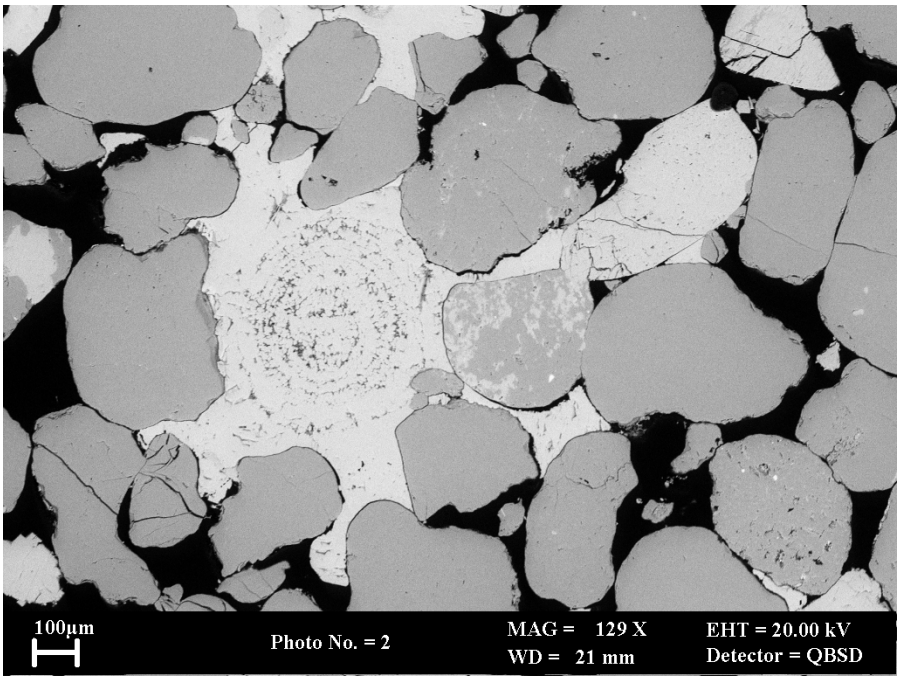

Plate 7.4 BSEM photomicrograph showing detail of concentric growth fabric of micronodular non-ferroan calcite cement (calcrete or 'cornstone' nodule). Later calcite forms overgrowths projecting into the adjacent intergranular porosity. Corrosion of the calcite along grain boundaries is evident at the margin of the calcrete nodule. Sample H684P1 (118.60–118.62 m).

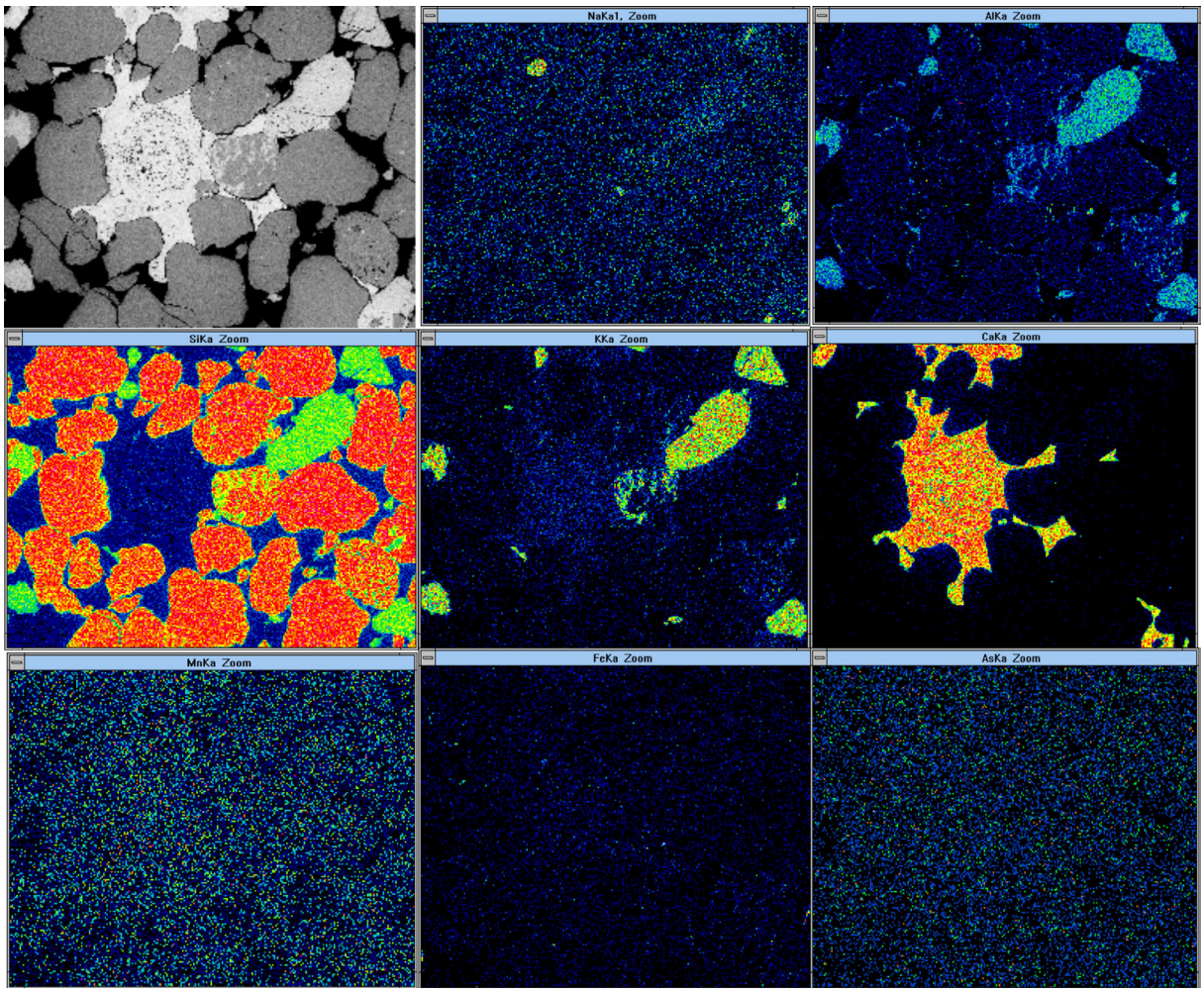

Plate 7. 5 Example of EDXA X-ray elemental mapping. Plate shows (a) BSEM image with bright nodular calcrete calcite cement, detrital quartz (dark grey) and K-feldspar (lighter grey). (b) Na map corresponding to grains of albite. (c) Al map corresponding to detrital K-feldspars, plagioclase and clay rims around detrital grains. (d) Si map with high concentrations (red) corresponding to quartz and lower concentrations (green) corresponding to feldspars and clay coatings on grain surfaces. (e) K map corresponding to detrital K-feldpars. Thin clay rims also show (green) on some grain surfaces. (f) Ca map corresponding to calcite cement. (g) Mn map showing mainly background noise. (h) Fe map showing only background noise. (i) As map showing only background noise. Sample H684P1 (118.60–118.62 m).

8 Conclusions

8.1 THE GEOLOGICAL AND HYDROGEOLOGICAL BACKGROUND

The Abbey Arms Wood borehole was successfully completed to 150 m in March 2002. The Helsby Sandstone-Wilmslow Sandstone boundary was found at 49 m bgl. The sandstone varied from coarse-grained fluvial channel-fill interbedded with smaller amounts of mudstones to aeolian sandstones and massive sandstones containing carbonate cementation. The Wilmslow Sandstone Formation consisted of stratified fine- to medium-grained silty sandstones developed in an aeolian sabkha environment. Both sandstone formations were fairly uniformly red in colour with occasional grey horizontally-bedded, bleached bands, most especially in the Helsby Sandstone. A number of faults and other large fractures were noted in the core log and in the CCTV tape of the borehole. A major fracture was observed at 103 m bgl. Geophysical logging suggested that this was the exit point of water flowing upwards from deeper in the borehole.

The water table was found at 40 m although observations from the lithological log, CCTV and the moisture content profile suggested that a perched water table occurred at about 26 m.

The porosity of the sandstones was typically in the range 19–24% although occasional lower porosities were found in well-cemented horizons. Horizontal permeability was greater than the vertical permeability and was broadly related to porosity. There were no consistent trends of permeability or porosity with depth. Results from a portable permeability probe agreed well with laboratory tests.

8.2 ARSENIC

The Delamere area is known for its occasional high-As groundwaters. Typically these groundwaters have As concentrations in the range 10–50 $\mu g\,L^{-1}$ which is not high by international standards but relatively high for the UK. Both depth sampling and porewater sampling in the project borehole indicated that As concentrations increase steadily with depth from about 8 $\mu g\,L^{-1}$ at 10 m to about 30 $\mu g\,L^{-1}$ at 150 m. Arsenic speciation suggested that approximately 2/3 of the As was present as As(III). However this is not consistent with the generally oxidising nature of the groundwaters and so should be viewed with caution. Although higher As concentrations were observed in 3 (out of 60) porewaters, these are believed to be an artefact, possibly due to the slow dissolution of an As-rich colloid.

This increasing trend of As concentration with depth was the opposite to that observed for most of the major solutes (except Mg) which tended to decrease in concentration with depth. Considering that the location of the borehole was in a forested area, surprisingly high nitrate concentrations (up to 17 mg L^{-1} NO_3-N) were found in the unsaturated zone (top 40 m).

The sediment chemistry was fairly typical of that of red-bed sandstones (Haslam and Sandon, 1991). Sediment arsenic concentrations appeared to be typical (5–12 mg kg^{-1}) of sandstones (Smedley and Kinniburgh, 2002) and if anything showed a decrease with depth. Erratic and high concentrations of porewater sulphate in the unsaturated zone of the Helsby Sandstone suggested possible barite mineralization. This was supported by high concentrations of SO_4 and Ba in the sediment solid in the corresponding depth intervals. No sulphide mineralization, as found in other mineralized areas of British red-bed sandstones (e.g. nearby Alderley Edge), was observed visually in the core during logging or in subsequent SEM-EDXA examination. No specific As-bearing minerals were observed.

The reason why arsenic concentrations are relatively high in the Delamere area is not clear. It is important to stress that while such concentrations are not widespread, they are not confined to the Delamere area since there are other high-As groundwaters in the region. Identifying the source of the arsenic is difficult since the quantities involved are so small. Given an average porosity of the sandstone (21%) and an average As content (8 mg kg^{-1}), it is only necessary to dissolve 0.04% of the As in the sandstone to give a groundwater concentration with an As concentration of 30 μg L^{-1}, three times the existing water quality standard for arsenic. This amount is extremely small and such dissolution clearly could not be detected by bulk chemical analysis. Indeed, given the sensitivity of groundwater to such small changes, it is perhaps surprising that high-As groundwaters are not more common.

The sediments were laid down some 240-245 million years ago and so the major geochemical changes following deposition (diagenesis) and groundwater flow probably occurred long ago. The drivers for change in the recent past must have been relatively small and over the last 100,000 years have probably been governed by the Ice Ages and resulting sea level changes. These would have affected groundwater flow patterns. and so would have altered the mixing patterns in the groundwater. However, it is likely that on a timescale of decades, a steady state would have existed with respect to most water quality parameters. Unfortunately, there are no data for water quality at that time and so it is not clear whether the arsenic concentrations have always been relatively high or whether this is a more recent phenomenon.

The extensive pumping of groundwater along with the possible introduction of pollutants, such as those derived from fertiliser leaching, are now likely to be the major drivers for change. Given that arsenic is currently being removed from the aquifer in the abstracted groundwater, it is likely that it is still being desorbed from the aquifer, most likely from the iron oxides since these are known to bind arsenic very strongly. How long this might last is difficult to judge without more detailed information about the desorption isotherms. There could also be very slow diagenetic changes taking place. Crystallization of the iron oxides may either reduce their surface area or change their structure, for example from hydrous ferric oxide to hematite, and this could be accompanied by the release of small amounts of arsenic. Other factors leading to increased arsenic concentrations could be an increase in pH, perhaps resulting from changes in groundwater flow patterns, and less likely, an increase in the concentration of competing anions (like phosphate, silicate, bicarbonate or DOC) or a decrease in the concentration of co-ions aiding As adsorption like Ca^{2+}.

There are insufficient detailed data on the As content of the Triassic Sandstones in the UK in general to know whether the As concentrations observed in the sediments examined in the present study are different from Triassic Sandstones from elsewhere in the UK. It could well be that the mineralization in the Cheshire Basin in general has led to a regionally slightly higher As concentration in the sediments (including that adsorbed by the iron oxides). This As could be dispersed via the extensive fracture and faulting systems observed in the area. The Abbey Arms Wood borehole was only 0.5 km from a major fault, the East Delamere Fault, and the CCTV footage showed fractures of various sizes intersecting the borehole.

Edwards (2001) noted that the proximity to major faults was a possible indicator of high-As groundwaters, although it proved not to be statistically significant. He also noted that there was a clear correlation between high-As groundwaters and the proximity to the mapped mudstone–sandstone boundary (here reflected by the Tarporley Siltstone Formation–Helsby Sandstone Formation boundary). Clearly, both the source of the As and the groundwater flow are important factors and faulting can in principle affect both.

It should be stressed that the analyses of water samples referred to in this report are for raw groundwaters prior to any treatment taking place. The samples were not taken for the purpose of assessing water quality from each of the boreholes tested for drinking, cooking or other domestic, agricultural, or industrial purposes and do not amount to certification of potability in

respect of groundwater in the region. If such information is required, specific tests should be carried out for this purpose.

8.3 IMPLICATIONS FOR WATER RESOURCES MANAGEMENT

The main conclusion from the present study is that the As concentration in groundwater in the Delamere area gradually increases with depth. In that sense, the shallower the borehole the better in terms of As concentration but of course this has to be set against the increase in yield that may occur with increasing depth. We have observed a large fracture and potentially water-yielding fracture at about 100 m, for example. Therefore completion just below this depth might provide an acceptable yield without excessive As. Nevertheless, the concentration is likely to be in the range 10–20 μg L^{-1} and so would still exceed the revised drinking water limit of 10 μg L^{-1}.

While the increase in As concentration with depth is somewhat erratic, it is sufficiently consistent that the possibility of finding dramatically lower As concentrations by drilling to a shallower (or deeper) depth is unlikely.

9 Further research

9.1 AQUIFER PROPERTIES AND HYDROGEOLOGY

- Undertake a dilution test under natural gradient flow conditions to characterise the flow distribution in the borehole. The results should be analyzed in the context of the geophysical flow logs and be used to provide a more refined interpretation of movement of water into and out of the borehole.
- Obtain an optical imager log to locate and characterize the faults and secondary fracturing in the borehole. Results should be analyzed in conjunction with existing geophysical flow logs and pore water quality profiles to provide a preliminary assessment of the contribution of fracture flow to the borehole.
- Systematic packer testing of the hole could then be undertaken following the dilution and packer tests. This would enable a head gradient profile to be generated for the borehole and would enable the characterization of the relative contribution of matrix and fracture flow down the borehole. Results should be analyzed in the context of the optical imager logs, geophysical flow logs and dilution tests to provide a sound basis for the interpretation of the pore water chemistry and the recent evolution of the aquifer at the site.
- MICP tests and thin section work should be undertaken on core already tested for poro-perm properties and for which there is also whole rock and pore water chemistry data available. The purpose of this work would be to investigate the relationships between cement content and type, pore-size distribution and matrix permeability and to provide insights into aquifer evolution at the matrix scale.

9.2 ARSENIC

- There is a need for a systematic review and mapping of all arsenic data in UK groundwaters to assess the true extent of arsenic contamination and to reveal any spatial or other patterns. For example, there is evidence for occasional 'high-As' groundwaters (greater than 10 $\mu g\ L^{-1}$) in other parts of the Triassic Sandstone aquifer (Edmunds et al., 1989). This would place the findings of this study in a broader context and should make the mechanisms of arsenic release clearer.
- A systematic study of the As content and As adsorption behaviour of UK sandstones should be undertaken. This should include a measure of total As as well as more labile forms released by selective dissolution. Adsorption isotherms should be measured under both oxidising and reducing conditions and with a realistic range of background groundwater compositions. This should enable the rate of transport of As through the sandstone aquifers to be calculated.
- Further work should be undertaken to try and identify As in minerals in sandstone samples from Delamere and elsewhere using modern methods such as EDXA, μ-PIXE and EXAFS. Especial care should be taken to examine the iron oxides. This analysis should include sandstone samples from known mineralised areas. Where EXAFS proves successful, an attempt should be made to determine the speciation.
- Systematic monitoring of water quality over time, including for arsenic, should establish the nature of the temporal variability which might itself give clues to the origin of the high-arsenic waters and could be used in the design of any future water treatment plants.

Appendix 1 Core physical properties data

Table A1 Porosity, bulk density and grain density results for plug samples.

Sample Number	Dry bulk density g cm^{-3}	Sat bulk density g cm^{-3}	Grain density g cm^{-3}	Porosity %
1575/1H	2.122	2.322	2.652	20.0
1575/2H	2.247	2.401	2.657	15.4
1575/3H	2.156	2.346	2.662	19.0
1575/4H	1.942	2.208	2.647	26.6
1575/5H	2.059	2.282	2.650	22.3
1575/6H	2.195	2.369	2.657	17.4
1575/7H	2.157	2.346	2.660	18.9
1575/8H	2.116	2.318	2.652	20.2
1575/9H	2.121	2.320	2.648	19.9
1575/10H	2.102	2.310	2.654	20.8
1575/11H	2.076	2.293	2.652	21.7
1575/12H	2.129	2.326	2.650	19.7
1575.13H	2.181	2.359	2.653	17.8
1575/14H	2.210	2.376	2.650	16.6
1575/15H	2.258	2.407	2.655	15.0
1575/16H	2.001	2.245	2.645	24.3
1575/17H	2.096	2.306	2.654	21.0
1575/18H	2.079	2.296	2.654	21.7
1575/19H	2.015	2.255	2.650	23.9
1575/20H	2.017	2.253	2.640	23.6
1575/21H	2.023	2.256	2.637	23.3
1575/22H	2.020	2.255	2.640	23.5
1575/23H	2.088	2.299	2.645	21.0
1575/24H	2.082	2.294	2.642	21.2
1575/25H	2.091	2.299	2.640	20.8
1575/26H	2.116	2.315	2.644	20.0
1575/27H	2.137	2.329	2.647	19.3
1575/28H	1.944	2.205	2.631	26.1
1575/29H	2.036	2.264	2.637	22.8
1575/30H	2.135	2.331	2.656	19.6
1575/31H	2.032	2.263	2.643	23.1
1575/32H	2.092	2.298	2.633	20.5
1575/33H	2.039	2.268	2.647	23.0
1575/34H	2.068	2.286	2.646	21.9
1575/35H	2.041	2.268	2.641	22.7
1575/36H	2.147	2.339	2.659	19.2
1575/37H	2.051	2.279	2.655	22.7
1575/38H	2.062	2.281	2.641	21.9
1575/39H	2.072	2.288	2.643	21.6
1575/40H	2.278	2.422	2.663	14.5
1575/41H	2.398	2.500	2.669	10.2
1575/42H	2.154	2.344	2.658	19.0
1575/43H	2.506	2.565	2.662	5.9
1575/44H	2.140	2.332	2.649	19.2
1575/45H	2.072	2.286	2.636	21.4
1575/46H	2.088	2.299	2.647	21.1
1575/47H	2.110	2.311	2.641	20.1
1575/48H	2.085	2.292	2.630	20.7
1575/49H	2.117	2.316	2.643	19.9
1575/50H	2.018	2.252	2.633	23.3
1575/51H	2.071	2.285	2.633	21.3

Table A2 Permeability results for plug samples

Sample Number	Sample depth (m bgl)	Standard gas permeametry permeability (mD)	Probe permeametry permeability (mD)
1575/1H	11.00	3181.5	1338.6
1575/1V	11.00	2622.8	1499.5
1575/2H	13.61	551.8	259.1
1575/2V	13.61	395.9	259.7
1575/3H	16.25	272.9	153.4
1575/3V	16.25	168.9	56.6
1575/4H	20.585	7916.8	5168.8
1575/4V	20.585	7585.8	4417.2
1575/5H	23.21	3539.0	2391.0
1575/5V	23.21	1627.4	2714.5
1575/6H	26.44	400.0	13.1
1575/6V1	26.44	4.0	123.7
1575/6V2	26.44	327.4	541.6
1575/7H	28.67	975.3	514.4
1575/7V	28.67	815.4	400.2
1575/8H	32.17	4020.5	1183.2
1575/8V	32.17	2181.7	1767.0
1575/9H	34.845	520.6	219.6
1575/9V	34.845	115.3	210.7
1575/10H	37.79	920.5	878.1
1575/10V	37.79	330.9	220.5
1575/11H	41.075	2141.5	1148.2
1575/11V	41.075	2198.5	2322.9
1575/12H	43.66	8.7	789.6
1575/12V	43.66	4.8	1236.2
1575/13H	46.07	9.9	917.7
1575/13V	46.07	10.2	1130.4
1575/14H	48.13	9.9	90.7
1575/14V	48.13	5.3	72.4
1575/15H	50.955	116.9	243.9
1575/15V	50.955	0.8	296.4
1575/16H	53.62	2377.4	2069.7
1575/16V	53.62	1881.5	1156.8
1575/17H	55.585	359.9	426.5
1575/17V	55.585	27.3	155.3
1575/18H	58.785	727.6	606.7
1575/18V	58.785	402.1	68.1
1575/19H	60.32	1592.4	471.0
1575/19V	60.32	225.0	362.2
1575/20H	63.79	2781.7	1843.2
1575/20V	63.79	449.7	707.1
1575/21H	65.55	2079.7	941.5
1575/21V	65.55	1269.8	1070.6
1575/22H	68.655	1156.1	1000.1
1575/22V	68.655	1625.3	2731.9
1575/23H	71.205	316.7	108.2
1575/23V	71.205	111.5	146.3
1575/24H	74.73	669.4	624.0
1575/24V	74.73	23.4	264.4
1575/25H	77.76	1757.7	1218.6
1575/25V	77.76	319.9	1220.4
1575/26H	80.715	271.2	214.8
1575/26V	80.715	100.9	91.0
1575/27H	84.03	136.0	165.0
1575/27V	84.03	82.5	150.2
1575/28H	86.685	1985.5	1657.8
1575/28V	86.685	1800.2	3402.2
1575/29H	88.315	1112.7	1188.6
1575/29V	88.315	450.9	513.3
1575/30H	89.49	244.1	3.1
1575/30V	89.49	3.4	22.4
1575/31H	91.425	506.6	172.1
1575/31V	91.425	9.7	180.5
1575/32H	94.51	538.7	255.7
1575/32V	94.51	400.7	1265.6
1575/33H	97.98	354.5	588.4
1575/33V	97.98	226.3	482.7
1575/34H	101.605	173.4	141.4
1575/34V	101.605	121.9	176.5
1575/35H	104.53	673.3	907.9
1575/35V	104.53	538.9	1292.5
1575/36H	105.95	40.2	50.5
1575/36V	105.95	20.0	136.2
1575/37H	109.855	155.0	113.0
1575/37V	109.855	47.8	13.5
1575/38H	113.725	559.6	114.8
1575/38V	113.725	703.1	1051.2
1575/39H	117.135	295.7	293.2
1575/39V	117.135	250.8	450.8
1575/40H	119.54	13.2	7.2
1575/40V	119.54	10.3	123.6
1575/41H	123.21	2.3	15.7
1575/41V	123.21	0.1	64.8
1575/42H	129.135	99.2	500.0
1575/42V	129.135	1.0	2210.3
1575/43H	132.475	0.8	1.4
1575/43V	132.475	54.9	26.6
1575/44H	135.48	25.5	103.6
1575/44V	135.48	17.4	104.0
1575/45H	136.575	148.4	105.7

Sample Number	Sample depth (m bgl)	Standard gas permeametry permeability (mD)	Probe permeametry permeability (mD)
1575/45V	136.575	102.6	423.1
1575/46H	140.265	124.4	124.5
1575/46V	140.265	39.7	44.3
1575/47H	142	166.2	327.4
1575/47V	142	73.6	36.6
1575/48H	144.115	1502.9	856.7
1575/48V	144.115	872.6	935.8
1575/49H	145.72	70.5	100.2
1575/49V	145.72	21.8	116.0
1575/50H	147.74	455.2	465.7
1575/50V	147.74	331.5	528.9
1575/51H	148.975	1978.8	1503.9
1575/51V	148.975	376.2	1370.7

Table A3 Correlation between horizontal and vertical gas permeability measurements on plug samples.

Standard gas permeametry sample number (H=horiz; V=vertical)	Horiztl. gas perm. mD	Vert. gas perm. mD	Standard K_h/K_v	Horiztl gas perm. mD	Vert. gas perm. mD	Probe K_h/K_v
1575/1H or V	3181.5	2622.8	1.2	1338.6		
1575/2H or V	551.8	395.9	1.4	259.1		1.0
1575/3H or V	272.9	168.9	1.6	153.4	56.6	2.7
1575/4H or V	7916.8	7585.8	1.0	5168.8	4417.2	1.2
1575/5H or V	3539.0	1627.4	2.2	2391.0	2714.5	0.9
1575/6H or V	400.0	4.0	100.5	13.1	123.7	0.1
1575/7H or V	975.3	815.4	1.2	514.4	400.2	1.3
1575/8H or V	4020.5	2181.7	1.8	1183.2	1767.0	0.7
1575/9H or V	520.6	115.3	4.5	219.6	210.7	1.0
1575/10H or V	920.5	330.9	2.8	878.1	220.5	4.0
1575/11H or V	2141.5	2198.5	1.0	1148.2	2322.9	0.5
1575/12H or V	8.7	4.8	1.8	789.6	1236.2	0.6
1575/13H or V	9.9	10.2	1.0	917.7	1130.4	0.8
1575/14H or V	9.9	5.3	1.9	90.7	72.4	1.3
1575/15H or V	116.9	0.8	143.6	243.9	296.4	0.8
1575/16H or V	2377.4	1881.5	1.3	2069.7	1156.8	1.8
1575/17H or V	359.9	27.3	13.2	426.5	155.3	2.7
1575/18H or V	727.6	402.1	1.8	606.7	68.1	8.9
1575/19H or V	1592.4	225.0	7.1	471.0	362.2	1.3
1575/20H or V	2781.7	449.7	6.2	1843.2	707.1	2.6
1575/21H or V	2079.7	1269.8	1.6	941.5	1070.6	0.9
1575/22H or V	1156.1	1625.3	0.7	1000.1	2731.9	0.4
1575/23H or V	316.7	111.5	2.8	108.2	146.3	0.7
1575/24H or V	669.4	23.4	28.6	624.0	264.4	2.4
1575/25H or V	1757.7	319.9	5.5	1218.6	1220.4	1.0
1575/26H or V	271.2	100.9	2.7	214.8	91.0	2.4
1575/27H or V	136.0	82.5	1.6	165.0	150.2	1.1
1575/28H or V	1985.5	1800.2	1.1	1657.8	3402.2	0.5
1575/29H or V	1112.7	450.9	2.5	1188.6	513.3	2.3
1575/30H or V	244.1	3.4	71.1	3.1	22.4	0.1
1575/31H or V	506.6	9.7	52.4	172.1	180.5	1.0
1575/32H or V	538.7	400.7	1.3	255.7	1265.6	0.2
1575/33H or V	354.5	226.3	1.6	588.4	482.7	1.2
1575/34H or V	173.4	121.9	1.4	141.4	176.5	0.8
1575/35H or V	673.3	538.9	1.2	907.9	1292.5	0.7
1575/36H or V	40.2	20.0	2.0	50.5	136.2	0.4
1575/37H or V	155.0	47.8	3.2	113.0	13.5	8.4
1575/38H or V	559.6	703.1	0.8	114.8	1051.2	0.1
1575/39H or V	295.7	250.8	1.2	293.2	450.8	0.7
1575/40H or V	13.2	10.3	1.3	7.2	123.6	0.1
1575/41H or V	2.3	0.1	16.5	15.7	64.8	0.2
1575/42H or V	99.2	1.0	97.2	500.0	2210.3	0.2
1575/43H or V	0.8	54.9	0.0	1.4	26.6	0.1

Standard gas permeametry sample number (H=horiz; V=vertical)	Horiztl. gas perm. mD	Vert. gas perm. mD	Standard K_h/K_v	Horiztl gas perm. mD	Vert. gas perm. mD	Probe K_h/K_v
1575/44H or V	25.5	17.4	1.5	103.6	104.0	1.0
1575/45H or V	148.4	102.6	1.4	105.7	423.1	0.2
1575/46H or V	124.4	39.7	3.1	124.5	44.3	2.8
1575/47H or V	166.2	73.6	2.3	327.4	36.6	8.9
1575/48H or V	1502.9	872.6	1.7	856.7	935.8	0.9
1575/49H or V	70.5	21.8	3.2	100.2	116.0	0.9
1575/50H or V	455.2	331.5	1.4	465.7	528.9	0.9
1575/51H or V	1978.8	376.2	5.3	1503.9	1370.7	1.1

Table A4 Probe permeability results on whole core.

Depth m	Probe permeability mD	Corrected permeability mD	Depth m	Probe permeability mD	Corrected permeability mD	Depth m	Probe permeability mD	Corrected permeability mD
10.2	684.8	459.4	22.275	28.9	67.5	37.435	168.3	196.4
10.41	850.1	523.7	22.4	89.9	134.3	37.74	69.3	114.7
10.6	1008.1	580.7	22.6	2700.0	1054.6	37.9	1796.9	824.1
11.2	1185.9	640.7	23.425	1097.4	611.3	38.1	1166.8	634.4
11.43	2045.0	891.2	23.6	2424.6	988.0	38.5	2269.0	949.1
11.79	23.7	59.9	24.07	3975.0	1333.0	38.725	2798.1	1077.6
11.8	1635.4	778.4	24.8	5963.2	1704.1	38.94	2412.0	984.9
11.98	3236.7	1177.0	25.005	494.9	377.4	39.105	1173.0	636.5
12.41	24.2	60.7	26.1	131.7	169.3	39.3	2716.6	1058.5
12.6	457.5	359.9	26.72	190.5	211.7	39.5	3533.7	1241.3
12.79	1440.5	720.8	26.88	441.3	352.1	39.71	1032.0	589.0
12.97	799.2	504.5	26.99	47.0	90.7	39.765	3097.7	1146.1
13.21	109.0	150.9	27.2	33.3	73.6	40	115.7	156.5
14	215.6	228.2	27.58	18.7	52.0	40.2	2853.9	1090.6
14.19	609.6	428.2	27.81	55.1	99.8	40.7	2844.8	1088.5
14.4	1096.0	610.8	28.87	236.3	241.2	41.6	170.0	197.5
14.8	1037.2	590.8	29.08	364.4	313.5	41.815	82.9	127.9
15.03	2360.7	972.2	29.79	32.4	72.4	42	21.0	55.6
15.6	13.3	42.1	30	634.1	438.5	42.21	10.9	37.5
15.6	1742.6	808.9	30.17	448.8	355.7	42.6	1340.4	690.0
15.895	1169.1	635.2	30.3	170.6	198.0	42.81	35.7	76.8
15.9	735.1	479.6	30.63	1596.7	767.2	43	129.4	167.5
16.2	1032.5	589.1	30.82	1563.5	757.5	43.275	199.6	217.7
16.46	4.1	20.6	30.95	1594.7	766.6	43.8	750.6	485.7
16.84	5254.9	1578.5	31.21	141.1	176.5	43.985	213.8	226.9
17.3	11.3	38.2	31.5	848.7	523.2	44.2	81.9	127.0
18.045	93.2	137.3	31.8	2547.8	1018.1	44.6	121.7	161.3
18.205	169.3	197.1	31.955	1201.4	645.8	44.8	866.7	529.9
18.3	138.0	174.1	32.91	474.9	368.0	45	192.1	212.7
18.42	50.7	95.0	33.1	3643.8	1264.5	45.21	74.5	119.9
18.56	13.0	41.6	33.4	49.3	93.3	45.4	167.7	195.9
18.85	44.3	87.5	33.53	288.3	272.0	45.625	1459.8	726.6
18.985	110.7	152.3	33.715	440.7	351.8	45.8	968.7	566.8
19.4	185.5	208.3	34.18	20.6	55.0	46.285	885.0	536.6
19.59	598.3	423.3	34.3	508.5	383.6	46.57	822.2	513.2
19.76	46.9	90.5	34.4	175.4	201.3	46.73	4.5	21.9
20.02	227.8	235.9	34.755	642.6	442.1	46.82	62.3	107.5
20.19	34.1	74.6	35.08	902.2	542.9	47	18.3	51.3
20.91	12.9	41.4	35.515	123.3	162.6	47.19	154.2	186.2
21.1	1141.9	626.2	35.8	25.6	62.7	47.37	17.4	49.7
21.33	2443.7	992.7	36.005	118.1	158.4	47.5	5016.5	1534.7
21.5	1603.0	769.0	36.2	1232.2	655.7	47.715	6.2	26.6
21.735	2112.8	909.0	37	725.4	475.7	48.5	178.9	203.8
21.865	1452.2	724.3	37.17	1613.3	772.0	48.735	445.9	354.3
22.05	250.3	249.7	37.27	1535.7	749.3	49	224.6	233.8

Depth m	Probe permeability mD	Corrected permeability mD
49.13	114.8	155.8
49.7	251.8	250.6
49.91	126.5	165.2
50.14	16.7	48.4
50.6	12.4	40.4
51.125	239.3	243.0
51.6	64.0	109.3
51.7	207.6	223.0
51.805	9.3	34.1
51.905	68.3	113.7
52	29.1	67.8
52.195	72.2	117.6
52.4	162.2	192.0
52.71	941.7	557.2
52.9	15.1	45.5
53.4	85.0	129.8
53.665	349.3	305.6
53.8	565.5	409.1
54.1	685.1	459.5
54.25	126.3	165.0
54.425	317.7	288.5
54.8	975.7	569.3
54.95	2831.8	1085.5
55.14	735.2	479.6
55.605	302.3	280.0
55.8	722.7	474.7
55.985	5.7	25.4
56.17	47.6	91.4
56.5	331.7	296.1
56.69	444.2	353.4
56.95	961.6	564.3
57.68	1426.5	716.5
58.045	1069.5	601.8
58.21	212.6	226.2
58.45	1173.6	636.7
58.67	509.9	384.2
58.875	1735.9	807.0
61.235	398.3	330.9
61.415	2263.1	947.6
61.6	178.3	203.3
61.87	577.2	414.2
62.4	230.0	237.3
62.69	1876.5	846.0
62.96	622.2	433.5
63.2	1546.2	752.4
63.4	474.5	367.9
63.61	2792.8	1076.4
63.77	1549.7	753.4
64	967.3	566.3
65.32	503.3	381.3
66.155	914.1	547.2
66.4	3172.1	1162.7
66.56	5144.3	1558.3
66.775	556.5	405.2
67.01	1891.8	850.2
67.2	1662.4	786.1
67.6	1003.8	579.1
67.78	2819.6	1082.6
68.2	4620.1	1460.1
68.36	499.8	379.6
68.8	210.5	224.8
69.1	1253.8	662.7
69.265	91.1	135.4
69.47	1525.0	746.1
69.685	793.9	502.5
70.1	1772.7	817.3
70.26	71.4	116.8
70.54	186.5	209.0
70.93	1051.0	595.5
71.995	31.1	70.5
72.185	196.4	215.6
72.4	262.7	257.2
73.16	36.3	77.5
74.15	58.3	103.3
74.4	16.9	48.8
74.8	806.5	507.2
76.57	1446.5	722.6
76.8	1678.5	790.7
76.985	283.3	269.2
77.25	1974.2	872.4
77.4	2156.4	920.3
77.57	4412.6	1420.0
77.8	748.4	484.8
78	379.0	321.1
78.675	902.4	543.0
78.9	367.2	315.0
79.07	2378.7	976.7
79.3	1723.6	803.5
79.555	826.6	514.9
79.72	2132.9	914.2
80.16	588.1	419.0
80.62	3005.8	1125.4
80.8	329.9	295.2
81.52	707.2	468.5
81.73	2849.4	1089.5
82	3744.7	1285.6
82.31	1686.3	793.0
82.895	201.3	218.8
83.055	173.6	200.1
83.3	173.7	200.1
83.9	94.4	138.3
84.95	2835.2	1086.3
85.1	1156.6	631.0
85.38	2433.4	990.2
85.97	2055.2	893.9
86.195	2406.1	983.5
86.41	2383.0	977.7
86.501	1812.7	828.5
86.8	1614.8	772.4
86.985	762.4	490.3
87.5	895.2	540.3
87.79	6444.5	1786.2
88	1636.7	778.7
88.45	1127.0	621.2
88.85	31.8	71.5
89.625	862.7	528.4
89.855	84.7	129.5
90.13	1529.8	747.5
90.385	940.2	556.6
90.95	128.8	167.0
91.27	513.2	385.8
91.14	400.5	332.0
91.41	364.2	313.4
91.61	231.4	238.1
92.54	954.4	561.7
92.75	1522.4	745.3
92.975	284.3	269.7
93.375	412.5	338.0
93.69	193.7	213.8
94.2	1472.1	730.3
94.425	838.7	519.4
95.335	2603.5	1031.6
95.555	1009.9	581.3
95.75	2222.0	937.2
96.765	1105.5	614.0
96.945	486.3	373.4
97.15	482.0	371.4
97.5625	461.3	361.6
97.7425	2135.5	914.9
97.9425	1003.2	578.9
98.14	1275.0	669.4
98.315	1300.8	677.6
98.35	2019.8	884.6
99.825	1093.7	610.1

Depth m	Probe permeability mD	Corrected permeability mD
100.155	314.6	286.8
100.5	160.5	190.8
101.03	1101.2	612.6
101.3	39.5	81.6
101.2	180.3	204.7
101.38	775.5	495.4
101.55	1927.1	859.7
101.735	749.1	485.1
102.495	452.3	357.3
102.685	485.9	373.2
102.905	828.6	515.6
103.1	434.9	348.9
103.68	1627.1	776.0
104.25	222.4	232.5
105.09	3056.1	1136.7
105.43	961.3	564.2
106.035	2203.1	932.3
106.25	1649.4	782.4
109	1839.9	836.0
110	992.8	575.3
111.795	134.7	171.6
112.15	347.8	304.8
113.375	468.0	364.8
113.55	311.3	285.0
113.935	270.3	261.6
114.4	164.7	193.8
116.295	994.9	576.0
116.675	313.1	286.0
117.07	1121.5	619.4
117	655.2	447.3

Depth m	Probe permeability mD	Corrected permeability mD
117.91	452.6	357.5
118.15	2412.2	985.0
119.045	176.3	201.9
119.2	1401.5	708.9
119.4	41.8	84.5
119.7	2240.7	942.0
122.65	731.5	478.1
123.04	254.0	251.9
125.55	50.2	94.3
126.822	1152.3	629.6
126.52	4307.3	1399.4
126.955	625.5	434.9
130.62	232.1	238.6
130.76	47.1	90.8
131	151.3	184.1
131.85	338.8	300.0
132.4	95.6	139.4
132.73	1164.7	633.7
133.115	317.9	288.6
133.775	97.0	140.6
134	165.0	194.0
134.22	63.2	108.5
134.64	436.5	349.7
134.9	647.9	444.3
135.25	196.9	215.9
135.37	419.8	341.6
135.6	1841.2	836.3
135.78	299.1	278.1
136	816.0	510.9
136.19	193.3	213.5

Depth m	Probe permeability mD	Corrected permeability mD
136.415	366.8	314.7
139.265	1594.3	766.5
140.01	105.9	148.3
139.945	64.5	109.8
140.17	299.3	278.3
140.95	91.5	135.8
142.1	107.3	149.5
142.47	138.4	174.4
142.75	3458.9	1225.3
143.8	1311.7	681.0
144.94	317.8	288.6
114.54	280.6	267.6
145.295	16.5	48.0
145.575	137.3	173.6
145.88	61.1	106.3
146.175	1085.2	607.2
146.69	938.0	555.9
147.345	33.8	74.3
147.475	44.9	88.2
147.615	97.0	140.7
147.82	568.4	410.4
148.1	905.6	544.1
149	824.6	514.1
149.185	1573.4	760.4
149.38	54.2	98.8
149.595	525.3	391.3

Appendix 2 Descriptive log of core

Top depth	Bottom depth	Lithology	Description
0.00	9.55		No core recovery
9.55	12.30	Sandstone	Moderate orange pink, medium grained, well-cemented, low-angle cross-bedded, mudclast-lined erosion surfaces at 20-70 cm intervals
12.30	14.60	Sandstone	Moderate orange pink, medium grained, well-cemented, faintly laminated, occasional mudclasts at 12.33 m. Mudclast lined erosion surface
14.60	16.10	Sandstone	Pale reddish brown, fine-medium grained, well cemented, faint lamination, micaeous
16.10	16.95	Sandstone	Greyish orange pink, medium-coarse grained, moderately sorted, moderately well-cemented, faint low-angle cross-bedding, common mudclasts
16.95	20.90	Sandstone AND Silty Sandstone	Moderate to dark reddish brown, fine-grained, diffuse bedding parallel zones of carbonate-cemented sandstone, massive
20.90	21.50	Sandstone	Moderate orange pink, medium-grained, moderately cemented, faint lamination
21.50	22.50	Sandstone	Dark reddish brown, fine-grained, moderately cemented, silty
22.50	23.70	Sandstone	Moderate Orange brown, medium-grained, moderately cemented, low angle lamination, more pronounced toward base
23.70	25.66	Sandstone	Orange brown, fine-grained, alternation of well cemented and poorly cemented sandstone, faint lamination
25.66	26.70		Core loss
26.70	27.05	Sandstone	Orange brown, medium-grained, moderately cemented, faint low angle lamination
27.05	27.50	Mudstone	Dark reddish brown, massive, becoming sandy and micaeous toward base
27.58	27.82	Clayey sandstone	Dark reddish brown, fine-grained, ripple-cross laminated
27.82	28.50	Sandstone	Reddish brown, fine-grained, well cemented, cross-laminated, micaeous, mudclasts
28.50	29.63	Sandstone	Reddish brown, Fine-medium grained, well cemented, ripple cross-laminated, scattered mica and mudflakes, bleached green toward base
29.63	33.00	Sandstone	Greyish orange pink, fine-medium grained, well cemented, faintly laminated, common mudclasts
33.00	33.68	Sandstone	Grey and greenish grey, fine-very coarse grained, well-cemented, faint lamination
33.68	34.75	Sandstone	Reddish brown, medium-coarse grained, moderately cemented, bimodal lamination
34.75	35.45	Sandstone	Reddish brown, fine-grained, weakly cemented, massive, silty
35.45	35.66	Sandstone	Laminated
35.66	35.97	Sandstone	Reddish brown, fine-medium grained, moderately cemented, wavy lamination, silty
35.97	36.35	Sandstone	Reddish brown, fine-medium grained, moderately cemented, high angle cross lamination
36.35	37.80	Sandstone	Reddish brown, fine-medium grained, moderately cemented, wavy laminated, silty
37.80	38.00	Sandstone	Reddish brown, fine-medium grained, moderately cemented to friable, laminated
38.00	38.40		Core loss
38.40	39.00	Sandstone	Reddish brown, fine-medium grained, moderately cemented to friable, laminated
39.00	39.84	Sandstone	Orange brown, medium-coarse grained, moderately cemented, high angle cross-lamination
39.84	41.40	Sandstone	Reddish brown, fine-medium grained, moderately cemented, low-angle lamination and wavy lamination
41.40	42.28	Sandstone	Reddish brown, fine-medium grained, well cemented, massive

Top depth	Bottom depth	Lithology	Description
42.28	42.43	Mudstone	Dark reddish brown, massive
42.43	44.40	Sandstone	Pale Reddish brown, medium-grained, moderately cemented, massive
44.40	46.68	Sandstone	Pale Reddish brown, fine-medium grained, well cemented, faint cross-bedding, some mudflakes overlying faint erosion surfaces, some greyish-green reduction
46.68	47.15	Sandstone	Greyish green, fine-grained, well cemented, ripple cross-laminated, micaeous
47.15	47.60	Sandstone	Pale Reddish brown, medium-grained, well cemented, cross lamination, mudclasts up to 12 mm
47.60	48.90	Sandstone	Pale Reddish brown, fine-medium grained, well cemented, faintly low-angle cross laminated
48.90	49.60	Sandstone	Reddish brown, medium-coarse grained, weakly cemented, faintly low-angle cross laminated, mottled greenish grey
49.60	50.05	Sandstone	Reddish brown and greenish grey, fine-medium grained, well cemented, massive/faint wavy lamination
50.05	51.10	Sandstone	Reddish brown and greenish grey, fine-medium grained, well cemented, faint lamination, irregular carbonate nodules and grey green mottling
51.10	53.00	Sandstone	Reddish brown and greenish grey, fine-medium grained, well cemented, faint wavy lamination, patchy carbonate cement
53.00	53.32	Sandstone	Pervasive carbonate cement, nodular
53.32	54.05	Sandstone	Reddish brown, fine-medium grained, moderately cemented, faint lamination
54.05	54.10	Sandy mudstone	Dark reddish brown, micaeous, ripple cross lamination
54.10	56.05	Sandstone	Reddish brown, medium-grained, moderately cemented, faint cross-bedding, silty @55.30-55.36 Pervasive carbonate cement
56.05	58.79	Sandstone	Reddish brown, medium-grained, friable, faint wavy to parallel lamination
58.79	61.10		Core loss
61.10	64.00	Sandstone	Reddish brown, fine-coarse grained, moderately cemented, wavy to parallel laminated, silty to clean
64.00	64.90		Core loss
64.90	65.50	Sandstone	Reddish brown, medium-grained, moderately cemented, faintly laminated
65.50	65.95		Core loss
65.95	71.34	Sandstone	Reddish brown, medium-grained, moderately cemented, wavy irregular lamination, common silty laminae
71.34	71.95		Core loss
71.95	74.75	Sandstone	Reddish brown, medium-grained, moderately cemented, wavy irregular lamination, common silty laminae
74.95	75.30		Core loss
75.30	77.00	Sandstone	Reddish brown, medium-grained, moderately cemented, faint low angle lamination
77.00	78.15	Sandstone	Dark reddish brown, fine-medium grained, moderately cemented, silty, wavy lamination, some well-developed erosion surfaces
78.15	78.30		Core loss
78.30	81.00	Sandstone	Dark reddish brown, fine-medium grained, moderately cemented, silty, wavy lamination
81.00	81.30		Core loss
81.30	82.85	Sandstone	Dark reddish brown, fine-medium grained, moderately cemented, low angle lamination
82.85	87.07	Sandstone	Dark reddish brown, fine-medium grained, moderately cemented, silty, wavy lamination, irregular zones of carbonate cementation and bleaching
87.07	87.30		Core loss
87.30	90.42	Sandstone	Dark reddish brown, fine-medium grained, moderately cemented, low angle lamination
90.42	90.50		Core loss
90.50	93.10	Sandstone	Dark reddish brown, fine-medium grained, moderately cemented, silty, wavy lamination @90.90-91.00 Greenish grey bleached zone
93.10	93.30		Core loss

Top depth	Bottom depth	Lithology	Description
93.30	96.10	Sandstone	Dark reddish brown, fine-medium grained, moderately cemented, silty, wavy lamination
96.10	96.30		Core loss
96.30	98.75	Sandstone	Dark reddish brown, fine-medium grained, moderately cemented, silty, wavy lamination, cemented bleached zone at 97.00
98.75	99.30		Core loss
99.30	102.11	Sandstone	Dark reddish brown, fine-coarse grained, moderately cemented, silty, wavy lamination, common coarse aeolian grains
102.11	102.30		Core loss
102.30	104.66	Sandstone	Dark reddish brown, fine-medium grained, moderately cemented, low angle lamination, clean
104.66	104.90	Core loss	Core loss
104.90	106.30	Sandstone	Dark reddish brown, fine-medium grained, moderately cemented, silty, wavy lamination
106.30	107.35		Core loss
107.35	108.80	Sandstone	Orange brown, loose, friable, clean, becoming firmer toward base
108.80	111.17	Sandstone	Dark reddish brown, fine-medium grained, weakly cemented, low angle lamination
111.17	111.60		Core loss
111.60	113.80	Sandstone	Reddish brown, fine-medium grained, weakly/moderately cemented, low angle lamination
113.80	114.60		Core loss
114.60	117.00	Sandstone	Reddish brown, fine-medium grained, weakly/moderately cemented, low angle lamination with some wavy lamination, bleached zone at 177.20
117.00	117.75		Core loss
117.75	118.14	Sandstone	Pale Reddish brown, medium-coarse grained, high angle cross-bedding, irregular carbonate cement
118.14	119.14	Sandstone	Dark reddish brown, massive, very silty, carbonate nodules
119.14	119.98	Sandstone	Reddish brown, medium-grained, moderately cemented, high to low angle cross-bedded
119.98	120.40		Core loss
120.40	122.25	Sandstone	Reddish brown, fine-medium grained, weakly cemented/friable, wavy lamination
122.25	123.40		Core loss
123.40	124.60	Sandstone	Reddish brown, fine-medium grained, moderately cemented, low angle lamination
124.60	126.40		Core loss
126.40	126.52	Sandstone	Reddish brown, medium-coarse grained, moderately cemented, low angle lamination
126.52	127.45	Sandstone	Dark reddish brown, fine-medium grained, moderately cemented, silty, wavy lamination
127.45	129.45		Core loss
129.45	129.60	Sandstone	Reddish brown, fine-medium grained, moderately cemented, low angle cross bedding
129.60	130.15	Sandstone	Dark reddish brown, fine-medium grained, moderately cemented, silty, wavy lamination
130.15	130.65		Core loss
130.65	131.10	Sandstone	Reddish brown, fine-medium grained, moderately cemented, low angle cross-bedding, irregular carbonate cementation
131.10	133.10	Sandstone	Dark reddish brown, fine-medium grained, moderately cemented, low angle lamination, slightly silty
133.33	133.65		Core loss
133.65	136.36	Sandstone	Dark reddish brown, fine-medium grained, moderately cemented, silty, wavy lamination

Top depth	Bottom depth	Lithology	Description
136.36	136.54	Sandstone	Reddish brown, fine-medium grained, weakly cemented, high angle cross-bedded
136.54	136.65		Core loss
136.65	137.35	Sandstone	Dark reddish brown, fine-medium grained, moderately cemented, low angle lamination
137.35	139.55		Core loss
139.55	142.05	Sandstone	Reddish brown, fine-medium grained, moderately cemented, silty, wavy lamination with some planar lamination
142.05	142.55		Core loss
142.55	143.73	Sandstone	Dark reddish brown, fine-medium grained, moderately cemented, low angle lamination
143.73	144.16	Sandstone	Pale Reddish brown, medium-grained, well cemented, high angle cross-bedding
144.16	149.80	Sandstone	Dark reddish brown, fine-medium grained, moderately cemented, low angle lamination alternating with wavy lamination, variably silty with some bleached, carbonate-cemented zones
149.80	150.00		Core loss

Appendix 3 Core physical properties

Table A5 Description of core as received by BGS at Wallingford (all depths in units of m).

Box	Top depth	Bottom depth	Cored interval	Core recovery	Core loss	Cumulative loss
1	9.55	11.60	2.05	1.96	0.09	0.09
2	11.60	14.60	3.00	2.99	0.01	0.10
3	14.60	16.95	2.35	2.35	0.00	0.10
4	16.95	17.70	0.75	0.75	0.00	0.10
5	17.70	20.70	3.00	2.94	0.06	0.16
6	20.70	23.70	3.00	2.95	0.05	0.21
7	23.70	26.70	3.00	1.96	1.04	1.25
8	26.70	29.70	3.00	2.93	0.07	1.32
9	29.70	32.70	3.00	2.98	0.02	1.34
10	32.70	35.45	2.75	2.75	0.00	1.34
11	35.45	38.40	2.95	2.55	0.40	1.74
12	38.40	41.40	3.00	2.90	0.10	1.84
13	41.40	44.40	3.00	2.96	0.04	1.88
14	44.40	46.80	2.40	2.32	0.08	1.96
15	46.80	49.50	2.70	2.70	0.00	1.96
16	49.50	51.25	1.75	1.68	0.07	2.03
17	51.25	54.05	2.80	2.76	0.04	2.07
18	54.05	56.15	2.10	2.10	0.00	2.07
19	56.15	61.10	4.95	2.64	2.31	4.38
20	61.10	64.90	3.80	2.90	0.90	5.28
21	64.90	65.95	1.05	0.60	0.45	5.73
22	65.95	68.95	3.00	2.97	0.03	5.76
23	68.95	71.95	3.00	2.39	0.61	6.37
24	71.95	75.30	3.35	2.80	0.55	6.92
25	75.30	78.30	3.00	2.85	0.15	7.07
26	78.30	81.30	3.00	2.70	0.30	7.37
27	81.30	84.30	3.00	2.98	0.02	7.39
28	84.30	87.30	3.00	2.77	0.23	7.62
29	87.30	88.50	1.20	1.00	0.20	7.82
30	88.50	90.50	2.00	1.92	0.08	7.90
31	90.50	93.30	2.80	2.60	0.20	8.10
32	93.30	96.30	3.00	2.80	0.20	8.30
33	96.30	99.30	3.00	2.45	0.55	8.85
34	99.30	102.30	3.00	2.81	0.19	9.04
35	102.30	104.90	2.60	2.36	0.24	9.28
36	104.90	109.10	4.20	3.05	1.15	10.43
37	109.10	111.60	2.50	2.07	0.43	10.86
38	111.60	114.60	3.00	2.20	0.80	11.66
39	114.60	117.75	3.15	2.40	0.75	12.41
40	117.75	120.40	2.65	2.23	0.42	12.83
41	120.40	123.40	3.00	1.85	1.15	13.98
42a	123.40	126.40	3.00	1.20	1.80	15.78
42b	126.40	129.45	3.05	1.05	2.00	17.78
43	129.45	130.65	1.20	0.70	0.50	18.28
44	130.65	133.65	3.00	2.68	0.32	18.60
45	133.65	136.65	3.00	2.89	0.11	18.71

Box	Top depth	Bottom depth	Cored interval	Core recovery	Core loss	Cumulative loss
46	136.65	139.55	2.90	0.70	2.20	20.91
47	139.55	142.55	3.00	2.50	0.50	21.41
48	142.55	145.00	2.45	2.38	0.07	21.48
49	145.00	148.00	3.00	3.00	0.00	21.48
50	148.00	150.00	2.00	1.80	0.20	21.68

10 References

Allen, D J, Brewerton, L J, Coleby, L M, Gibbs, B R, Lewis, M A, MacDonald, A M, Wagstaff S J, and Williams, A T. 1997. The physical properties of major aquifers in England and Wales. *Technical Report* WD/97/34, British Geological Survey, Keyworth.

Bellis, L. 2002. A study of the variation in cation exchange capacity within the Triassic Sandstone of the Cheshire Basin, and its implications for risk assessment. M.Sc. Thesis, University of Reading.

Bloomfield, J P, and Williams, A T. 1995. An empirical liquid permeability-gas permeability correlation for use in aquifer properties studies. *Quarterly Journal of Engineering Geology*, Vol. 28, S143–S150.

Bloomfield, J P, Brewerton, L J, and Allen, D J. 1995. Regional trends in matrix porosity and dry density of the Chalk of England. *Quarterly Journal of Engineering Geology*, Vol. 28, S131–S142.

Chadwick, R A, 1997. Fault analysis of the Cheshire Basin, north-west England. In: Meadows, N S, Trueblood S, Hardman, M, and Cowan, G (Editors), *The Petroleum Geology of the Irish Sea and adjacent areas*., Special Publication of the Geological Society of London, No. 124., pp. 297–313.

Edwards, G. 2001. An investigation into the controls on arsenic distribution in groundwaters of north west England. M.Sc. Thesis, University of Birmingham.

Edmunds, W M, Cook, J M, Kinniburgh, D G, Miles, D L, And Trafford, J M. 1989. Trace-element occurrence in British groundwaters. *Research Report* SD/89/3, British Geological Survey, Keyworth.

Goldstein, J E, Newbury, D E, Echlin, P, Joy, D C, Fiori, C, and Lifshin, E. 1981. Scanning Electron Microscopy and X-ray Microanalysis. A Text for Biologists, Materials Scientists, and Geologists. (New York: Plenum Press).

Griffiths, K J, Shand, P and Ingram, J. 2002. Baseline Report Series: 2. The Permo-Triassic Sandstones of west Cheshire and the Wirral. *Commissioned Report*, CR/02/109N, British Geological Survey, Keyworth.

Haslam, H, and Sandon. P T S.1991. The geochemistry of some red-bed formations in the United Kingdom. *British Geological Survey Technical Report*, WP/90/2, British Geological Survey, Keyworth.

Kinniburgh, D G, and Trafford, J M. 1996. Unsaturated zone porewater chemistry and the edge effect in a beech forest in southern England. *Water Air and Soil Pollution* Vol. 92, 421–450.

Meadows, N S And Beach A. 1993. Structural and climatic controls on facies distribution in a mixed fluvial and aeolian reservoir: the Triassic Sherwood Sandstone in the Irish Sea. In: C P North and D P Prosser (Editors), *Characterization of fluvial and aeolian reservoirs*. Geological Society Special Publication No 73, pp. 247–263. The Geological Society, London.

Naylor, H, Turner, P, Vaughan, D J, Boyce, A J, and Fallick, A E. 1989. Genetic studies of red bed mineralization in the Triassic of the Cheshire Basin, northwest England. *Journal of the Geological Society of London*, Vol. 146, 685–699.

Plant, J A, Jones, D G, and Haslam, H W. 1999. The Cheshire Basin: Basin Evolution, Fluid Movement and Mineral Resources in a Permo-Triassic Rift Setting. British Geological Survey, Keyworth, Nottingham, United Kingdom.

Smedley, P L, and Edmunds, W M. 2002. Redox patterns and trace-element behaviour in the East Midlands Triassic Sandstone aquifer, U.K. *Ground Water* Vol. 40, 44–58.

Smedley, P L, Gallois, R W, Edmunds, W M, and Edmunds, W M. 1995. Trace elements in Anglian-Water Lower-Cretaceous aquifers. *British Geological Survey Technical Report*, WD/95/45R, British Geological Survey, Keyworth.

Smedley, P L, and Kinniburgh, D G. 2002. A review of the source, behaviour and distribution of arsenic in natural waters. *Applied Geochemistry* Vol. 17, 517–568.

Thompson, D B. 1970. The stratigraphy of the so-called Keuper Sandstone Formation (Scythian-?Anisian) in the Permo-Triassic Cheshire Basin. Quarterly *Journal of the Geological Society of London*, Vol. 126, 151–181.

Warrington, G, Audley-Charles, M G, Elliott, R E, Evans, W B, Ivimey-Cook, H C, Kent, P E, Robinson, P L, Shotton, F W, and Taylor, F M. 1980. A correlation of Triassic rocks in the British Isles. *Special Report of the Geological Society of London*, No. 13, 77 pp. The Geological Society, London.